Improved reaction loads incorporated in sea fastening designs of offshore wind turbine components

A study on preparing the reaction loads calculation method for the future

Davi van Slobbe

TU Delft   TWD   NTNU

Cover image source: https://breakbulk.news/ohts-hlv-hawk-brings-10-jackets-to-moray-east/
Back cover image source: https://acebrongroup.com/en/offshore-wind-power-saint-brieuc/

Improved reaction loads incorporated in sea fastening designs of offshore wind turbine components

A study on preparing the reaction loads calculation method for the future

by

Davi van Slobbe

MSc student European Wind Energy Master

University	Degree
TU Delft	MSc Offshore Engineering
NTNU	MSc Technology - Wind Energy

Thesis committee:	TU Delft chair	Dr. H. C. Seyffert
	NTNU supervisor	Prof. Dr. B. J. Leira
	TU Delft committee member	Dr. A. Grammatikopoulos
	NTNU external censor	Dr. A. Bjørset
	TWD supervisor	Ir. J. Remmers
	TWD supervisor	Ir. J. Hogerheijde
Company:	TWD	

Preface

This Master's thesis, titled "*Improved reaction loads incorporated in sea fastening design of offshore wind turbine components*", was written in fulfillment of the Offshore Engineering track of the European Wind Energy Master (EWEM). Upon finalizing this Master's thesis, a Master's degree in Offshore Engineering is awarded by the TU Delft and a Master's degree Technology - Wind energy is awarded by the NTNU. As part of this thesis, a literature project was conducted from September 2022 until the end of December at the NTNU in Norway.

This research project was executed in collaboration with TWD. After finalizing the literature project in Trondheim, the research in this thesis was performed from February 2023 until the end of August from the Rotterdam office of TWD. The thesis project was initiated by Joost Remmers of TWD who convinced me of the future challenges and obstacles that are expected to arise in future transports of offshore wind turbines and their support structures.

First and foremost, I would like to express my gratitude to all my supervisors for guiding me through this thesis project and for sharing their knowledge and expertise with me. I would like to thank you all for taking the time to have regular progress meetings with me to provide me with your thoughts and feedback. In addition, I am grateful to Bernt Leira for instructing the *Stochastic theory of sea loads* course at the NTNU. The contents of this course have been very helpful for conducting this research. My gratitude also extends to Bernt for our productive interactions, both in person and digitally, which have played a significant role in shaping this work. I also wish to convey my sincere thanks to Harleigh Seyffert for your enthusiasm towards this research topic and for your insightful questions and feedback during the regular progress meetings. Furthermore, I wish to extend my gratitude to you for taking on the role of chair for this Master's thesis and for your dedicated organizational efforts in fulfilling this responsibility. Joost Remmers, your introduction to this thesis project and your shared passion for refining the existing calculation method of the reaction loads have played a crucial role for this thesis project. Your commitment of time and effort has greatly contributed to the success of this research. Joost Hogerheijde, your willingness to assist me and to always joyfully help me with my motion analysis related questions is very much appreciated. Apostolos Grammatikopoulos, I am appreciative of the constructive feedback which you have provided during the green-light meeting. Not to forget, I extend my gratitude to my colleagues at TWD for the enjoyable moments shared within the office.

Finally, my thanks go to my friends and family for their unconditional support and understanding during this Master's degree. Most importantly, I would like to thank my parents for their hard work and efforts in shaping the perfect conditions for me to successfully conclude my studies. I am very grateful and I am aware that I am very lucky with all the support you have always provided me with. In addition to being very lucky with my parents, I acknowledge being very fortunate to be born and raised in a part of the world where access to quality education and promising prospects are readily accessible.

Davi van Slobbe
Rotterdam, September 2023

Abstract

The offshore wind energy market is expanding and the number of offshore wind turbines being installed in the near future is rising. Offshore wind turbines are being installed further offshore and in deeper waters. Besides, to lower the cost of wind energy offshore wind turbines are increasing in size and power output. Both wind turbines and their support structures are expected to keep increasing in size and weight in the coming years. After fabrication, wind turbine components and support structures have to be transported to onshore storage depots or to their offshore location. To enable safe transports, wind turbine components and support structures are constraint to heavy transport vessels or transport barges by sea fastening structures. As a result of wind turbine components and support structures increasing in size and weight, the reaction loads for which sea fastening structures need to be designed are increasing as well. Since increasing reaction loads have various negative consequences which are expected to become more critical for future transports, there is a need for an optimized reaction load calculation.

The current method of calculating the reaction loads which is widely used in the industry is often referred to as being a conservative method. The aim of this thesis was to enhance the existing calculation method of the reaction loads by shifting from a conservative approach towards a method of calculating reaction loads based on an acceptable probability of occurrence during transports. By calculating the reaction loads for an acceptable probability of occurrence it is avoided that sea fastening structures are designed for overly conservative reaction loads while the structural reliability of these structures will still be ensured.

In this thesis an existing sea fastening design project from the industry was used to perform a case study. Data and information from this project was used as input to perform motion analyses of a vessel which is transporting a jacket support structure. The obtained linear wave-induced accelerations of the jacket CoG were used as the main input for calculating the reaction loads. It was first investigated how these 6-DoF accelerations of the CoG are used in the current method of calculating the reaction loads. This was followed by introducing statistical extreme value theory with the purpose of using the accelerations of the jacket CoG as input for a probabilistic method of calculating the reaction loads.

The findings of this research show that optimized reaction loads can be obtained by replacing the current calculation method by a long-term probabilistic method. It was found that this long-term probabilistic method could be derived by combining 3-hour extreme value density functions of reaction loads with the probabilities of encountering the various sea states at the location on the route for which the most severe environmental conditions are expected. The long-term probabilistic method was used to perform a probabilistic investigation of the reaction loads calculated with the current calculation method. It was found that the return periods of the reaction loads calculated with the current method were significantly different for the individual jacket legs. Moreover, it was found that the sea fastening design for at least one of the jacket legs was expected to be over-conservative. By presenting the long-term probabilistic calculation method, a methodology was introduced which determines reaction loads based on acceptable return periods while avoiding over-conservative sea fastening designs.

This research has provided a new insight into the method of designing sea fastening structures. The long-term probabilistic calculation method can be applied in practice to determine optimized reaction loads incorporated in sea fastening designs. This research therefore makes a valuable contribution to preparing the reaction load calculation method for future transports which are expected to become more critical due to wind turbine components and their support structures growing in size and weight.

Contents

Nomenclature

Abbreviations

Abbreviation	Definition
CDF	Cumulative Distribution Function
CoG	Centre of Gravity
DoF	Degree of Freedom
EVT	Extreme Value Theory
FEM	Finite Element Method
HTV	Heavy Transport Vessel
LCD	Load Case Determination
LRFD	Load and Resistance Factor Design
OWF	Offshore Wind Farm
OWT	Offshore Wind Turbine
PDF	Probability Density Function
RAO	Response Amplitude Operator

1
Introduction

1.1. Background

Offshore wind industry

Due to the demand of carbon neutral energy sources the offshore wind energy market is growing at a rapid pace. In the last 20 years the installed capacity of this new energy source has expanded significantly [12]. This is graphically shown in Figure 1.1. As many countries have targets to become carbon neutral in the coming decades, the offshore wind energy market is expected to keep expanding.

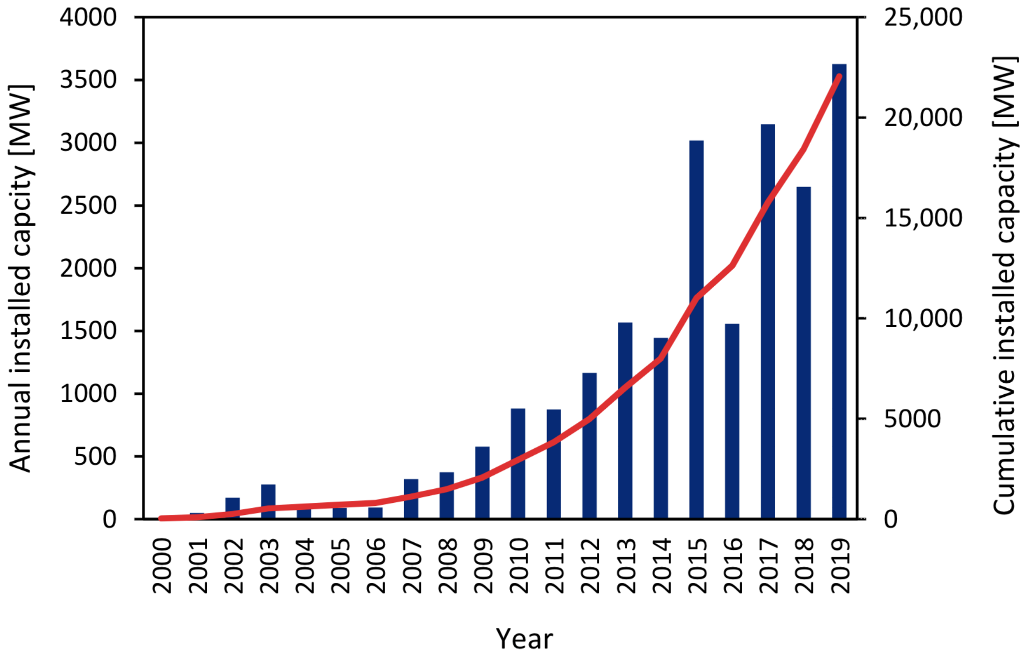

Figure 1.1: Annual and cumulative installed capacity of offshore wind farms in Europe between 2000 and 2019, taken from [12]

Although the offshore wind energy market is expanding, the market is still facing challenges. To compete with other sources of energy, the cost of offshore wind energy should be kept low. However, Offshore Wind Turbines (OWTs) require expensive support structures, transport, installation and grid connection which makes offshore wind energy 1.5-2 times more expensive than onshore wind energy [19].

In order to lower the cost of wind energy, wind turbine manufacturers are working on up-scaling wind turbines. Technological progress has enabled an impressive growth in size and power output of OWTs in the last decades. The average power output of OWTs ordered in 2022 in Europe was 12.2MW and this is expected to keep increasing in the coming years [4]. In Figure 1.2 an illustration is given of wind turbines increasing in size and power output over the years. Although up-scaling of wind turbines might lower the cost of wind energy, up-scaling of wind turbines also brings challenges such as increased weight and dimensions.

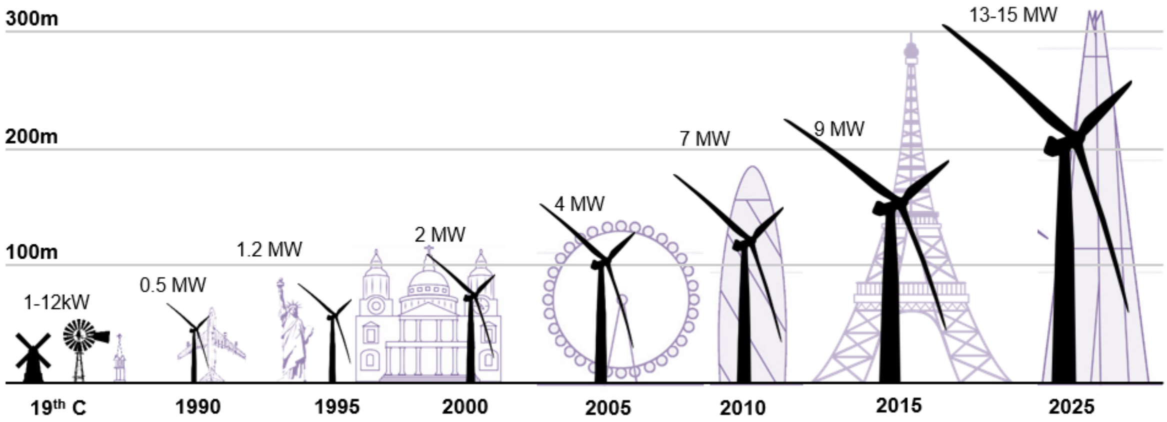

Figure 1.2: Wind turbines of increasing rated power, their hub heights and rotor diameters, taken from [3]

On top of OWTs and Offshore Wind Farms (OWFs) growing in size and power output, OWF locations are moving further from shore and into deeper waters. Due to the increase in installations in the last two decades, possible OWF locations in shallow waters close to shore are becoming scarce. Besides, wind conditions are more stable, impact on other economic activities are reduced and visual pollution is less of a problem further offshore [20]. It is also stated that technological advances in support structures and high voltage direct current technology make this trend feasible. In Figure 1.3 the distances offshore and the water depths of existing and planned European OWFs are given in a chart.

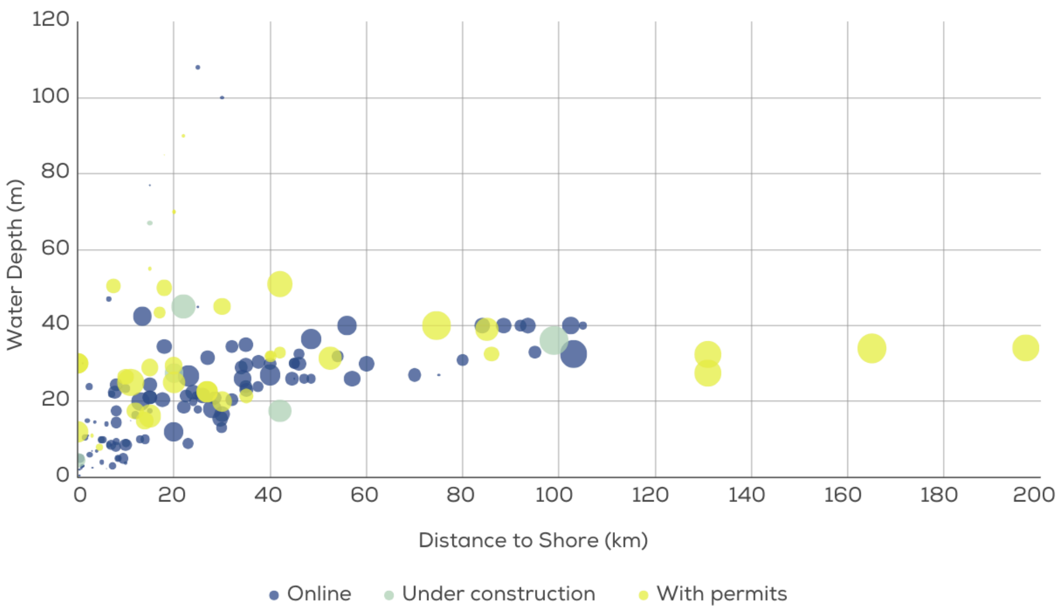

Figure 1.3: Distance to shore and water depths of European OWFs where bubble size denotes the total capacity of the wind farm, taken from [20]

OWT components and support structures

OWTs consist of multiple components which all have to be transported to the location of the OWF. The main components of an OWT are the rotor blades, turbine tower, nacelle and hub as can be seen in

Figure 1.4. The turbine tower often consist of multiple steel tubulars mounted on top of each other. The nacelle which contains the generator and in some cases also a gearbox is installed on top of the turbine tower. The rotor blades are secured to the hub which is fixed to the shaft going into the nacelle.

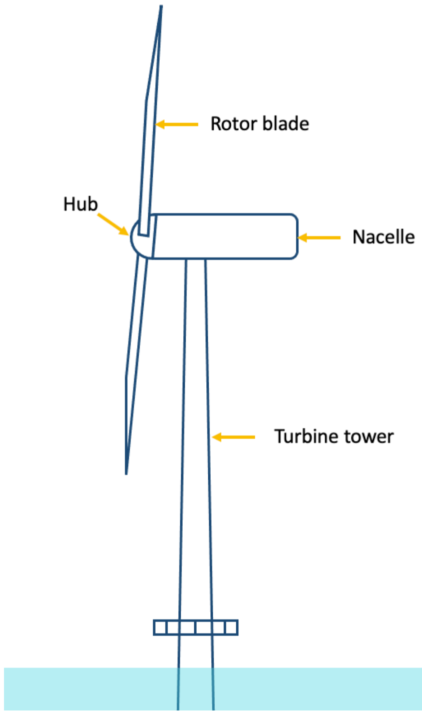

Figure 1.4: Main components of an OWT

Where onshore wind turbines only require a foundation to support the turbine tower at ground level, OWTs require a support structure to support the tower at a certain distance above the water level. Besides the OWT components, these support structures also have to be transported from their fabrication yard to the OWF location. Different types of bottom-founded support structures are being used in practice which are shown in Figure 1.5.

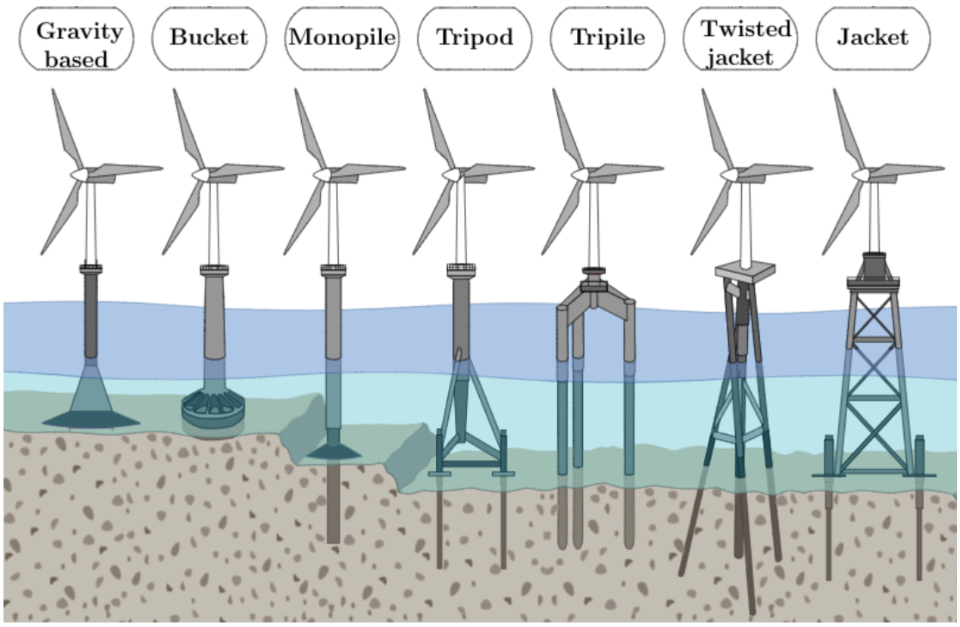

Figure 1.5: Different types of bottom-founded support structures, taken from [21]

In Figure 1.6 the number of installed support structure types in Europe by the end of 2010 and by the end of 2019 are given in a chart. As can be seen from the figure, the amount of gravity based structures has increased relatively little. This can be explained by the fact that these structures have advantages in shallow waters whereas OWTs are more often being installed in deeper waters. It can also be noted that monopiles remained to have the greatest share in this time period. For water depths up to 30m monopiles commercially and technically remain the best option [8]. The share of jacket support structures has increased between 2010 and 2019. Jacket support structures are favoured for water depths of 30m up to 50m [8]. It is also stated that jacket structures are suited for larger wind turbines with higher power output. Therefore the share of jacket structures is expected to keep growing in the coming years.

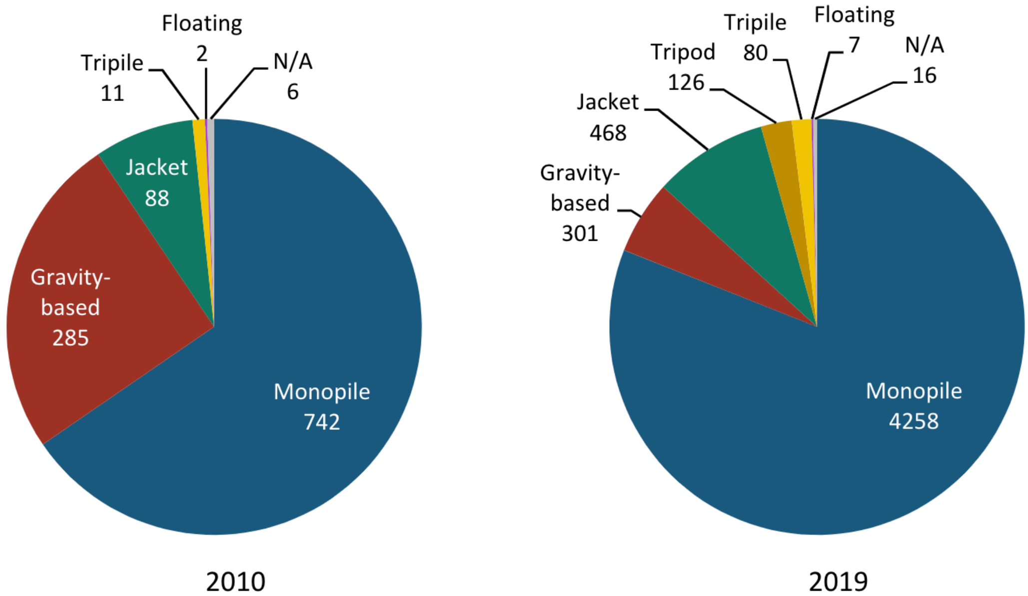

Figure 1.6: Numbers of installed support structure types in Europe by the end of 2010 and 2019 respectively, taken from [12]

Sea fastening during transports

After fabrication, wind turbine components and their support structures are often first transported from their production facilities to onshore storage locations after which they are transported in badges to the location of the OWF. To enable safe transport of wind turbine components and support structures without damaging these items or the vessel, these items are constrained to the vessel by sea fastening structures as can be seen in Figure 1.7. Sea fastening structures are designed to constrain undesired motions of the items during transport. In some cases it is not desired to constrain all motions of the to be transported structures. Constraining all possible motions of a structure might lead to unwanted internal stresses in a structure. This is especially the case when hogging and sagging is expected and long structures are being transported horizontally. Sea fastening structures should be able to withstand static loads as well as dynamic inertial loads of the structures which are caused by the response motions of the vessel in the six Degrees of Freedom (DoF).

Figure 1.7: Picture of jacket support structures which are sea fastened to a transport barge during transport, taken from [22]

The structural capacity of Heavy Transport Vessels (HTVs) and transport barges is an important aspect when designing the sea fastening. The reaction loads on the sea fastening have to be transferred into the structure of the vessel or barge. The points of a vessel that provide structural strength are web frames, transverse- and longitudinal bulkheads. To transfer the reaction loads on the sea fastening into these points of the vessel, the to be transported items are often supported by grillages. Grillages are support frames which often consist of steel beams or box girders as shown in Figure 1.8. It can also be seen here that a large amount of steel is involved in the construction of sea fastening structures as these structures have to be designed to withstand high reaction loads. The capacity of the vessel can be used efficiently by choosing the optimal deck layout and smart design of grillages.

Figure 1.8: Close up of sea fastening structures designed for the transport of jacket structures, taken from [18]

1.2. Problem statement

As described in section 1.1, wind turbines and therewith their support structures are expected to keep growing in size and weight. This increase in size and weight is associated with higher reaction loads on the sea fastening during transports of these items. Besides, these reaction loads are also being transferred into the structure of the vessel by the sea fastening. Although there is a lot of experience in transporting large and heavy structures in the oil and gas industry, the increase in size and weight of turbine components and support structures in the offshore wind industry brings new challenges:

- The numbers involved in the transport and installation of wind turbines are significantly higher than in the oil and gas industry. Recent OWFs may consist of more than 100 wind turbines and support structures which all have to be transported to their offshore location. Due to the expanding wind industry the demand for HTVs and transport barges is increasing which might cause problems in the future due to limited availability of HTVs and transport barges.
- Besides, HTVs need to increase in size as well to be able to transport the turbines and their support structures which are increasing in size. However, port accessibility might cause HTVs to be limited in size since vessels should be able to navigate safely and efficiently into and out of ports. Some reasons that might limit vessel dimensions are draught restrictions, channel width and depth and turning radii.
- Another concern are the increasing reaction loads as a result of larger and heavier turbines and support structures. These increased reaction loads on the sea fastening requires HTVs and transport barges to have increased structural capacity. In addition to being more expensive, higher capacity HTVs and transport barges are also scarcer.
- Apart from the challenges related to HTVs and transport barges, the increased reaction loads ask for more robust sea fastening designs. A large amount of steel is required for fabrication of sea fastening structures which brings both costs and emissions with it.
- Wind turbine components and support structures are designed for their functionality and not for structural integrity during transport. When loads acting on these items during transports are increasing, the structural integrity of these objects might become a problem.

These are all negative consequences of increasing reaction loads on the sea fastening during the transport of wind turbine components and their support structures. However, the current method of calculating the reaction loads which is widely used in the industry is often referred to as being conservative.

This presumption often lacks adequate support and even if arguments are presented, the probabilities of experiencing the calculated reaction loads during a transport remain uncertain. In the absence of a clear understanding of this probability, the structural reliability of sea fastening structures designed for reaction loads obtained with the current method also remains undetermined.

Since the increasing reaction loads are expected to become more critical for future transports, there is a need for optimized reaction loads. While it is essential to ensure sufficient structural reliability in a sea fastening design, it is not desired to design for overly conservative reaction loads. Therefore, there is a demand for an optimized calculation method that determines the reaction loads for an acceptable probability of experiencing these loads during transports such that structural reliability of sea fastening designs is ensured.

1.3. Research objective

As stated in the problem statement, the expansion of wind turbine components and support structures results in increased reaction loads on sea fastening structures, leading to various adverse effects. To mitigate the unfavorable consequences associated with increasing reaction loads, the research objective of this thesis is formulated as:

> *The aim of this research is to enhance the current calculation method of the reaction loads by shifting from a conservative approach towards an optimized method of calculating reaction loads based on an acceptable probability of occurrence during transports.*

By calculating the reaction loads for an acceptable probability of occurrence it is avoided that sea fastening structures are designed for overly conservative reaction loads while the structural reliability of these structures is still ensured. In order to achieve this research objective the following main research question is presented for this thesis:

- *How can the current calculation method be optimized to calculate reaction loads incorporated in sea fastening designs for an acceptable probability of occurrence during transports?*

Besides this main research question, sub-questions are formulated. The first sub-question is formulated to investigate the current calculation method while focusing on identifying the main uncertainties of the method and how the results of this method are affected by these uncertainties:

1. *What are the main uncertainties in the current calculation method of the reaction loads?*

The second sub-question is introduced to investigate the possibility of substituting deterministic steps of the current method with probabilistic techniques such that the resulting reaction loads can be interpreted in terms of probability:

2. *Which elements of the current calculation method should be modified to make the calculation method probabilistic?*

Finally, a third sub-question is presented which aims to quantify the probability of occurrence of the reaction loads calculated with the current method:

3. *What is the probability of occurrence during transports of reaction loads obtained with the current calculation method?*

In conclusion, the research conducted in this thesis aims to offer recommendations and methodologies that not only improve the understanding of reaction loads in terms of probability, but also contribute to preparing the method of designing sea fastening structures for future transports of wind turbine components and support structures.

1.4. Approach

To reach the presented research objective, investigations in this thesis are conducted on the basis of a chosen case study. An example of a typical sea fastening design project performed by TWD is chosen to serve as a case study. The chosen project concerns the vertical transportation of wind turbine support jackets. This case study is chosen for as it serves as a good illustration since the share of jacket support structures is expected to keep rising in the near future. Besides, these already large and heavy structures already cause some transports to be performed at the limits of the capacities of available HTVs and transport barges. Additionally, this type of support structure serves as a good illustration since it has a high CoG position relative to the deck such that high reaction loads are expected. The case study is introduced in more detail in section 2.1. From the example project which serves as a case study in this thesis, the following data and information is used:

- Complex transfer functions of the vessel containing the jacket structures on deck. These complex transfer functions are obtained with radiation-diffraction software.
- Jacket properties such as dimensions, weight and CoG location.
- Environmental conditions which have been agreed on together with the client for which the project is executed.

This data is used as input to perform time-domain motion analyses in Orcaflex. The OrcaFlex software is used to obtain linear-wave induced response motions of the vessel and jackets. For the calculation of the reaction loads, only the jacket is considered for which the highest reaction loads are expected based on its position on the vessel. The 6-DoF response accelerations of the CoG for this jacket is the main input used for reaction loads calculations. In this thesis it is investigated how the accelerations input is used in the current calculation method and how this could be used in a probabilistic approach by using statistical extreme value theory.

1.5. Scope

The scope of this thesis is the method of calculating the reaction loads incorporated in the design of sea fastening structures for jacket support structures. However, in practice the reaction loads which are calculated for the sea fastening design might be used for other purposes as well such as HTV capacity checks, structural integrity analysis and fatigue analysis of wind turbine components and support structures during transport. Besides, the method of calculating the reaction loads could be applied to design sea fastening structures for the transport of all types of structures such as horizontally transported monopiles or vertically transported transition pieces.

The research objective of this thesis is to introduce a method of calculating the reaction loads based on an acceptable probability of occurrence during transports. However, determining acceptable probabilities of occurrence of the design reaction loads to ensure a specific structural reliability of sea fastening designs is not part of the scope of this thesis. Although the introduced probabilistic approach to calculate reaction loads could be used to perform a structural reliability analysis of sea fastening designs, it's important to clarify that a comprehensive structural reliability analysis is not within the scope of this thesis

1.6. Thesis outline

In chapter 2 the current method of calculating the reaction loads which is widely used in the industry is elaborated. Besides, the current method is applied to calculate the reaction loads for the sea fastening design for the introduced case study.

The main uncertainties of the current method and the influence on the reaction loads calculated with this method are described in more detail in chapter 3.

Statistical extreme value theory for narrow-banded and non-narrow-banded processes is introduced in chapter 4, to describe stochastic response motions and loads during transport. In addition, the validity of applying theory for narrow-banded processes to the response accelerations of the jacket CoG which are non-narrow-banded is investigated.

In chapter 5 the introduced extreme value theory is used to obtain short-term extreme value distributions of the reaction loads for the different sea states. These extreme value distributions of the reaction loads are used to perform a probabilistic investigation of the current method of combining loads.

In chapter 6 a long-term probability based calculation method is introduced based on the 3-hour extreme value density functions of the reaction loads and the long-term probability on the different sea states. This long-term probability based method is used to perform a probabilistic investigation of the current calculation method.

The results and the main findings of this research are discussed in chapter 7. After which the final conclusions and recommendations for future work are presented in chapter 8. A schematic illustration of the thesis outline is presented in Figure 1.9.

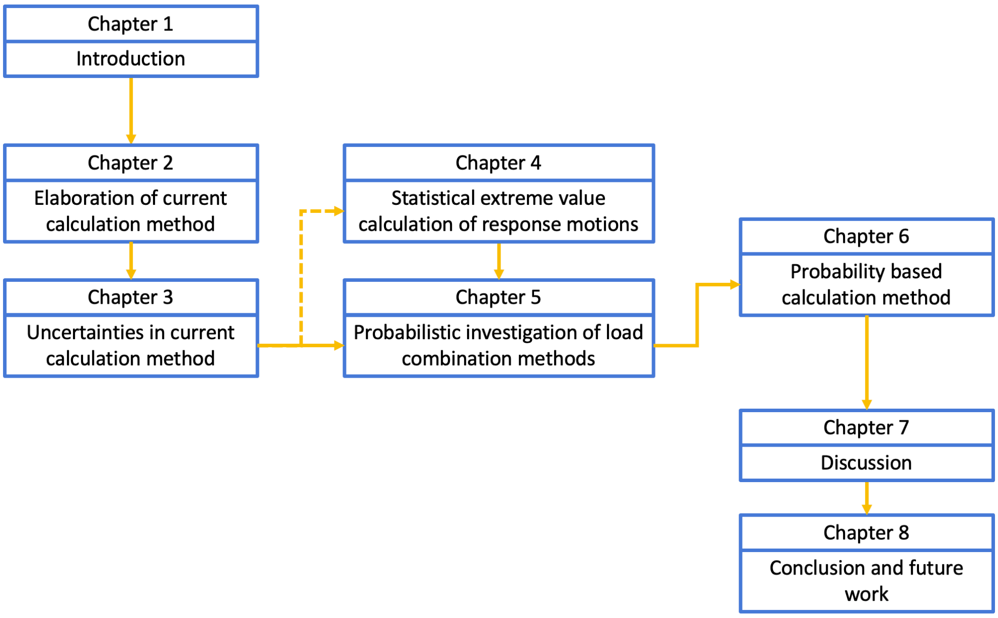

Figure 1.9: Schematic illustration of thesis outline

2 Elaboration of current calculation method

In this chapter, first the chosen project from industry that will be used for the case study which is performed in this thesis is introduced in section 2.1. The chosen project concerns the design of a sea fastening structure for the transport of wind turbine support jackets. The focus of this section will be on presenting the essential data and information which will be used to perform the case study in this research.

Once the case study is introduced, the current method of calculating the reaction loads which is widely used in the industry is introduced and elaborated. The different stages of the current calculation method are introduced in section 2.2, section 2.3, section 2.4 and section 2.5. Finally, in section 2.6 the current method is applied to the chosen project to calculate the reaction loads for the design of the sea fastening structure.

2.1. Jacket transport case study

The chosen project which is chosen to perform a case study, concerns the vertical transportation of wind turbine support jackets. As mentioned before, this project is chosen for as it serves as a good illustration since the number of installed jacket support structures is expected to keep rising in the coming years. Besides, some transports of jacket support structures are already performed at the limits of the capacities of available HTVs and transport barges while these jacket structures are foreseen to keep increasing in size and weight. In addition, the high CoG position of the jacket relative to deck is likely to cause high reaction loads. Moreover, these are all reasons why the chosen project forms a good illustration of the challenges involved in future sea fastening designs.

In the case study the vertical transport of multiple three-legged jacket structures on a single vessel will be considered. All jackets will have to be taken into consideration during the motion analysis of the vessel carrying the jackets. However, the focus of this thesis will be only on designing the sea fastening structure for the jacket for which the highest reaction loads are expected. It is assumed that all jackets have equal geometry, weight and orientation on the vessel. However, the jacket positioned on the aft of the vessel will be considered for the calculation of the reaction loads on the sea fastening as the response motions and the resulting reaction loads for this jacket are likely to be governing.

Jacket properties

The considered three-legged jacket structures have heights of ?m and maximum design masses of ? tonne. This mass is including an initial guess of the weight of the sea fastening. The height of the jacket CoG relative to the vessel deck is ?m. This height includes the initial guess of the sea fastening height. The legs of the jacket have a centre to centre distance of ?m as can be seen in Figure 2.2.

Table 2.1: Jacket properties

Height	?	m
Maximum design mass	?	tonne
CoG height relative to deck	?	m
Centre to centre distance legs	?	m

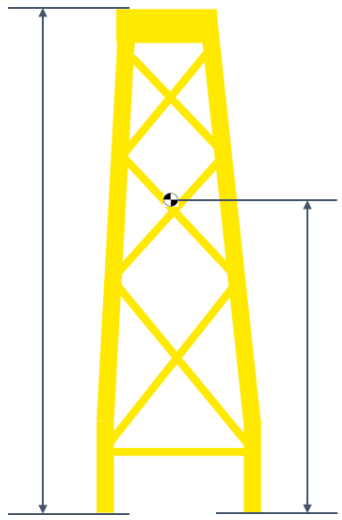

Figure 2.1: Height of the jacket and its CoG position relative to the vessel deck, dimensions are in mm

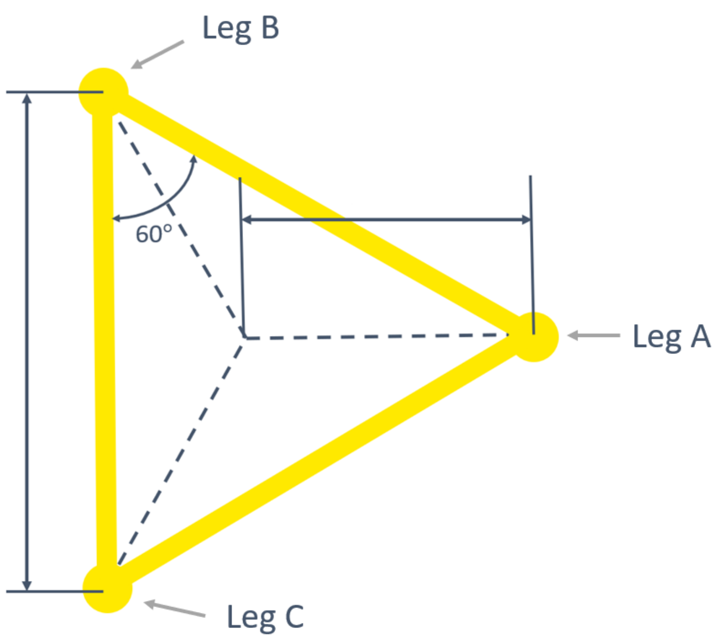

Figure 2.2: Top view of jacket's lowest frame elevation, dimensions are in mm

Jacket position and orientation on vessel

The governing jacket is positioned on the aft of a typical transportation vessel. A vessel-bound coordinate system will be used to express the position of the jacket CoG relative to the vessel. The properties of the vessel-bound coordinate system are given in Table 2.2. In Figure 2.3 and Figure 2.4 the assumed position of the jacket CoG when the jacket is sea fastened to the vessel is given in the vessel-bound coordinate system. From these figures it can also be seen that the jacket is oriented with jacket leg A on the center line of the vessel and that jacket legs B and C are positioned closer to the side shell.

Table 2.2: Properties of the vessel-bound coordinate system

Coordinate	Origin	Positive direction
X	Aft	Towards bow
Y	Center plane	Towards portside
Z	Base line	Upwards

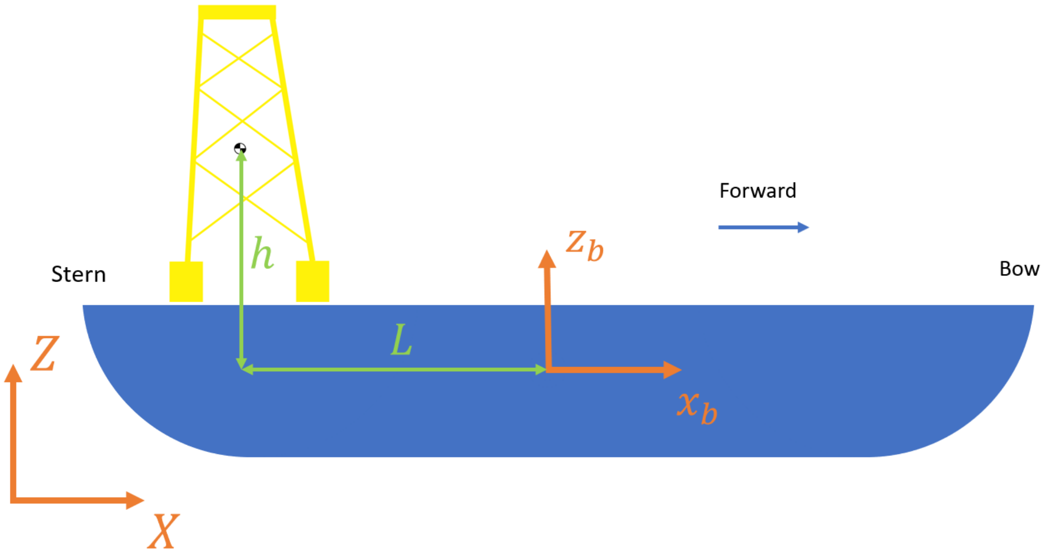

Figure 2.3: Position of jacket CoG expressed in the vessel-bound (x_b, y_b, z_b)-coordinate system

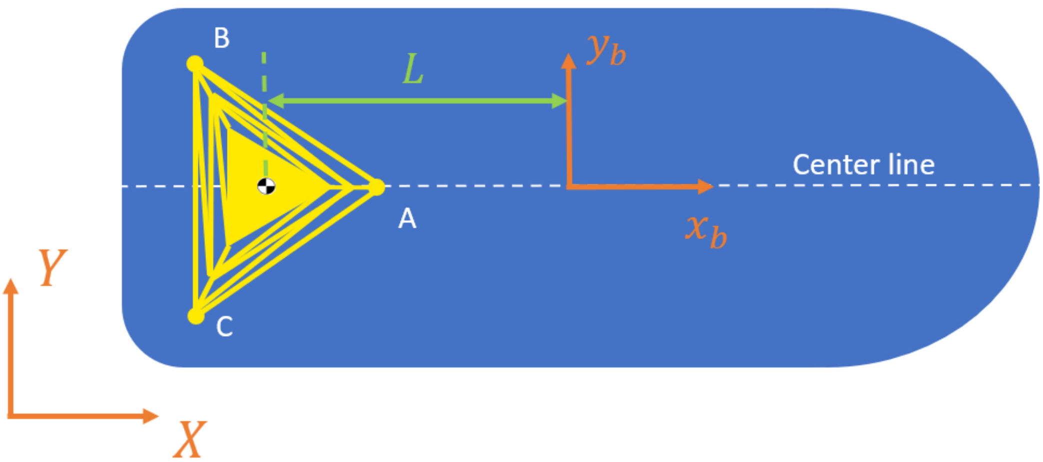

Figure 2.4: Position of jacket CoG expressed in the vessel-bound (x_b, y_b, z_b)-coordinate system

Environmental conditions

For marine operations in general the design environmental conditions consist of wave height, wind speed, current and other relevant conditions. According to DNV-ST-N001 [6] these design environmental conditions should be based on both extreme statistical data and short-term variations representative for the geographical area of the marine operation. The data from which the design environmental conditions are to be determined should cover a sufficient long time period. For meteorological and oceanographic data a minimum of three to four year of data is recommended in the guideline. It should be pointed out that the environmental conditions used as input for the case study have been specified by the client for which TWD has executed the considered project.

Design sea states can be represented by wave energy spectra which are described by significant wave height H_s and zero up-crossing period T_z or peak period T_p. In DNV-ST-N001 [6] it is prescribed that a range of peak periods should be investigated when performing a motion analysis for a marine operation. In the example project from which the environmental conditions are taken, swell waves are considered with a design significant wave height $H_s =$?m and peak periods T_p ranging from ? to ?s with intervals of 0.5s. A peak shape parameter γ ranging from ? for short peak periods up to ? for longer peak periods will be used. Besides, a spreading exponent of $n =$? is considered. In this case study current is not neglected. The design sea state parameters are summarized in the following table:

Table 2.3: Design sea state characteristics

	Symbol	Value	Unit
Significant wave height	H_s	?	m
Peak period	T_p	? - ?	s
Peak period interval	ΔT_p	0.5	s
Peak shape parameter	γ	?	
Spreading exponent	n	?	

In addition to wave-induced loads also wind loading is considered. However, wind loading is neglected in the motion analysis and is only accounted for in the structural analysis of the jacket. A design wind velocity U_w of ?m/s is assumed and the air density ρ_{air} used to calculate the wind load is expected to be ?kg/m^3 at -20° Celsius. The design wind velocity is the wind velocity averaged over a given time period T at a reference height z above the mean water level. In the case study a forward vessel speed of ?kn is considered.

Table 2.4: Wind conditions and forward vessel speed

	Symbol	Value	Unit
Design wind speed	U_w	?	m/s
Air density (at -20° Celsius)	ρ_{air}	?	kg/m^3
Forward vessel speed	V_{fwd}	?	kn

2.2. Response motion analysis

After the design sea state and other environmental conditions have been defined, the next step in the calculation process of the reaction loads is to perform a response motion analysis of the vessel containing the jackets. In Figure 2.5 the conventions of the six motions of a vessel are defined.

In DNV-ST-N001 [6] it is described that once the vessel has been selected, the draught and trim of the vessel for the given cargo should be determined before performing the motion response analysis. Besides performing a motion response analysis it is prescribed that the response motions of a vessel could be obtained by model tank testing or by using default equivalent motion values given in the guideline. In practice, performing a motion response analysis is preferred because model tank testing is a time consuming and costly method and the default motion criteria values can be considered very general and conservative. However, when conservativeness is not a problem and there is no need to know the exact motions of a vessel the default motion criteria can save a lot of time and costs because a motions response analysis will not have to be performed.

It is mentioned that the motion analysis shall be performed for zero vessel speed and a range of headings including head, bow quartering, beam, stern quartering and following seas. In Figure 2.6 wave

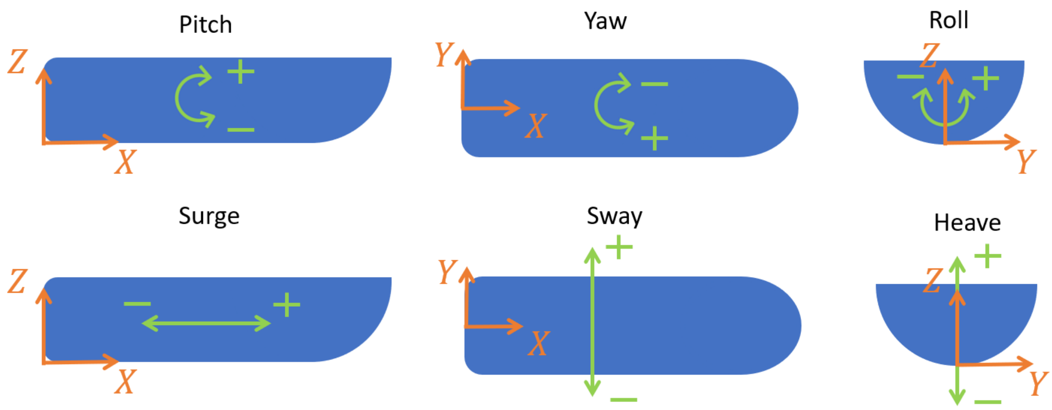

Figure 2.5: Vessel motion conventions

direction and vessel definitions are given. The analysis should also be performed for the maximum vessel speed during a transport for non-beam seas. In the guidelines it is recommended to use recognised and well proven 6-DoF linear or linearized computer programs based on strip theory or 3D panel methods. However, it is stated that 3D panel methods are preferred.

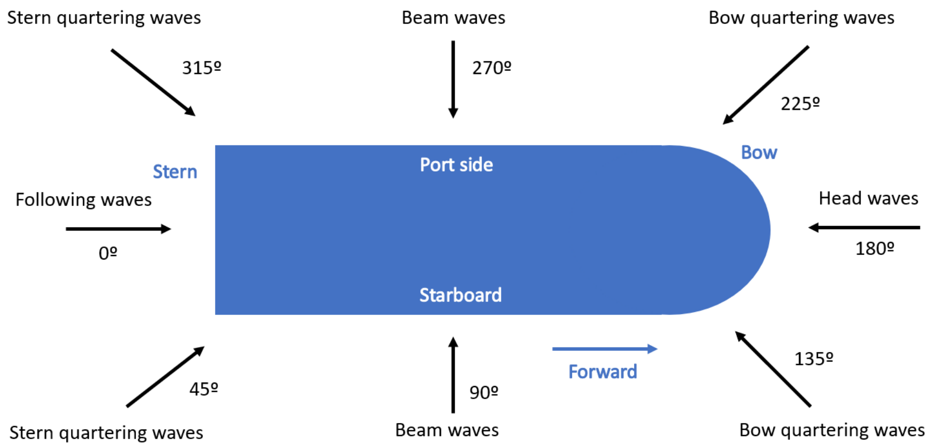

Figure 2.6: Vessel and wave direction definitions

Radiation-diffraction software

Linear wave-induced motions and loads in irregular seas can be obtained by superposition of the results of a vessel in regular waves. These motions and loads on large volume-structures at zero forward speed can be predicted with the help of three-dimensional based numerical tools [7]. It is stated that the most used methods for calculating the linear steady state response of large-volume structures in regular waves are 3D panel methods. Panel methods are based on potential energy and software using panel methods is therefore also called radiation-diffraction software.

Panel methods make use of Green's integral theorem which enables to numerically calculate the flow around a vessel [9]. With this theorem a three-dimensional linear homogeneous differential equation can be written as a two-dimensional integral equation. Therefore, the three-dimensional Laplace equation can be transformed to a surface integral equation representing a distribution of sources or sinks on the vessel hull surface. By dividing the hull of the vessel into panels, as can be seen in Figure 2.7, the surface integral can be solved numerically.

It should be noted that the method only accounts for damping due to radiation of waves and that damping caused by viscous effects such as skin friction and vortices cannot be accounted for [9]. It is stated

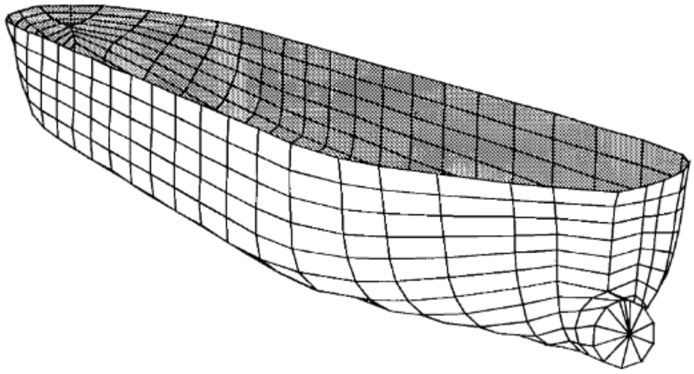

Figure 2.7: Example of a vessel hull divided in panels, taken from [9]

that for vessels these viscous effects are often neglected for sway, heave, pitch and yaw motions as the contribution of viscous damping to the total damping is relatively small compared to potential wave damping. However, especially for roll motion the contribution of viscous damping can be significant [9]. It is suggested that in many cases the empirical Ikeda method can be used which estimates viscous damping due to forward speed, skin friction, eddy making, lift and bilge keels.

Motion analysis performed in practice

Before performing the motion analysis, the stability characteristics of the vessel are determined for the case that the vessel is being loaded with all jackets. The radii of gyration and the metacentric height of the loaded vessel are determined. Subsequently, a frequency domain analysis of the vessel is performed with radiation-diffraction software. As a first step the vessel hull is imported into the software after which the hull is divided into panels as has been done in Figure 2.7 for an example vessel. Besides, the stability characteristics of the vessel are given as input to the software.

When the software has performed a radiation-diffraction analysis the complex motion response functions of the six vessel motions are given as an output. The complex response functions contain the Response Amplitude Operators (RAOs) and phase angle information of the response motions. For linear wave-induced motions RAOs give the ratio between the amplitude of a regular wave of frequency ω and the amplitude of the response motion to this regular wave. Phase angles of the motions give the phase difference between a regular wave of frequency ω and the response motions to this regular wave.

When the frequency domain analysis of the vessel is performed and the complex response functions are obtained with potential theory, viscous roll damping effects are determined with the Ikeda method as recommended in DNV-ST-N001 [6]. The roll damping is corrected for non-linear damping effects and effects due to forward speed. These effects are linearized and the complex response functions are updated to account for these effects. In subsection 3.3.1 it is described in more detail how the roll damping and complex response functions are corrected to take into consideration viscous effects. The corrected complex response functions are used as input for the software which performs time domain simulations of the vessel. However, in the time domain simulations linear steady state response motions are obtained with frequency domain calculations.

In the time domain analysis the calculated vessel frequency response characteristics are used to perform three hour motion response simulations for the design sea state. Response motion simulations are performed for each wave spectrum corresponding to a significant wave height and peak period combination. In total a range of 29 peak periods are considered and therefore simulations for 29 wave spectra are performed. Besides, for each wave spectrum the simulations are performed for intermediate wave angles in steps of 15°. The output of the time domain simulations are response motion time series from which the Most Probable Extreme (MPE) response motions of the vessel are calculated for all simulations with the formula for narrow-banded processes [17]:

$$\text{MPE} = \sqrt{2 \cdot m_0 \cdot \ln(n)} \tag{2.1}$$

where the zeroth spectral moment of the responses is given by m_0 and the number of response maxima n are given by:

$$n = \frac{t_e}{T_z} \tag{2.2}$$

with the zero up-crossing period T_z and the exposure time t_e which is equal to three hours.

After the MPE accelerations of each motion are calculated for all simulation corresponding to a specific wave spectrum and wave heading angle, the maximum MPE accelerations for each motion are obtained from all these MPE accelerations. For each motion the maximum MPE acceleration is given in Table 2.5 together with the corresponding wave spectrum parameters and the wave heading angles for which the maximum MPE is expected.

Table 2.5: Maximum MPE accelerations with corresponding sea state parameters and wave heading angle

Motion	Symbol	MPE [deg/s^2]	MPE [m/s^2]	H_s [m]	T_p [s]	Wave angle [°]
Surge	a_x	-	?	?	10.5	195
Sway	a_y	-	?	?	12.0	75
Heave	a_z	-	?	?	8.5	255
Roll	r_x	?	-	?	12.5	270
Pitch	r_y	?	-	?	9.5	150
Yaw	r_z	?	-	?	8.0	240

In section 2.4 these maximum MPE accelerations are used to calculate the inertia loads acting on the jacket. In this section it is also described how these loads are be combined by defining different load cases. From Table 2.5 it can be seen already that combining these maximum MPE accelerations is physically not realistic because:

- The maximum MPE acceleration of each motion is expected for different peak periods and therefore for different wave spectra
- The maximum MPE acceleration of each motion is expected for different wave heading angles
- Besides, a MPE is a statistical value based on the three hour simulation output. It gives information on the extreme value of the motions only and not on which moment in time this extreme happens during the simulation. By combining the maximum MPE accelerations it is assumed that these happen at the same moment in time.

2.3. Wind loading

The wind loading on the jacket is calculated based on what is prescribed in DNVGL-RP-C205 [5]. In this guideline is stated that wind induced loads are in general time dependent loads due to fluctuations in the wind velocity. For open structures such as a jacket the wind loads act on both the primary wind exposed surfaces as well as on the secondary wind exposed surfaces. In Figure 2.8 it is shown how the total wind exposed surface A_w normal to the wind velocity is determined by the superposition of the primary exposed surface and the secondary exposed surface. The wind exposed surfaces normal to the wind direction can easily be determined from a 3D model of the jacket in most software.

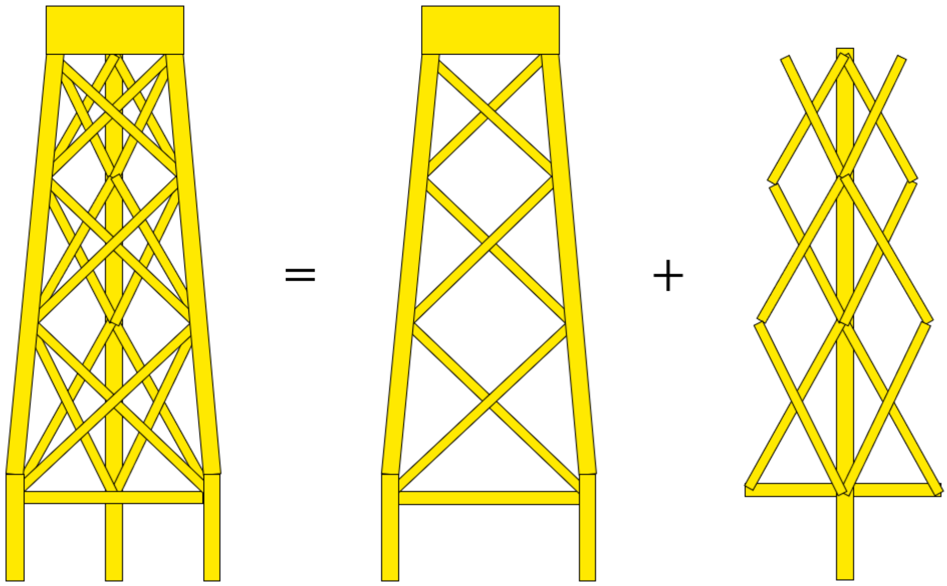

Figure 2.8: Illustration of the superposition of the primary and secondary wind exposed surfaces

The wind profile is not constant over height and therefore the height of the structure should be taken into account to determine the design wind velocity. Therefore, often a reference height of the wind velocity is given together with the design wind velocity. In the guideline it is mentioned that the response to wind loading has a static part and a resonant part due to wind excitations close to the natural frequencies of the structure. When the wind field contains frequencies close to the natural frequencies of the structure a dynamic analysis using a wind frequency should be carried out. In this case study the wind loading is assumed to be a static loading only for which the basic wind pressure is calculated with:

$$q = \frac{1}{2} \cdot \rho_{air} \cdot U_w^2 \tag{2.3}$$

The wind force F_w on the jacket structure can now be calculated with:

$$F_w = C \cdot q \cdot A_w \tag{2.4}$$

Where C is the shape coefficient of the tubular members out of which the jacket is constructed. The shape coefficient is determined to be $C = 1.05$ for the members of the jacket.

2.4. Load Case Determination (LCD)

Loads acting on the jacket

As the jacket is to be supported by the sea fastening, part of the reaction loads are caused by the self weight of the jacket. To obtain the maximum design weight an initial guess of the sea fastening weight is made and added to the maximum weight of the jacket given in the weight report. In DNV-ST-N001 [6] it is prescribed that conservative weight values should be used for calculation purposes. Once the expected sea fastening weight is added to the jacket weight a weight contingency factor $\gamma_{wc} = 1.10$ is applied to this total design weight. The weight contingency factor which is given in the guideline holds for structures which are not to be weighed and which are not weight and CoG critical. Besides, a CoG inaccuracy factor $\gamma_{CoG} = 1.05$ is recommended. This factor is to be applied to the height of the jacket CoG which is likely to result is higher reaction loads on the sea fastening.

Besides the static weight of the jacket the motions of the vessel containing the jacket cause inertia loads of the jacket. These inertia loads are calculated for all DoFs except for yaw motion. The inertia forces due to translational motions are calculated by multiplication of the jacket weight with the translational accelerations of the jacket CoG. The inertia moments due to the rotational motions are obtained by multiplication of the jacket moments of inertia with the rotational accelerations of the jacket CoG. As jackets are complex structures the moments of inertia I_{xx} and I_{yy} around the CoG of the jacket can best be extracted from 3D models to give accurate results. The calculation of the inertia loads is summarized in the following equations:

$$\begin{aligned} F_{surge} &= W_{jacket} \cdot a_x \\ F_{sway} &= W_{jacket} \cdot a_y \\ F_{heave} &= W_{jacket} \cdot a_z \\ M_{roll} &= I_{xx} \cdot r_x \\ M_{pitch} &= I_{yy} \cdot r_y \end{aligned} \tag{2.5}$$

As described in section 2.3, also wind loads are acting on the jacket. Although the wind loading and inertia loading are distributed loads on the jacket, both load types are assumed to be acting on the CoG of the jacket for calculation purposes.

Load combinations

Different load cases can be defined to combine the loads which are acting on the jacket. The static weight load is always present but the different inertia loads due to motions are expected to be more severe for specific wave directions. Load cases for head waves, following waves, beam waves from both directions and quartering waves from four directions are considered. The wind direction is assumed to be in the same direction as the waves as this results in the highest reaction loads. Besides, in DNV-RP-C205 [5] it is stated that for wind generated seas it is often a good approximation to assume that wind and waves have the same direction.

In every load case the vertical static weight and heave force are combined with the horizontal loads which are governing for a given wave direction. Load cases LC1 and LC2 consider beam waves and therefore besides the vertical loads the sway force, the roll moment and wind loading in Y-direction are acting on the jacket CoG. Head and following waves are considered in load cases LC3 and LC4 and next to the vertical loads the surge force, pitch moment and wind loading in X-direction are acting on the jacket. In load cases LC5, LC6, LC7 and LC8 quartering waves are considered. The horizontal loads for the quartering wave load cases are assumed to be comprised of 80% of the sway force, roll moment and wind load in Y-direction and of 60% of the surge force, pitch moment and wind load in X-direction. In DNV-ST-N001 [6] it is described that motions in quartering seas can be described by combining 60% of transverse accelerations and 60% of longitudinal accelerations. However, to be conservative the transverse accelerations are accounted for by 80% as these wave-induced loads are governing for most vessels.

Table 2.6: Considered load cases for compressive vertical reaction loads

Load case	Combination of loads	Wave angle
LC1	Static weight + Heave + Sway - Roll + Wind-Y	90°
LC2	Static weight + Heave - Sway + Roll - Wind-Y	270°
LC3	Static weight + Heave + Surge + Pitch + Wind-X	0°
LC4	Static weight + Heave - Surge - Pitch - Wind-X	180°
LC5	Static weight + Heave + $0.8\cdot$ (Sway - Roll + Wind-Y) + $0.6\cdot$ (Surge + Pitch + Wind-X)	45°
LC6	Static weight + Heave - $0.8\cdot$ (Sway - Roll + Wind-Y) + $0.6\cdot$ (Surge + Pitch + Wind-X)	315°
LC7	Static weight + Heave + $0.8\cdot$ (Sway - Roll + Wind-Y) - $0.6\cdot$ (Surge + Pitch + Wind-X)	135°
LC8	Static weight + Heave - $0.8\cdot$ (Sway - Roll + Wind-Y) - $0.6\cdot$ (Surge + Pitch + Wind-X)	225°

Load cases LC1 to LC8 are chosen such that these load cases result in the maximum compressive vertical reaction loads on the sea fastening. The combination of loads is chosen such that all loads contribute to the maximum compressive load in a governing leg of the jacket. Besides the eight load cases to calculate the maximum compressive reaction loads in one of the jacket legs, load cases LC9 to LC16 are introduced to calculate the maximum tensile loads (if present) on the sea fastening. The directions of the loads are combined such that they all contribute to the maximum tensile load for a governing jacket leg. Conservatively, in DNV-ST-N-001 [6] it is prescribed that uplift restraints should be accounted for in the sea fastening design when the overturning moment of the jacket is greater than the restoring moment due to gravity which is reduced by 15%. Therefore, a factor of 0.85 is applied to the static weight in these load cases. Negative vertical reaction forces obtained with these load cases are an indication for tensile forces in the sea fastening which means that the sea fastening should be designed to constrain uplift forces of this magnitude.

Table 2.7: Considered uplift load cases

Load case	Combination of loads	Wave angle
LC9	$0.85\cdot$ Static weight - Heave + Sway - Roll + Wind-Y	90°
LC10	$0.85\cdot$ Static weight - Heave - Sway + Roll - Wind-Y	270°
LC11	$0.85\cdot$ Static weight - Heave + Surge + Pitch + Wind-X	0°
LC12	$0.85\cdot$ Static weight - Heave - Surge - Pitch - Wind-X	180°
LC13	$0.85\cdot$ Static weight - Heave + $0.8\cdot$ (Sway - Roll + Wind-Y) + $0.6\cdot$ (Surge + Pitch + Wind-X)	45°
LC14	$0.85\cdot$ Static weight - Heave - $0.8\cdot$ (Sway - Roll + Wind-Y) + $0.6\cdot$ (Surge + Pitch + Wind-X)	315°
LC15	$0.85\cdot$ Static weight - Heave + $0.8\cdot$ (Sway - Roll + Wind-Y) - $0.6\cdot$ (Surge + Pitch + Wind-X)	135°
LC16	$0.85\cdot$ Static weight - Heave - $0.8\cdot$ (Sway - Roll + Wind-Y) - $0.6\cdot$ (Surge + Pitch + Wind-X)	225°

It should be noted that although the load cases described in this section are commonly applied in practice, the choice of load cases may differ as they often depend on client or project requirements. The choice of load cases might also depend on whether it is desired to know the exact reaction loads for fatigue analysis for example or whether it is preferred to use more conservative values of the reaction loads as is often the case in the early design phase of for example the sea fastening.

2.5. Structural analysis of jacket

The reaction loads on the sea fastening can be determined by performing a structural analysis of the jacket. In a structural analysis the relationships between the external loads acting on the jacket and the internal stresses and deformations that occur in the members of the structure are to be established. Besides, the support reactions in the supports of the jacket should be obtained. The load cases considered in the previous section describe which external loads are acting on the jacket. The structural analysis is to be performed for all load cases. As a jacket is a complex structure and multiple load cases are considered, it is therefore more convenient to use a numerical method rather than a analytic method to perform the structural analysis of a jacket.

Finite Element Method (FEM) analysis of the jacket

The FEM method is a numerical method which can be used to calculate displacements, stresses and strains in structures when external loads are applied. The FEM method discretizes continuous geometries into a collection of finite elements. For each finite element a system of algebraic equations can be formulated to solve a boundary value problem. By combining the system of equations of each element a large set of equations is constructed which can often only be solved with the help of computers. The jacket is analyzed with the static second-order P-delta analysis. This analysis accounts for second-order effects that can result in higher stresses and deflections in the jacket. P-delta effects are caused by deformations due to axial loads on slender structures or members in a structure. P-delta effects occur both on member level as well as on the level of the overall structure.

The FEM model of the jacket is taken from the example project in the company. The FEM model of the jackets consists of nodes and finite 1D-elements. The 1D-elements represent the members of the jacket and for each element the geometric and material properties are specified. In Figure 2.9 two different views of the FEM model of the jacket are shown. In Figure 2.9a it can be seen that the FEM model is built up by nodes and 1D-elements. The red dots represent the nodes and the colored lines represent the 1D-elements. In Figure 2.9b the geometries of the members are visualized. In both figures it can be seen that groups of 1D-elements and members with equal geometries are categorized by color.

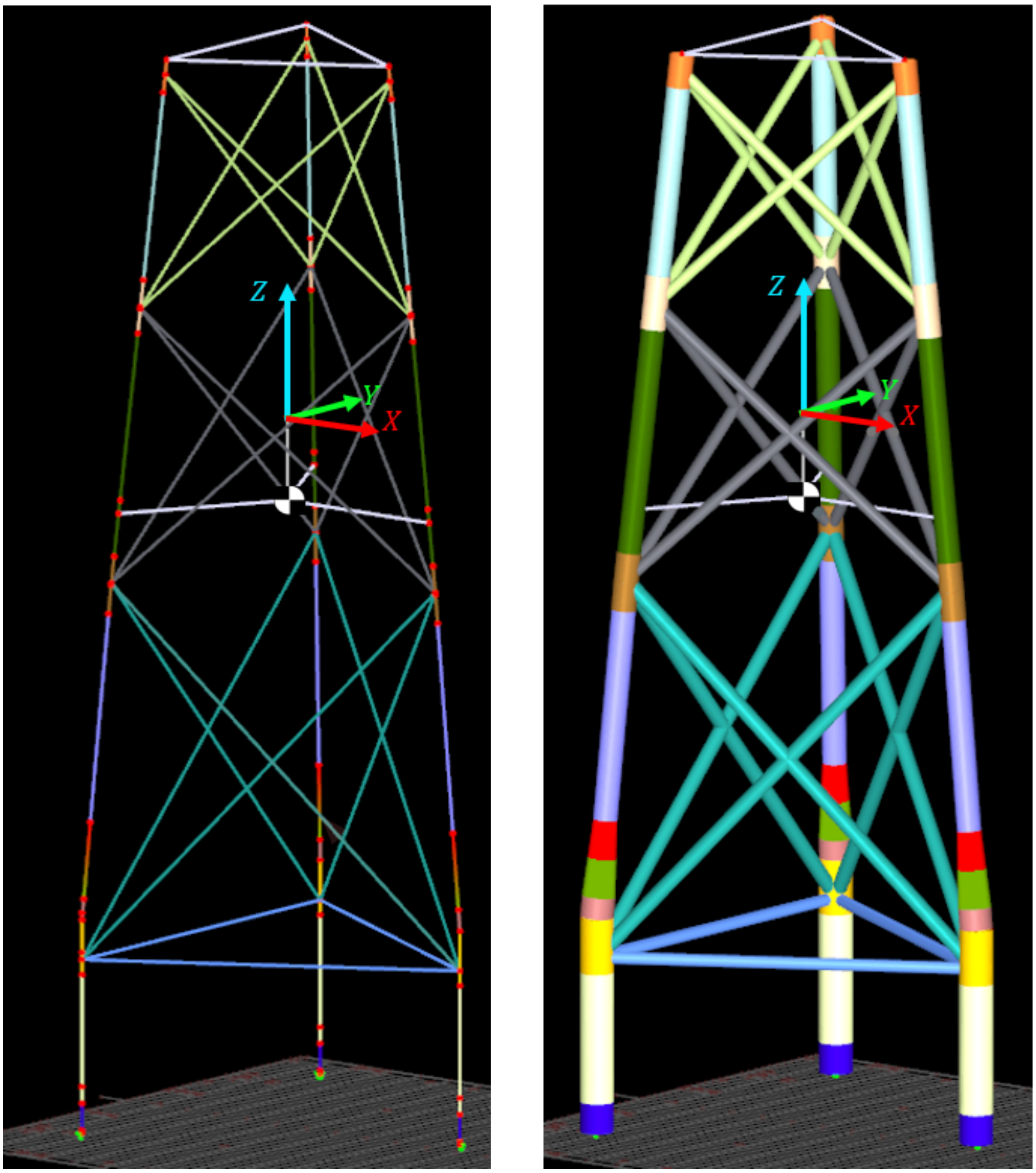

(a) Nodes and 1D-elements of FEM model

(b) Visualization of member geometries

Figure 2.9: FEM model of jacket in which groups of members with equal geometries are given the same color

As mentioned in the previous section it is assumed that all loads are acting on the CoG of the jacket. In Figure 2.10 a close up of the jacket local coordinate system and CoG is shown. As the CoG is a floating point in space, rigid dummy elements are introduced which transfer the loads on the CoG to three nodes on the jacket legs. In the figure the rigid dummy elements are represented by the white lines. On the top of the jacket three more rigid dummy elements have been introduced as can be seen in Figure 2.11. These rigid elements represent a triangular platform supporting the OWT which can be assumed very stiff relative to the jacket structure.

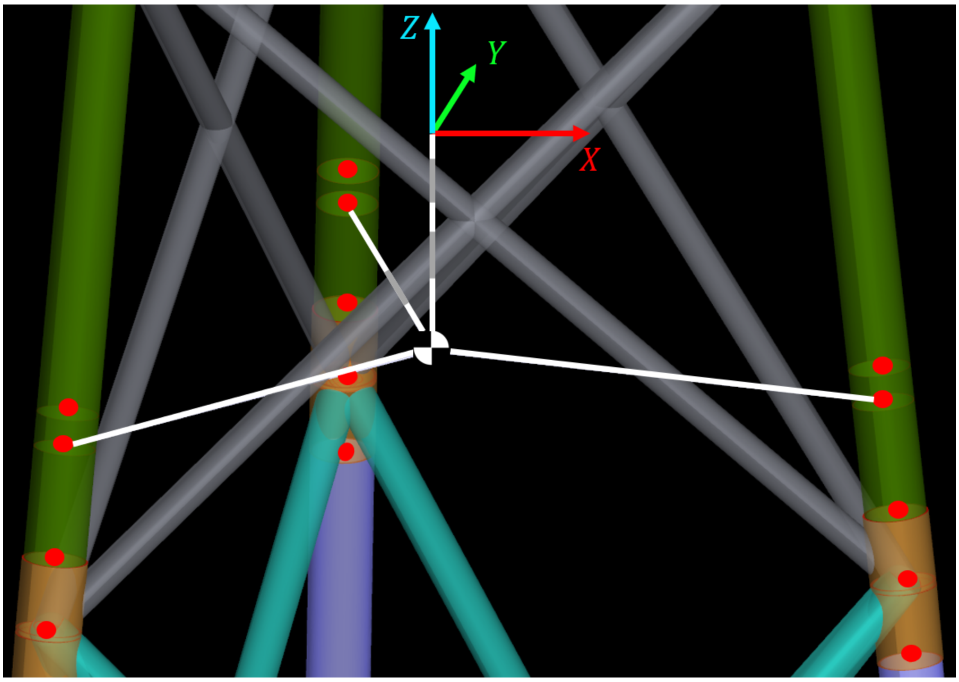

Figure 2.10: Rigid dummy elements connecting the CoG with three nodes on the jacket legs

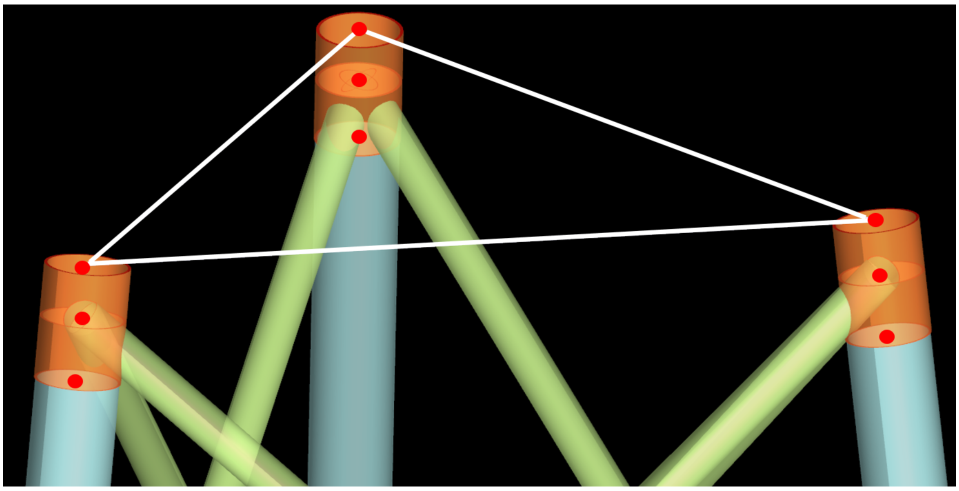

Figure 2.11: Rigid dummy elements at top of the jacket

During a transport the jacket is sea fastened to the deck of the vessel to constrain the undesired motions of the jacket relative to the vessel. Sea fastening structures often consist of beams or box girders which are secured to the deck by wing plates, stoppers or braces. The bottom members of the jacket legs are assumed to be rigidly connected to the sea fastening. The sea fastening structure and the deck of the vessel are not completely rigid and will therefore deform when reaction loads are applied on the sea fastening. The stiffness of the vessel deck and the sea fastening of the jacket can be modeled by spring supports in the FEM model. As the bottom members of the jacket legs are assumed to be rigidly connected to the sea fastening structure the spring supports are applied at the lower nodes of these bottom supports as can be seen in Figure 2.12.

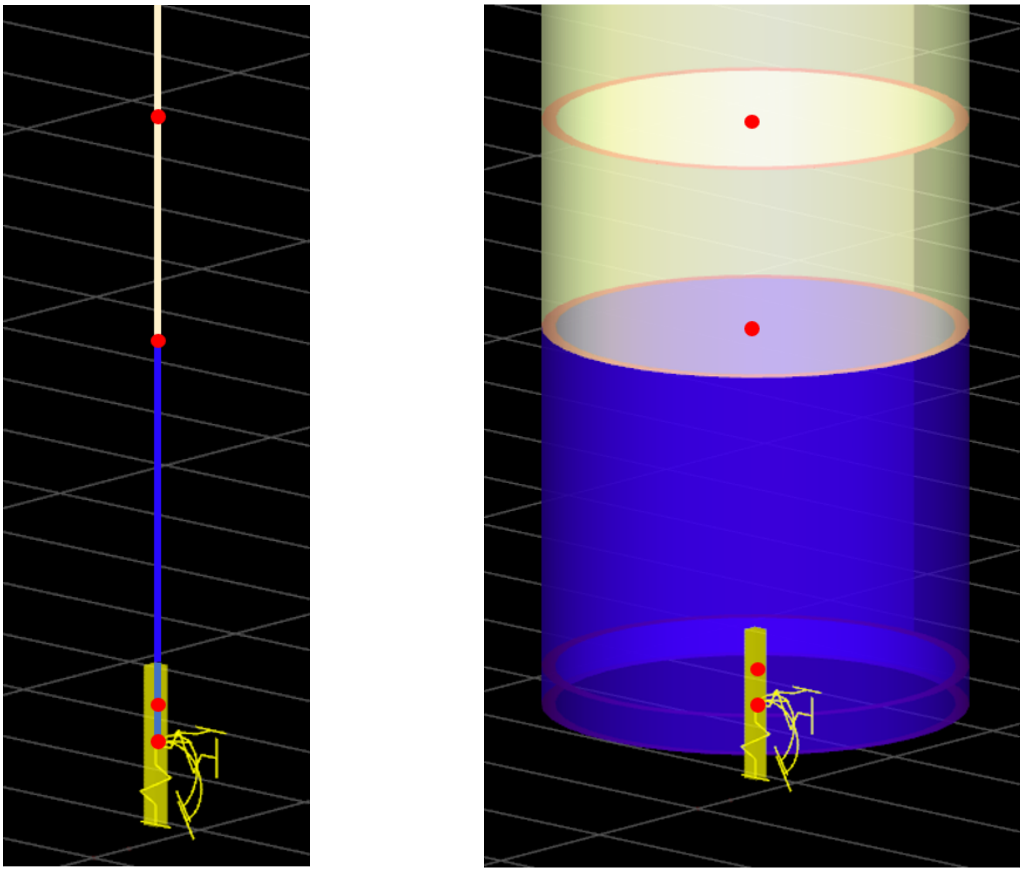

(a) (b)

Figure 2.12: In the FEM model the jacket is supported by spring supports which model the combined stiffness of the sea fastening structure and vessel deck

The relative stiffness of the supports depends how the reaction loads are distributed over the supports of the three legs. It is therefore essential to know the combined stiffness of the vessel deck and sea fastening when performing a structural analysis of the jacket. Besides the FEM model of the jacket, also the sea fastening design of each jacket leg and the corresponding stiffnesses are taken from the example project in the company. The combined stiffnesses of the vessel deck and the sea fastening design are specified in Table 2.8 for each jacket leg.

Table 2.8: Combined stiffnesses of the vessel deck and the sea fastening design specified for each jacket leg

Support legs	k_x [MN/m]	k_y [MN/m]	k_z [MN/m]	φ_x [MNm/rad]	φ_y [MNm/rad]	φ_z [MNm/rad]
B, C	?	?	?	?	?	?
A	?	?	?	?	?	?

As mentioned previously it is desired to perform the structural analysis of the jacket numerically as the analysis is to be performed for all load cases presented in the previous section. With the FEM software results are obtained for every load case and from all these results the governing results can be extracted.

2.6. Calculation of reaction loads with current method

In this section the reaction loads on the sea fastening will be calculated with the current calculation method which has been described in this chapter. The reaction loads will be calculated for the case study which is earlier defined in this chapter.

Motion analysis
The motion analysis of the vessel transporting the jackets is performed as described in section 2.2. Here it is also explained that the maximum MPE accelerations of the motions are used to calculate the inertia loads on the jacket CoG. The maximum MPE accelerations obtained with the motion analysis are given in Table 2.9.

Table 2.9: Maximum MPE accelerations obtained in motion analysis

Surge [m/s^2]	Sway [m/s^2]	Heave [m/s^2]	Roll [deg/s^2]	Pitch [deg/s^2]	Yaw [deg/s^2]
?	?	?	?	?	?

Loads and load cases
In Table 2.10 some additional properties of the considered jacket are given. As explained before a weight contingency factor $\gamma_{wc} =$ 1.10 is applied to the mass of the jacket to calculate the jacket weight. The moments of inertia of the jacket around both the $X-$axis and $Y-$axis are obtained from the model of the jacket in 3D software.

Table 2.10: Input for calculating the inertia loads on the jacket

	Symbol	Formula	Value	Unit
Maximum design mass	$m =$		?	tonne
Weight contingency factor	$\gamma_{wc} =$		1.10	
Factored design mass	$m_{jacket} =$	$m \cdot \gamma_{wc} =$	?	tonne
Gravitational acceleration	$g =$		9.81	m/s^2
Moment of inertia around $X-$axis	$I_{xx} =$		?	m$^2\cdot$ tonne
Moment of inertia around $Y-$axis	$I_{yy} =$		?	m$^2\cdot$ tonne

With the jacket properties of given in Table 2.10 the static weight and the inertia loads acting on the jacket CoG are calculated in Table 2.11.

Table 2.11: Calculation of static weight and inertia loads acting on jacket

	Symbol	Formula	Value	Unit
Static weight	$W_{jacket} =$	$m_{jacket} \cdot g =$	?	kN
Surge force	$F_{surge} =$	$m_{jacket} \cdot a_x =$	?	kN
Sway force	$F_{sway} =$	$m_{jacket} \cdot a_y =$	?	kN
Heave force	$F_{heave} =$	$m_{jacket} \cdot a_z =$	?	kN
Roll moment	$M_{roll} =$	$I_{xx} \cdot r_x =$	?	kN $\cdot$ m
Pitch moment	$M_{pitch} =$	$I_{yy} \cdot r_y =$	?	kN $\cdot$ m

The wind loading is calculated as explained in section 2.3. First the wind exposed area is determined from the jacket model with 3D software. The wind exposed area of the jacket is assumed to be equal for all wind directions. The total wind exposed area obtained with software is $A_w =$?m^2. The static wind force acting on the jacket is calculated in Table 2.12.

Table 2.12: Calculation of static wind force acting on the jacket

	Symbol	Formula	Value	Unit
Design wind speed	$U_w =$		?	m/s
Air density	$\rho_{air} =$		?	kg/m^3
Shape coefficient	$C =$		?	
Wind exposed area	$A_w =$		?	m^2
Wind pressure	$q =$	$0.5 \cdot \rho_{air} \cdot U_w^2 =$	?	N/m ^{2}
Wind force	$F_w =$	$C \cdot q \cdot A_w =$	?	kN

Now that all loads acting on the jacket have been calculated in Table 2.11 and Table 2.12, the loads and considered load cases can be implemented in the FEM model. In Figure 2.13 a graphical example is given of the combination of loads of LC1 acting on the jacket CoG in the FEM software. The units of the forces are kN and the unit of the moment is kN·m. It should be noted that the static self weight of the jacket is accounted for in the properties of the members and therefore no additional force is applied on the jacket CoG.

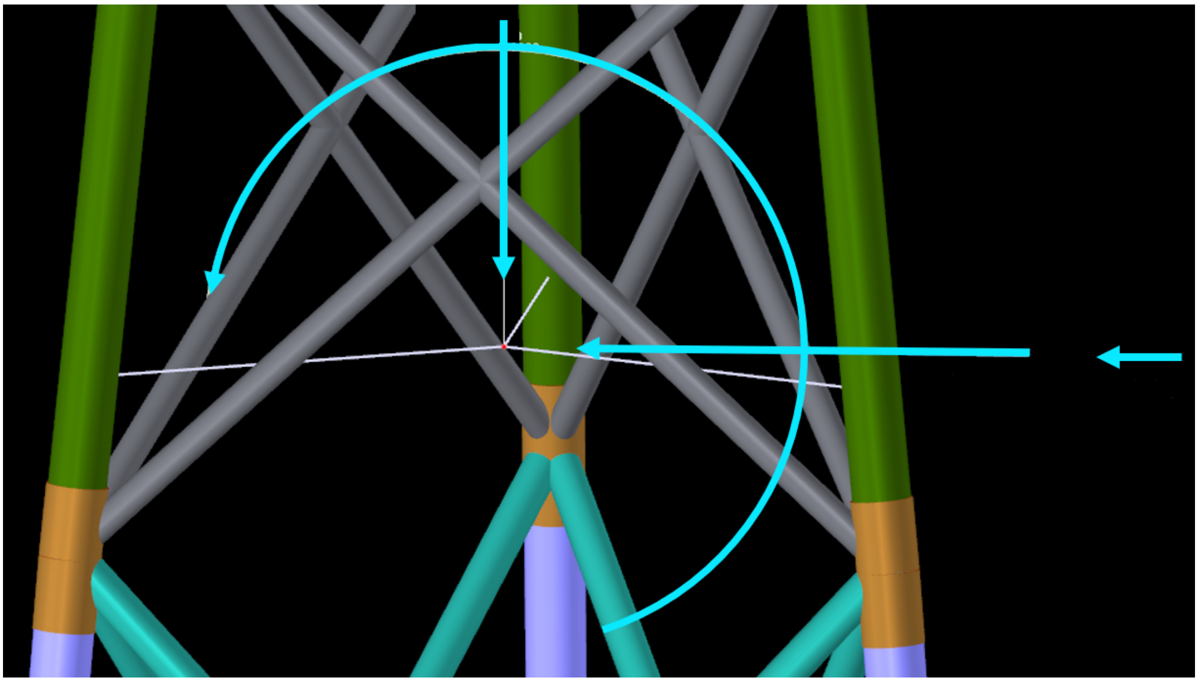

Figure 2.13: The combination of loads for LC1 applied on the jacket CoG in the FEM software

Results structural analysis of jacket

With the structural FEM analysis of the jacket the reaction loads on each leg are obtained for all the load cases. For the design of the sea fastening and the structural integrity check of this design the governing minimum and maximum reaction loads are most interesting. The resulting governing loads for legs A, B and C are given in Table 2.13, Table 2.14 and Table 2.15 respectively. More information on which load cases cause the governing loads for each leg and what the corresponding other loads are for this load case is given in Appendix A. In the following tables the maximum and minimum forces and moments in the supports of all legs are given. These are the governing maximum and minimum values out of all considered load cases. It should be noted that positive values of F_z are associated with compressive forces in the sea fastening and that negative values represent tensional forces which would result in uplift when this motion would not be constraint by the sea fastening.

Table 2.13: Governing reaction loads jacket leg A

	F_x [kN]	F_y [kN]	F_z [kN]	M_x [kNm]	M_y [kNm]	M_z [kNm]
Max.	?	?	?	?	?	?
Min.	?	?	?	?	?	?

Table 2.14: Governing reaction loads jacket leg B

	F_x [kN]	F_y [kN]	F_z [kN]	M_x [kNm]	M_y [kNm]	M_z [kNm]
Max.	?	?	?	?	?	?
Min.	?	?	?	?	?	?

Table 2.15: Governing reaction loads jacket leg C

	F_x [kN]	F_y [kN]	F_z [kN]	M_x [kNm]	M_y [kNm]	M_z [kNm]
Max.	?	?	?	?	?	?
Min.	?	?	?	?	?	?

Besides the support reaction loads, additional results can be obtained from the structural FEM analysis of the jacket such as deflections and stresses in all members of the jacket. Since the focus of this thesis is on the design of the sea fastening and not on the structural integrity of the jacket these results are not provided in this thesis.

3
Uncertainties in current calculation method

In the previous chapter the current calculation method has been described and some of the uncertainties of this method have been identified. In this chapter some of the main uncertainties will be described in more detail to be able to understand what impact they might have on the reaction loads calculated with the current calculation method. In addition, by improving understanding of the main uncertainties it can be assessed whether mitigating these uncertainties would be beneficial for the optimization of the reaction load calculation.

3.1. Uncertainty classification

In the calculation process of the reaction loads on the sea fastening there exist many sources of uncertainty. In most literature uncertainties are categorized as epistemic or aleatory uncertainties. In [10] it is claimed that the categorization of an uncertainty being either epistemic or aleatory is a pragmatic choice which depends on the purpose of the application. It is mentioned that the nature of an uncertainty and how the uncertainty should be dealt with depends on the content and application as an uncertainty might be aleatory in one model while the uncertainty might be epistemic in another model. Furthermore, according to [10] the distinction between epistemic and aleatory uncertainty can be defined as:

- **Epistemic uncertainties** - uncertainties that can be reduced by gathering more data or by refining models.
- **Aleatory uncertainties** - uncertainties that cannot be reduced.

By using this definition to categorize the sources of uncertainty in the calculation process it is clear which uncertainties could be reduced and which not. In most models and applications both types of uncertainty are present which is also the case in this thesis. Often the types of uncertainty are combined as for example input data which contains aleatory uncertainty is inserted into a model which contains epistemic uncertainty.

Uncertainties related to human errors
Besides epistemic and aleatory uncertainties, an additional category of uncertainties caused by human errors and omission is introduced in [15]. These uncertainties could for example be related to:

- Planning of the transport
- Choice or design of equipment
- Fabrication of jacket and sea fastening
- Execution of the transport

In [15] it is stated that uncertainties caused by human errors should not be accounted for by design factors. Other measures are proposed to reduce uncertainties caused by human errors such as quality assurance and quality control during design, fabrication and execution. Besides, methods for risk reduction during the planning of the transport can be applied and adequate training of personnel can reduce operational uncertainties. The focus of this thesis is on the calculation method and therefore uncertainties due to human factors are not in the scope of this thesis.

Types of uncertainty
In DNV-CN-30.6 [1] four different types of uncertainty are presented in which most sources of uncertainty can be subdivided. It should be noted that besides these four types there may also exist other types of uncertainty. The four types of uncertainty which are described in DNV-CN-30.6 [1] are:

- **Physical uncertainty** - is also known as intrinsic or inherent uncertainty. This type of uncertainty is caused by the natural randomness of quantities [1]. Given examples of physical uncertainties are uncertainties in yield strength of steel caused by production variability, variation in physical dimensions of structural components or variability in wave and wind loading. This type of uncertainty might be reduced with greater availability of data or in some cases by performing better quality control but in most cases this uncertainty cannot be eliminated [13]. It is also mentioned that generally the physical uncertainty for basic variables is not known a priori and must be estimated from observations of the variable or assessed subjectively. This type of uncertainty can be categorized as aleatory uncertainty.
- **Measurement uncertainty** - is caused by imperfect instruments and sample disturbances when observing a quantity by measuring equipment [1]. Precision errors can be reduced by improving the precision of a measurement instrument or by increasing the sample size whereas systematic measurement errors can be reduced by using more accurate calibration data or by using multiple measurement techniques or instruments.
- **Statistical uncertainty** - is uncertainty caused by limited information to statistically describe variables [1]. From available data, statistical estimators like the sample mean or higher moments can be determined which can be used to suggest a probability density function (PDF) representing a variable [13]. This introduces statistical uncertainty as observations do often not perfectly represent the variable and different sample data sets usually produce different statistical estimators. Statistical uncertainty can be mitigated by for example increasing the data sample size or increasing the data quality.
- **Model uncertainty** - is due to the use of one or more simplified relationships and assumptions between basic variables which represent the physical behaviour of the phenomenon [13]. It is mentioned that modelling uncertainty is often due to a lack of knowledge and can be reduced with research or increased availability of data. Therefore, this type of uncertainty is typically categorized as an epistemic uncertainty.

3.2. Uncertainties in environmental conditions

Uncertainties in environmental conditions have a significant impact on the reliability level of a sea transport operation as the reaction loads on the sea fastening are mostly caused by environmental loads. In DNV-ST-N001 [6] it prescribed how the environmental uncertainties could be accounted for when planning for a marine operation. The duration of marine operations is an important aspect in the planning process. In DNV-ST-N001 [6] an operation reference period T_R is introduced which is given by:

$$T_R = T_{POP} + T_C \tag{3.1}$$

Where T_{POP} is the planned operation period and T_C is the estimated maximum contingency time. The planned operation period is to be determined based on a detailed schedule of the operation. An estimated maximum contingency time T_C of 50 to 100% of the planned operation period T_{POP} is accepted according to DNV-ST-N001 [6] depending on the level of planning of the operation. Marine operations are categorized as either weather-restricted or weather-unrestricted operations based on their operation reference period T_R.

Weather-restricted operations
In DNV-ST-N001 an operation is defined as weather-restricted when it has a reference period $T_R < 96$ hours and a planned operation time $T_{POP} < 72$ hours. These operations should be planned to be executed within a reliable weather window. The design environmental conditions may be selected by the

owner, operator or contractor independent of statistical data but it should be noted that these conditions should be chosen selected based on an acceptable probability of obtaining the required weather window. If this probability is too low it is expected that this would results in waiting on weather which delays the operation. Operations which have a duration which is too long to consider a weather-restricted operation, may still be defined as weather-restricted operations on conditions given in DNV-ST-N001 [6]. During these operations continuous surveillance of actual and forecasted weather conditions should be implemented and it should be possible for the operation to be halted and brought into safe conditions within the maximum allowable period for a weather-restricted operation.

To account for uncertainty in monitoring and forecasting of the environmental conditions the alpha factor α is introduced. As the forecasted operational criteria OP_{WF} must be less than the operational limiting criteria OP_{LIM} used in the design of the operation, the alpha parameter $\alpha \leq 1$ is applied to the design operational criteria:

$$\text{OP}_{\text{WF}} = \alpha \cdot \text{OP}_{\text{LIM}} \tag{3.2}$$

The alpha factor depends on the duration of the operation and the level of forecasting or monitoring of the environmental conditions. The alpha factor for waves is also dependent on significant wave height H_s. In DNV-ST-N001 [6] tables are presented which contain alpha factors for wind and waves for operations which have different duration and operational limits.

Weather-unrestricted operations
Marine operation which cannot be defined as weather restricted operations due to their duration shall be defined as weather-unrestricted operations according to DNV-ST-N001 [6]. These operations are not planned based on weather forecasts because the duration of these operations are longer than the period for which a weather forecast is considered reliable. The environmental criteria for these operations should instead be based on extreme value statistics. It is mentioned that when the design environmental conditions for an operation are based on extreme value statistics, the operation could theoretically be performed with acceptable risk without considering the weather forecast. However, for most weather-unrestricted operations start criteria are defined as it is not desired to start an operation in extreme weather conditions. The uncertainty in the environmental criteria of this type of operations is dependent on the amount and quality of the environmental data, the duration of the operation, the season of the year and the geographical area.

3.3. Uncertainties in motion analysis

In section 2.2 it is explained how the current motion response analysis of the vessel is performed. In this section it is elaborated in more detail how non-linear effects are accounted for in the linear motion analysis.

3.3.1. Uncertainty in implementing non-linear viscous effects

As described in section 2.2 radiation-diffraction software based on potential theory is used to determine the response behaviour of the vessel to regular waves of different frequencies. The radiation diffraction analysis is performed for a forward speed of 7kn. The obtained frequency behaviour of the vessel is stored in the complex response functions. With a linear frequency-domain calculation the spectra of the wave induced vessel motions can be calculated from the wave spectra and the complex response functions. However, in many cases the linear assumption is not valid because of non-linear viscous damping, second order wave loads on horizontally restrained structures or loads caused by currents and wind [9]. For non-linear systems the frequency domain approach which is based on the superposition of regular waves is not applicable. Alternatively, to account for non-linear effects time-domain simulations can be performed to solve the equations of motions as a function of time.

The current motion analysis is performed as a linear analysis in the time-domain. It should be noted that in the current motion analysis time-domain simulations are performed only for the purpose of obtaining response time series and not to account for time dependent non-linear effects.

Potential damping effects which are calculated with radiation-diffraction software are often adequate to describe the motion of vessels in surge, sway, heave, pitch and yaw motion [2]. However, viscous damping effects can be significant for the roll motion of many vessel types. Depending on the vessel type, the viscous roll damping might be relatively high compared to potential roll damping [9]. In Figure 3.1 it can be seen that potential wave roll damping is minimal for vessel types with a breadth to draught ratio of the cross section of about 2.5. For vessels with breadth-draught ratios in this range viscous roll damping is expected to be significant relative to the potential roll damping. Potential roll damping increases for vessels with very low and very high breadth-draught ratios. Even for vessel types with cross sections like these, viscous roll damping might still be relatively high due to the presence of bilge keels for example.

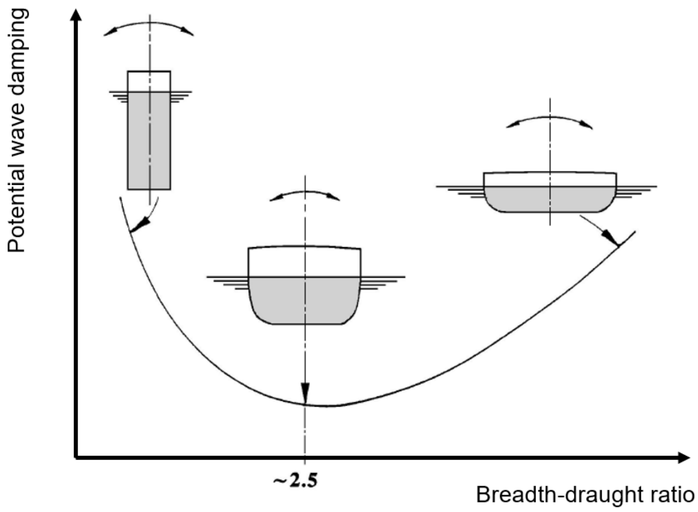

Figure 3.1: Potential wave roll damping as a function of breadth-draught ratio of the vessel cross section, taken from [9]

For this reason, viscous non-linear roll damping effects are not neglected in the current motion analysis. Instead the method described in [2] is used in which the non-linear damping term in the equations of motion of the vessel is replaced by an equivalent linear damping term. The equation of motion for roll is given by:

$$I\ddot{\phi} + B(\dot{\phi})\dot{\phi} + C(\phi, t) = M \cdot \cos(\omega t) \tag{3.3}$$

Where the damping term B is given by:

$$B(\dot{\phi}) = B_1\dot{\phi} + B_2|\dot{\phi}|\dot{\phi} + B_3\phi^3 \tag{3.4}$$

Besides first term which is linear, the second term is quadratic and the third term is cubic. When this non-linear damping term is replaced by an equivalent linear damping term the damping is given by:

$$B(\dot{\phi}) = B_{\mathrm{eq}}\dot{\phi} \tag{3.5}$$

The idea behind the equivalent linear damping coefficient is that the same amount of energy is dissipated from the system by the linear roll damping coefficient as by the non-linear damping coefficient. As the roll damping has multiple contributions, the equivalent linear damping coefficient given in [2] consists of multiple components:

$$B_{\mathrm{eq}} = B_{\mathrm{f}} + B_{\mathrm{e}} + B_{\mathrm{w}} + B_{\mathrm{L}} + B_{\mathrm{BK}} \tag{3.6}$$

The different components represent skin friction of the hull, eddy making damping, free surface waves damping, lift damping and bilge keel damping. It is mentioned that due to hydrodynamic interaction between the different components, this subdivision of the roll damping may not be justifiable hydrodynamically. However, the subdivision allows to determine the damping of the individual components analytically and experimentally. In [2] linear empirical formulas for the different components are presented which are mostly obtained by Ikeda from a series of model experiments. The formulas are presented for both zero forward speed cases as well as cases of forward speed.

In the motion analysis for this example project, first a radiation-diffraction analysis of the vessel is performed for a forward speed of 7kn. With this analysis the complex response functions based on potential theory are obtained. Thereafter, an equivalent roll-damping coefficient is determined to account for viscous non-linear effects. To determine the equivalent roll damping coefficient the following components from Equation 3.6 are considered: eddy making damping B_e, wave damping B_w and lift damping B_L.

According to [2], the initial potential wave roll damping coefficient obtained with the radiation-diffraction analysis for zero forward speed should be corrected to account for forward speed of the vessel. Even though in this case a radiation-diffraction analysis is performed for a forward vessel speed, the potential damping is still corrected. The potential damping is found to increase by a factor of 5 due to the forward speed of the vessel. This factor is calculated with the natural roll period of the vessel which is T_n = 12.6s, whereas for this given forward speed the highest wave damping coefficient is found for a roll period of T = 11.4s according to [2].

Subsequently, the non-linear viscous eddy damping component for zero forward speed B_{e0} is determined. The linearized eddy damping coefficient is given by a linear function of the roll angle and wave frequency. In the current motion analysis the eddy damping coefficient is calculated only for the wave heading angle and sea state combination for which the greatest roll motion is expected. An iterative calculation is performed which uses the natural roll frequency of the vessel and the significant roll angle obtained in simulations for beam waves described by a sea state that results in the highest roll motions.

In Figure 3.2 the iterative calculation of the linearized eddy damping coefficient is illustrated. A high significant roll angle corresponding to a simulation with only potential damping is used as a starting point. Since the significant roll angle is too high for the case with only potential damping, this roll angle will result in a eddy damping coefficient that is too high as well. However, when this high eddy damping coefficient is applied in a new simulation a lower significant roll angle will be obtained which in turn can be used to calculate a new eddy damping coefficient which will be lower. By repeating this process the equivalent eddy damping coefficient converges to a certain value. Once the eddy damping coefficient has been determined for the zero forward speed case, the converged coefficient should be corrected for forward speed. The eddy damping coefficient decreases with forward speed and for this specific motion analysis a factor of 0.3 is to be applied to the eddy damping coefficient for zero forward speed.

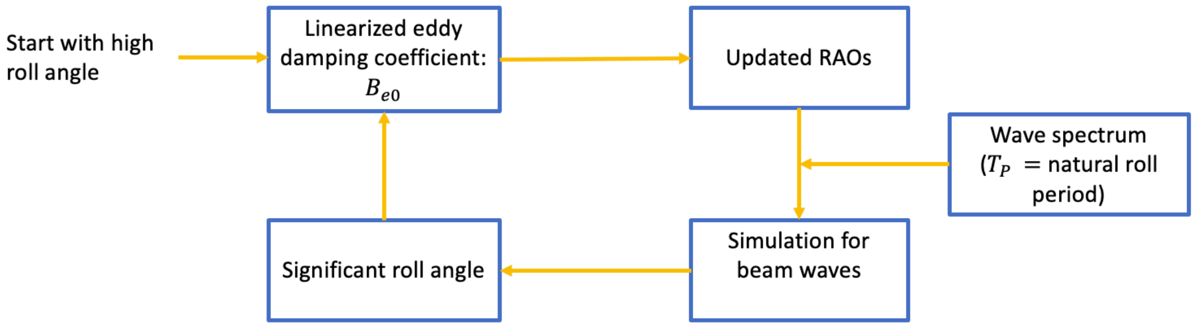

Figure 3.2: Illustration of iterative process of obtaining a linearized eddy damping coefficient

Due to the forward vessel speed also a lift damping component is introduced in the equivalent roll damping coefficient. This component can become significant for vessels with high forward speed [2]. In this case the contribution of the lift damping component to the equivalent damping coefficient is 8%, while the contribution of the wave damping component is 56% and for the eddy making damping component this is 36%.

Once the equivalent roll damping coefficient B_eq has been determined, the B_{44} coefficient in the original equation of motions of the vessel is replaced by this equivalent coefficient. From the updated equation of motions new complex response functions are determined containing the RAOs and phase angle information of the vessel. To illustrate the influence of applying additional roll damping, displacement RAOs of the vessel for beam waves with a wave heading angle of $\theta = 90°$ are presented in

Figure 3.3. In this figure the original RAOs based on potential damping only are presented together with the damped RAOs taking into consideration viscous damping effects. Since roll, sway and yaw are coupled motions, it can be seen that the damped RAOs for sway and yaw motion are also influenced by applying additional roll damping.

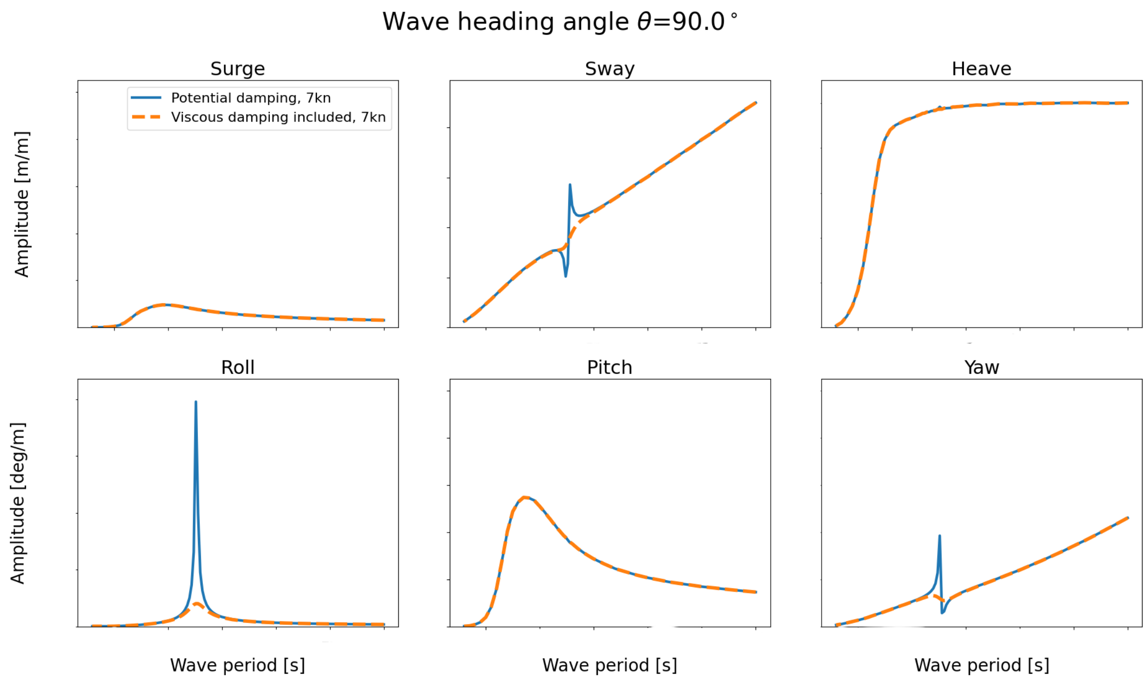

Figure 3.3: Displacement RAOs for 7kn forward speed for the potential damping only case and the case in which viscous roll damping is also included

As the eddy damping accounts for 36% of the equivalent roll damping, it is important to keep in mind that the equivalent roll damping is only calculated for the simulation in which the highest roll motion and therefore the highest eddy making damping is expected. However, in the current motion analysis the RAOs which are updated for this equivalent damping coefficient are used as input for the simulations for all sea states and all wave heading angles. As a result the roll, sway and yaw response motions for the other sea states and wave angles are expected to be underestimated because the maximum equivalent roll damping coefficient is used. This is especially important to keep in mind in case of zero or low forward speeds as the contribution of the eddy damping component to the equivalent roll damping coefficient will be governing. However, as mentioned the wave damping component has a maximum for a roll period T = 11.4s while the natural roll period T_n = 12.6s is used to calculate the contribution of this component. Since the wave damping component accounts for 56% of the equivalent damping coefficient, the motions for sea states described by a peak period in the range of T_p = 11.4s are less likely to be underestimated.

Another consequence of linearizing the non-linear damping effects is that this influences how wave-induced response signals $\eta(t)$ are distributed. In the current motion analysis the damping coefficient is determined for a single significant roll angle and a chosen roll frequency while the non-linear damping coefficient is is a function of roll angle and velocity according to Equation 3.4. As can be seen, the damping coefficient increases for greater roll angles and roll velocities. Whereas for the linear motion analysis the damping coefficient remains constant, in a non-linear motion analysis the greater roll amplitudes are expected to be damped more than the smaller roll amplitudes. Since it is stated in [9] that wave elevation signals for irregular seas follow the normal distribution quite well, the response signals obtained with a linear motion analysis are expected to be Gaussian distributed as well. On the other hand, when non-linear damping effects are not linearized the response signals are not expected to be normally distributed as the responses in the tail of the distribution will be damped more. This is illustrated in Figure 3.4.

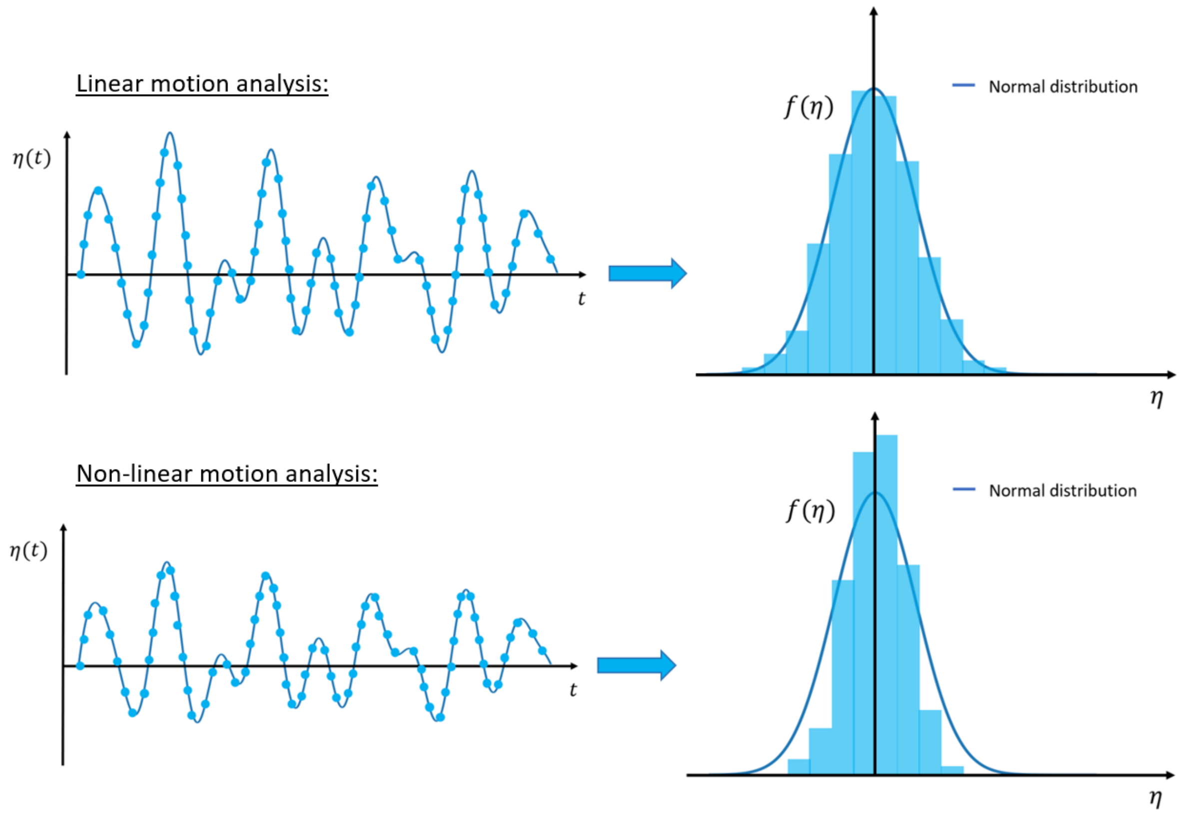

Figure 3.4: Difference in PDFs $f(\eta)$ of response signals $\eta(t)$ which are obtained with linear and non-linear motion analyses

3.4. Uncertainties in LCD

In section 2.4 the LCD of the current calculation method is described. In the LCD it is defined which loads are acting on the jacket and how these loads are combined with the various load cases. The calculation of loads and the combinations of these loads is based on assumptions and simplifications. Instead of using the acceleration time series obtained in the motion analysis, in the current calculation method 3-hour MPE values of the accelerations are used as input to calculate the inertia loads acting on the jacket. For all simulations which are performed for the different sea state and wave heading angle combinations, the 3-hour MPE values are determined from the acceleration time series for each motion. For each motion, the maximum 3-hour MPE value calculated in all simulations are extracted. Subsequently, the maximum 3-hour MPE values for each motion are used to calculate the inertia loads acting on the jacket. These inertia loads are then combined according to the specified load cases. This method of using the 3-hour MPE values of acceleration time series to calculate inertia loads and to combine these loads according to the specified load cases has the following consequences:

- A MPE value is the extreme value that is most likely to be observed in a certain period of time. The theoretical probability that this MPE value is exceeded by the extreme value in this same period of time is 0.632 according to [17]. The resulting reaction loads calculated with 3-hour MPE values of different motion accelerations might therefore also have a high probability of being exceeded depending on how the inertia loads are combined. Therefore, it might be more intuitive to work with extreme values which have a lower probability of being exceeded by by the extreme value in a certain period of time.
- 3-hour MPE values of accelerations time series coming from simulations for different sea states and different wave heading angles are combined.
- The MPE value is just a statistical value describing the most probable extreme magnitude of a process of a certain duration. The MPE value does not give any information on the exact moments when the process has values equal to or exceeding the MPE value. This means that even tough it is unclear if values of this magnitude happen at the same moment in time, the inertia loads

calculated with these 3-hour MPE values are combined as if the acceleration signals would have a value equal to the 3-hour MPE values at the same moment in time.

- Even if acceleration signals of different motions would have values equal to the 3-hour MPE value at the same moment in time, it remains unclear whether the accelerations have positive or negative directions at this moment. Since the signs of the acceleration directions are unknown, it is unclear if the combination of the inertia loads would contribute to higher or lower reaction loads. In the defined load cases the signs of the acceleration directions are chosen such that the combination of the inertia loads calculated with 3-hour MPE values of accelerations result in the highest possible reaction loads.

From these consequences it can be concluded that quite some uncertainties are involved in combining inertia loads which are calculated with 3-hour MPE values of acceleration signals.

3.5. Uncertainties in structural analysis of jacket

As mentioned in section 2.5 a static structural FEM analysis is performed to calculate the reaction loads on the sea fastening. However, as the wave-induced loads acting on the jacket and the resulting stresses and deformations of the jacket members are time-varying the structural analysis of the jacket should be considered as a dynamic problem. In a dynamic structural analysis additional characteristics of the jacket are investigated which are not considered in a static analysis such as the damping, natural frequencies and modes of vibrations of the jacket. A dynamic structural analysis is more extensive than a static analysis and it requires the system of equations to be solved for multiple time steps which makes the analysis more time-consuming. Besides dynamic analyses requires more extensive software which is often more expensive.

For these reasons, in practice it is preferred to just perform the static analysis as this analysis is less time consuming and cheaper. In this section it investigated if the static structural analysis gives a satisfactory approximation of the results which would have been obtained with a dynamic analysis of a jacket during transport.

4 Statistical extreme value calculation of response motions

During transports of wind turbine components and their support structures, HTVs and transport barges are exposed to wind and wave loads which have an irregular or stochastic nature. The stochastic nature of these loads leads to response motions and loads which are similarly stochastic. This makes it hard to predict the response motions and loads with deterministic methods. For this reason, statistical and probabilistic methods are often used to describe response motions and loads of vessels and structures exposed to wind and ocean waves. When analyzing extreme and rare events like large waves and severe storms that might be encounter during transport, statistical Extreme Value Theory (EVT) is often applied.

In section 4.1 EVT is introduced such that stochastic response motions and loads can be described in a probabilistic way. In section 4.2 it is described how EVT is often used to determine MPE values of responses which are known to be narrow-banded. In section 4.3 the same is done for response processes which are non-narrow-banded. Finally, in section 4.4 a probabilistic analysis is performed of the response acceleration processes obtained with the motion analysis. In the current calculation method the 3-hour MPE values of the acceleration processes are calculated by assuming the processes to be narrow-banded. In the final section of this chapter it is investigated if these processes are indeed narrow-banded and whether the applied theory to calculate the 3-hour MPE values of the acceleration processes is valid.

4.1. Extreme value theory

Extreme value density function

The maximum value of a random variable X that is observed in a certain number of observations n or a period of time T is known as the extreme value. The extreme value itself can also be considered a random variable that can be denoted by Y_n [17]. The PDF $f(x)$ and the cumulative distribution function (CDF) $F(x)$ of the random variable X are described as the initial PDF and the initial CDF. If the random variables $X_1, X_2, ..., X_n$ are statistically independent and all have the same PDF $f(x)$ it is shown with order statistics that the PDF $g(y_n)$ of the extreme value Y_n of the maxima can be expressed in terms of the initial PDF and the initial CDF and the number of observations n [16]:

$$\begin{aligned} g\left(y_n\right) &= n! \cdot f\left(y_n\right) \cdot \frac{\left[F\left(y_n\right)\right]^{n-1}}{(n-1)!} \\ &= n \cdot f\left(y_n\right) \cdot \left[F\left(y_n\right)\right]^{n-1} \end{aligned} \tag{4.1}$$

It is shown that the CDF $G(y_n)$ is given by:

$$G\left(y_n\right) = \int_{-\infty}^{y_n} g\left(y_n\right) dy_n = \left\{F\left(y_n\right)\right\}^n \tag{4.2}$$

For the extreme value Y_1 of the minima it is shown that the PDF $g(y_1)$ and the CDF $G(y_1)$ are given by:

$$\begin{aligned} g\left(y_{1}\right) &= n \cdot\left[1-F\left(y_{1}\right)\right]^{n-1} \cdot f\left(y_{1}\right) \\ G\left(y_{1}\right) &= \left[1-F\left(y_{1}\right)\right]^{n} \end{aligned} \tag{4.3}$$

MPE value determination

The MPE value of the maxima is defined as the value of y_n for which the extreme value PDF $g(y_n)$ has its peaks. To calculate the MPE value of the maxima, the PDF $g(y_n)$ of the extreme value Y_n has to be determined first. With Equation 4.1 the extreme value density function $g(y_n)$ can be constructed from the initial PDF $f(x)$ and $F(x)$ of random variable X which represents the local maximum peaks of a process. In Figure 4.1 it is illustrated how the local maximum peaks of a normally distributed response signal might be distributed.

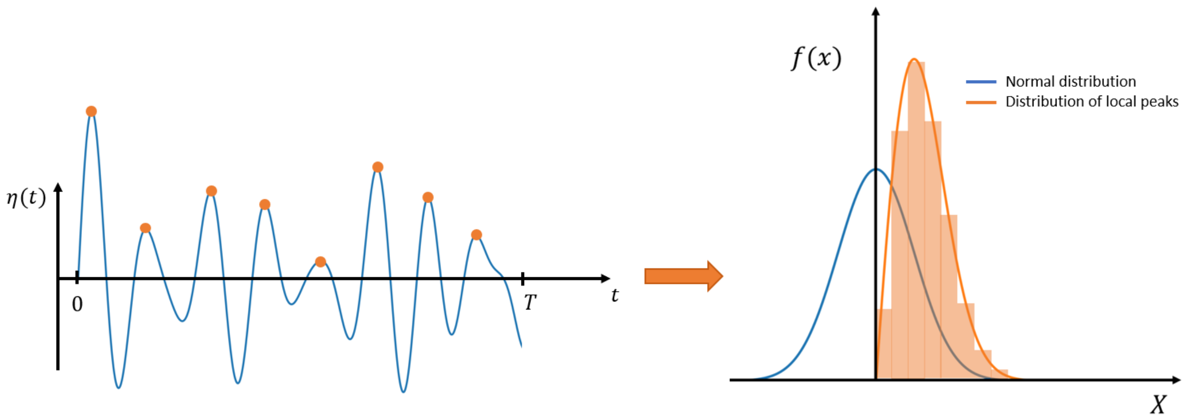

Figure 4.1: Example PDF $f(x)$ of the local maximum peaks of a normally distributed response signal $\eta(t)$

Once the initial PDF $f(x)$ and CDF $F(x)$ of the local maximum peaks are known, the distribution $g(y_n)$ of the extreme value can be obtained with Equation 4.1 as is shown in Figure 4.2 for a low number of peaks n. The MPE value for a process with a given number of peaks n or a given time period can now be determined as the value of y_n for which $g(y_n)$ has its peak.

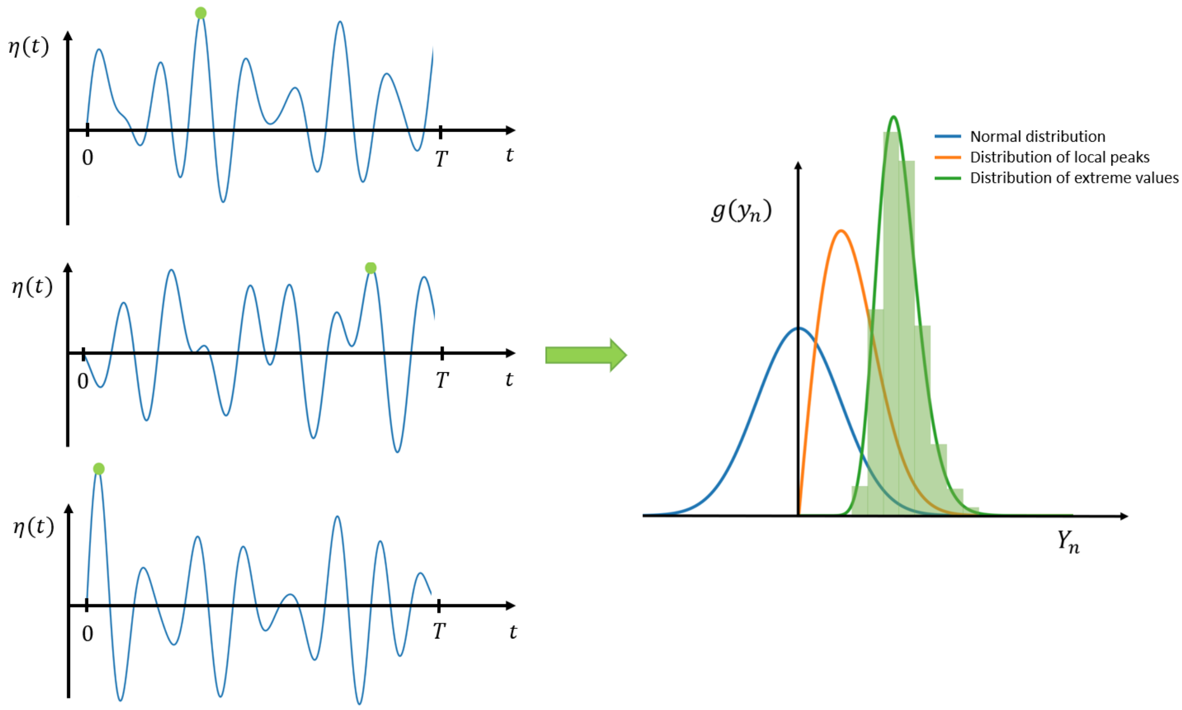

Figure 4.2: Example PDF $g(y_n)$ of the extreme value Y_n of a normally distributed response signal $\eta(t)$

4.2. MPE values of narrow-banded processes

As mentioned before it is stated in [9] that wave elevation signals for irregular seas follow the Gaussian distribution quite well. Besides, it is stated in [9] that if the range of frequencies in a wave field is not too large, the wave field can be described by a narrow-banded frequency spectrum. Besides, it is mentioned that both sea and swell waves generally satisfy this condition quite well. It is claimed in [17] that the local maximum peaks of a narrow-banded stationary random process, which is Gaussian distributed with zero mean, are Rayleigh distributed. Since wave elevation signals are said to be Gaussian distributed and quite narrow-banded in general, it follows that the wave amplitudes are expected to be Rayleigh distributed.

Narrow-banded processes

A process is considered strictly narrow-banded when the process only has one local maximum and one local minimum peak per zero up-crossing period. Processes which are not strictly narrow-banded may have multiple local maximum and minimum peaks per zero up-crossing period as these processes are comprised of wave components which cover a significant range of frequencies. An illustration of a narrow-banded and a non-narrow-banded process is shown in Figure 4.3.

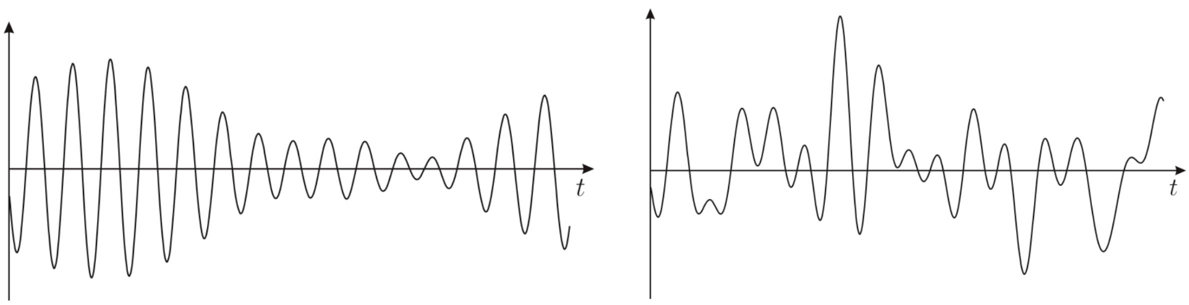

Figure 4.3: Illustration of a narrow-banded process on the left and a non-narrow-banded process on the right, taken from [14]

For Gaussian narrow-banded processes whose local maximum peaks follow the initial Rayleigh PDF and CDF, the following formula is derived in [17] to calculate the MPE value:

$$\begin{aligned} \text{MPE} &= \sqrt{2 \cdot m_0 \cdot \ln(n)} \\ &= \sigma\sqrt{2 \cdot \ln(n)} \end{aligned} \tag{4.4}$$

Where m_0 represents the zeroth moment of the response spectrum, σ represents the standard deviation of the acceleration time series and n the number of local peaks during a certain time period. The number of peaks is determined by dividing the time period t by the zero up-crossing period T_z:

$$n = \frac{t}{T_z} \tag{4.5}$$

MPE value calculation in current method
In the current calculation method, linear motion analyses are performed for 3-hour stationary sea states. The output of these simulations are 3-hour long acceleration time series of the jacket CoG in the 6-DoFs. Since linear motion analyses are performed, the wave-induced response motions have a linear relation with the wave elevation signals. Therefore, the response motions are assumed to be Gaussian distributed just like the wave elevation signals, as is illustrated in Figure 3.4. Besides, the acceleration signals are assumed to be narrow-banded and the local maximum peaks of the acceleration signals are therefore assumed to be Rayleigh distributed. For this reason, the MPE values are calculated from the acceleration time series by using Equation 4.4. Since the acceleration signals are Gaussian distributed with zero mean, the MPE values of the maxima and minima can be expected to be the same. Therefore, only the MPE values of the maxima are calculated.

4.3. MPE values of non-narrow-banded processes

Although it is stated in [9] that both sea and swell waves can generally be described by narrow-banded frequency spectra, it is observed that most of the acceleration time series obtained with the linear motion analyses are not strictly narrow-banded. Most obtained acceleration time series show at least several zero up-crossing periods containing multiple local maximum peaks which can be both positive and negative. The energy spectra of the time series can therefore be considered broad-banded or not strictly narrow-banded. Depending on the sea state some acceleration time series might have many local peaks for every zero up-crossing period while for other sea states only a few zero up-crossing periods experience more than one local peak. In [17] the bandwidth parameter ϵ of an energy density spectrum $S(\omega)$ is introduced to describe the width of the spectrum. For random processes having a narrow-banded spectrum the bandwidth is $\epsilon = 0$ while for a wide-banded spectrum the bandwidth is $\epsilon = 1$. The bandwidth parameter ϵ is given by:

$$\epsilon = \sqrt{1 - \frac{m_2^2}{m_0 \cdot m_4}} \tag{4.6}$$

Where m_0, m_2 and m_4 are the zeroth, second and fourth moments of the energy density spectrum respectively. They are given by:

$$\begin{aligned} m_0 &= \int_0^\infty S(\omega)d\omega \\ m_2 &= \int_0^\infty \omega^2 S(\omega)d\omega \\ m_4 &= \int_0^\infty \omega^4 S(\omega)d\omega \end{aligned} \tag{4.7}$$

For the remainder of this section only the positive local maximum peaks will be considered which will be referred to as positive maxima. In [17] the PDF of the positive maxima ξ of a stationary Gaussian process with zero mean is derived:

$$
\begin{aligned}
f(\xi) = \frac{\left(\frac{2}{\sqrt{m_0}}\right)}{1+\sqrt{1-\epsilon^2}} \Bigg[& \frac{\epsilon}{\sqrt{2\pi}} \exp\left\{ -\frac{1}{2\epsilon^2}\left(\frac{\xi}{\sqrt{m_0}}\right)^2 \right\} \\
& + \sqrt{1-\epsilon^2}\left(\frac{\xi}{\sqrt{m_0}}\right) \exp\left\{ -\frac{1}{2}\left(\frac{\xi}{\sqrt{m_0}}\right)^2 \right\} \\
& \times \left\{ 1 - \Phi\left(-\frac{\sqrt{1-\epsilon^2}}{\epsilon}\frac{\xi}{\sqrt{m_0}} \right) \right\} \Bigg] \quad 0 \leqq \xi < \infty
\end{aligned}
\tag{4.8}
$$

Where $\Phi(u)$ denotes the CDF of the standardized normal distribution given by:

$$
\Phi(u) = \frac{1}{\sqrt{2\pi}} \int_{-\infty}^{u} \exp\left\{ -\frac{u^2}{2} \right\} du \tag{4.9}
$$

Besides, the CDF of the positive maxima ξ of a stationary Gaussian process with zero mean is derived:

$$
\begin{aligned}
F(\xi) = & \frac{2}{1+\sqrt{1-\epsilon^2}} \Bigg[-\frac{1}{2}\left(1-\sqrt{1-\epsilon^2}\right) + \Phi\left(\frac{\xi}{\epsilon\sqrt{m_0}}\right) \\
& - \sqrt{1-\epsilon^2} \exp\left\{ -\frac{1}{2}\left(\frac{\xi}{\sqrt{m_0}}\right)^2 \right\} \\
& \times \left\{ 1 - \Phi\left(-\frac{\sqrt{1-\epsilon^2}}{\epsilon}\frac{\xi}{\sqrt{m_0}} \right) \right\} \Bigg] \quad 0 \leqq \xi < \infty
\end{aligned}
\tag{4.10}
$$

The extreme value distribution $g(\zeta_n)$ of the extreme value ζ_n can now be obtained from the initial PDF $f(\zeta_n)$ and CDF $F(\zeta_n)$ with Equation 4.1:

$$
g(\zeta_n) = n \cdot f(\zeta_n) \cdot [F(\zeta_n)]^{n-1} \tag{4.11}
$$

Where the number of positive maxima is given by n. For illustration, PDFs of the positive maxima $f(\zeta_n)$ are plotted in non-dimensional form $f(\frac{\zeta_n}{\sqrt{m_0}})$ in Figure 4.4. The non-dimensional PDFs are plotted for multiple processes whose energy spectra are described by different values of the bandwidth parameter ϵ. It is derived in [17] that the positive maxima of a narrow-banded process for which $\epsilon = 0$ are Rayleigh distributed. On the other hand, the positive maxima of a wide-banded process for which $\epsilon = 1$ are derived to be Gaussian distributed. It should be noted that the normal distribution is truncated at $\zeta_n = 0$ since only positive maxima are considered.

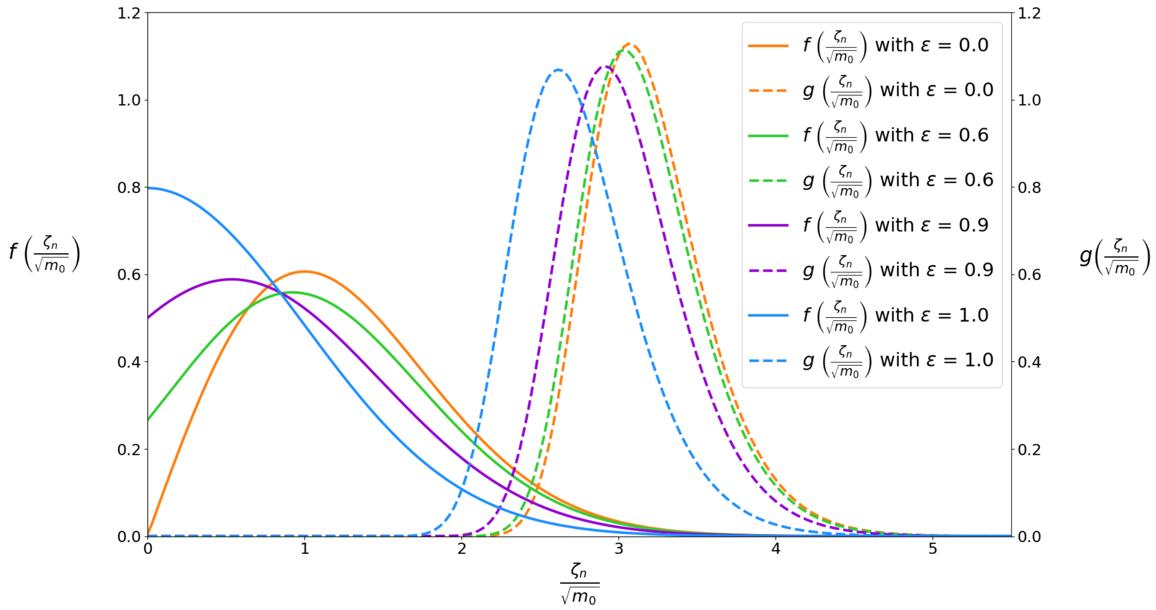

Figure 4.4: PDFs of the positive maxima and the corresponding extreme value distributions plotted as a function of non-dimensional extreme value $\frac{\zeta_n}{\sqrt{m_0}}$ for processes described by different bandwidth parameters ϵ

Besides the PDFs of the positive maxima for the different processes, also the corresponding extreme value PDFs $g(\zeta_n)$ are plotted for the different processes. The extreme value PDFs are determined for a fixed number of positive maxima $n = 100$ which is chosen just for the purpose of illustration. It can be seen that for a fixed number of positive maxima n, the extreme value PDF and therewith the MPE value for strictly narrow-banded processes form an upper limit.

However, the extreme value PDF and corresponding MPE value are not only dependent on how the positive maxima are distributed, but also on the number of positive maxima n. In [17] the following formula is presented which computes the expected number of positive maxima n as a function of the duration T in hours and the spectral moments of a process:

$$E[n] = (60)^2 \left(\frac{T}{4\pi}\right) \left(\frac{1+\sqrt{1-\epsilon^2}}{\sqrt{1-\epsilon^2}}\right) \sqrt{\frac{m_2}{m_0}} \cdot 2\pi \tag{4.12}$$

Once the spectral moments m_0, m_2 and m_4 of a process are known it is thus possible to determine the expected number of positive maxima n with Equation 4.12. Equation 4.8 and Equation 4.10 can now be used to determine the initial PDF and CDF of these positive maxima. Finally, Equation 4.11 can be used to obtain the extreme value distribution $g(\zeta_n)$ of the extreme value ζ_n in a time period T.

The MPE value of a process which is not strictly narrow-banded is defined as the value of ζ_n for which $g(\zeta_n)$ has its peak. In [17] a formula is derived to calculate the MPE value for processes which have a large number of positive maxima n. Besides, the formula is only valid for processes with energy spectra which are described by $\epsilon \leqq 0.9$. For these processes the MPE value $\bar{\zeta}_n$ can be calculated with:

$$\bar{\zeta}_n = \sqrt{2 \ln \left\{\frac{2\sqrt{1-\epsilon^2}}{1+\sqrt{1-\epsilon^2}} n\right\}} \cdot \sqrt{m_0} \qquad \text{for } \epsilon \leqq 0.9 \tag{4.13}$$

Besides the MPE value $\bar{\zeta}_n$, the extreme value $\hat{\zeta}_n$ is introduced which is the extreme value which has a small probability α of being exceeded by an extreme value ζ_n. The formula for $\hat{\zeta}_n$ is given by:

$$\hat{\zeta}_n = \sqrt{2\ln\left(\frac{\sqrt{1-\epsilon^2}}{1+\sqrt{1-\epsilon^2}} \cdot \frac{2n}{\alpha}\right)} \cdot \sqrt{m_0} \qquad \text{for small } \alpha \text{ and } \epsilon \leqq 0.9 \tag{4.14}$$

4.4. Probabilistic analysis of response acceleration signals

In the current calculation method the 3-hour MPE values of the accelerations are calculated by assuming that the response acceleration signals are narrow-banded. However, the obtained response acceleration signals were observed to be wide-banded or not strictly narrow-banded. For this reason, the obtained response acceleration signals are investigated in terms of bandwidth in this section. In addition, for the response acceleration signals it is investigated whether it is valid to use Equation 4.4 which is derived to calculate MPE values for narrow-banded processes. To do this, the theory introduced in the previous section for non-narrow-banded Gaussian processes with zero mean is used.

The introduced theory is based on the spectral moments of the energy spectrum of a process. The first step is therefore to obtain the zeroth, second and fourth spectral moments of the acceleration processes. The acceleration time series are obtained by performing motion simulations with time-domain software. As described, the software performs motion simulations of the vessel for different sea states and wave headings. The output of these simulations are acceleration time series of the jacket CoG. Besides, the software offers the option to extract the statistical properties of the acceleration time series.

As the time-domain software computes response time series instead of response energy spectra, the spectral moments are approximated by statistical properties of the acceleration time series. The zeroth spectral moment m_0 is estimated as the variance of the time series:

$$m_0 = \sigma^2 \tag{4.15}$$

To approximate the second and fourth spectral moments m_2 and m_4 the relations between the average zero up-crossing period T_z, the average crest period T_c and the spectral moments are used. In [11] the following relations are given:

$$\begin{aligned} T_z &= \sqrt{\frac{m_0}{m_2}} \\ T_c &= \sqrt{\frac{m_2}{m_4}} \end{aligned} \tag{4.16}$$

These relations are used as follows to approximate the spectral moments from the acceleration time series:

$$\begin{aligned} m_2 &= \frac{m_0}{T_z^2} \\ m_4 &= \frac{m_2}{T_c^2} \end{aligned} \tag{4.17}$$

Where T_z is determined from the acceleration time series by dividing the total duration of the simulation in seconds by the number of identified mean up-crossing of the signal during the simulation. The average crest period T_c for wave signals or the average period between the local maxima of these acceleration signals is determined by dividing the total duration of the simulation in seconds by the number of local maxima identified during the simulation.

Once the spectral moments are extracted from the time-domain software, the acceleration time series are investigated. For all time series the positive maxima are identified. In Figure 4.5 a segment of the acceleration time series for surge motion of the jacket CoG is shown for a simulation performed for a sea state described by $T_p =$ 10.5s and a wave heading angle of $\theta =$ 195°. The segment has a length of 50 average zero up-crossing periods. This surge acceleration signal is chosen for since for this signal the highest 3-hour MPE value for surge acceleration is expected according to Table 2.5. In Appendix B results which are presented for this signal are also presented for the governing acceleration signals of the other DoFs. For the acceleration motions of the other DoFs it is also chosen to present the results for the simulation for which the highest 3-hour MPE values were calculated. These specific acceleration signals are chosen for since these signals are likely to cause the highest reaction loads. Besides, these signals have bandwidth parameters ϵ ranging from low values to values approaching 1 and therefore these signal serve as a good example to show the results. However, the analysis has been performed for all simulations and all 6-DoF motions of the vessel.

In the figure below, the identified positive maxima are marked with orange dots. From the acceleration signal it can be seen that in several zero up-crossing periods multiple local maxima can be identified which are either positive or negative. It can therefore be expected that the acceleration energy spectrum corresponding to this signal contains a wide range of frequencies. This is confirmed in Table 4.1 in which the bandwidth parameter ϵ and other statistical properties of the acceleration signal are presented which have been extracted from the time domain software.

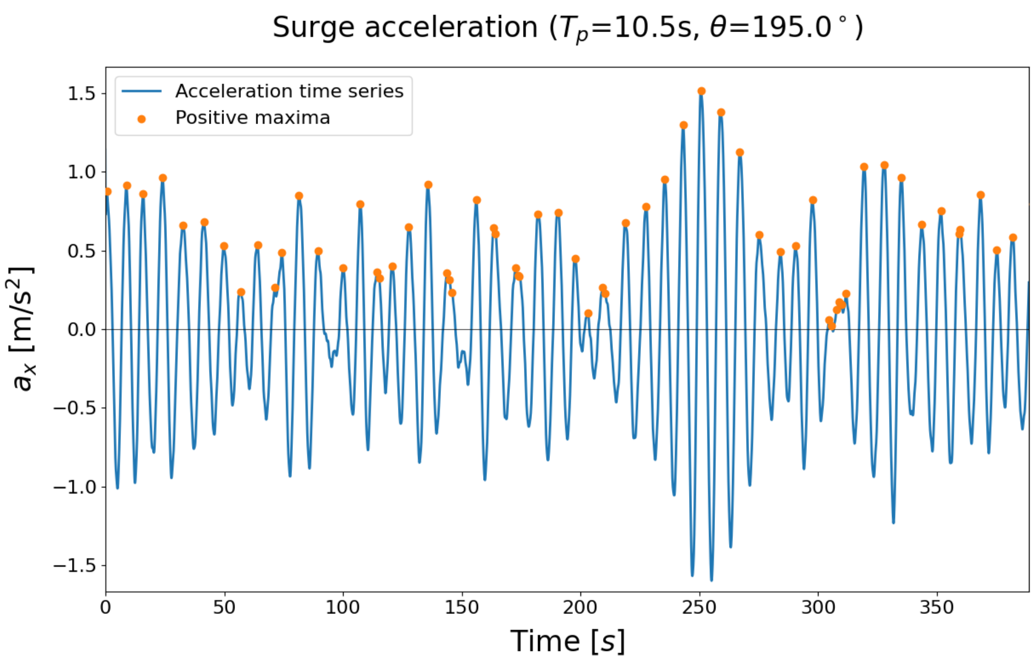

Figure 4.5: Time series of surge acceleration of the jacket CoG for which the positive maxima have been identified and marked with orange dots

Table 4.1: Statistical properties of the surge acceleration signal of the jacket CoG for T_p = 10.5s and θ =195°

T_p [s]	Heading [deg]	σ [m/s^2]	m_0 [m^2/s^4]	m_2 [m^2/s^6]	m_4 [m^2/s^8]	T_z [s]	T_c [s]	ϵ [-]
10.5	195	0.490	0.241	$3.98 \cdot 10^{-3}$	$1.73 \cdot 10^{-4}$	7.78	4.80	0.787

After the positive maxima have been identified, Equation 4.12 is used to calculate the expected number of positive maxima. The expected number of positive maxima is compared with the number of identified positive maxima. The results for this signal can be found in Table 4.2. The comparison is made for all other acceleration signals as well. For all signals the expected number of positive maxima is assumed to give a very accurate estimation of the number of identified positive maxima. The results for the acceleration signals considered for the other DoF motions can be found in Appendix B.

It should be noted that Equation 4.12 is expected to give an accurate estimation of the number of positive maxima. The spectral moments and the bandwidth parameter of the signals have been determined directly from the number of identified mean up-crossings, the number of identified positive maxima and the standard deviation of the signals. Subsequently, these statistical properties of the signals are used in Equation 4.12 to calculate the expected number of positive maxima.

Besides the number of positive maxima, it is investigated if the PDF given in Equation 4.8 gives an accurate approximation of the histogram of identified positive maxima. The identified positive maxima are presented in a histogram in Figure 4.6. With the spectral moments and Equation 4.8 the theoretical density function of the maxima is obtained and plotted on top of the histogram of the maxima. By visual inspection the mathematical approximation is considered to be accurate for all signals independent of bandwidth parameter ϵ. In Appendix B the approximated distributions of the positive maxima for the acceleration signals of the other DoFs motions are presented as well.

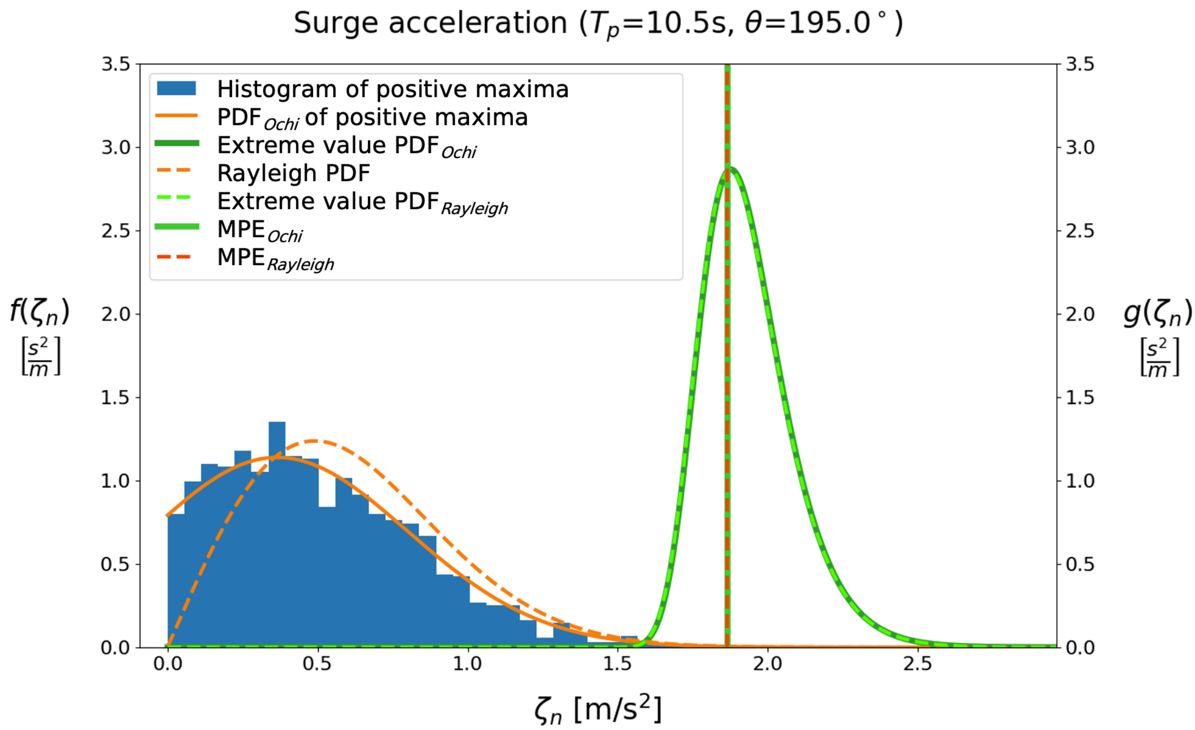

Figure 4.6: Extreme value theory introduced in section 4.3 is applied to the surge acceleration time series for the simulation given by T_p = 10.5s and θ = 195.0

Once the initial theoretical PDF of the local maxima $f(\zeta_n)$ is obtained, the corresponding initial CDF $F(\zeta_n)$ is obtained with Equation 4.10. With Equation 4.11 the extreme value density function $g(\zeta_n)$ of the 3-hour extreme value of the maxima ζ_n can be constructed from $f(\zeta_n)$, $F(\zeta_n)$ and the number of positive maxima. This theoretical extreme value density function $g(\zeta_n)$ is plotted alongside the histogram and the theoretical PDF $f(\zeta_n)$ in Figure 4.6.

In addition, the Rayleigh PDF $f(\zeta_n)$ for narrow-banded signals and thus $\epsilon = 0$ is plotted on top of the histogram of the positive maxima. It can be clearly seen that the Rayleigh PDF is not a valid representation of how the positive maxima are distributed. For comparison, the 3-hour extreme value distribution $g(\zeta_n)$ obtained with the initial Rayleigh PDF and CDF and the number of positive maxima computed with Equation 4.5 is plotted on top of the theoretical extreme value density function for the non-narrow-banded signal. Where it was observed that the initial theoretical PDF and the initial Rayleigh PDF for this signal with $\epsilon = 0.787$ are quite different, it can be seen that the obtained extreme value density functions are very similar.

In Figure 4.4 it was shown what is the influence of the shape of the initial density function $f(\zeta_n)$ of the positive maxima on the extreme value density function $g(\zeta_n)$ for a fixed number of positive maxima n. From this figure it can be concluded that if the same number of positive maxima n would have been used to obtain both extreme value density functions, these extreme value density functions would not be similar. However, for a non-narrow-banded signal the number of positive maxima is greater than the number of positive maxima for a narrow-banded signal as can also be seen in Table 4.2. This difference in number of positive maxima is concluded to cause the extreme value density functions of both the narrow-banded and non-narrow-banded signal to be as good as similar. This is concluded by examining not only the extreme value density functions given in this section but also those in Appendix B. Only for the pitch acceleration signal with bandwidth parameter $\epsilon = 0.970$ a slight difference in extreme value density functions is observed. The difference is very little and will only have a slight influence on the MPE value. In addition, almost no difference is observed in the right tail of the extreme value density functions which is often most important for engineering purposes.

Now that the extreme value density functions have been obtained, Equation 4.4 to calculate the MPE value MPE$_{Rayleigh}$ for narrow-banded signals and Equation 4.13 to calculate the MPE value MPE$_{Ochi}$ for non-narrow-banded signals can be examined. For the calculation of MPE$_{Ochi}$ the number of identified positive maxima is used. Equation 4.13 is only valid for signals with $\epsilon \leq 0.9$ Therefore, for signals with $\epsilon > 0.9$ MPE$_{Ochi}$ is taken to be equal to the extreme value ζ_n for which the extreme value density function $g(\zeta_n)$ has its peak. The resulting MPE values are shown in Figure 4.6 and presented in Table 4.2 for the example signal and in Appendix B for the other DoF motions.

Table 4.2: Comparison of number of positive maxima and MPE values

T_p [s]	Heading [deg]	$n_{identified}$ [-]	$E[n]$ [-]	MPE$_{Ochi}$ [m/s^2]	$n_{Rayleigh}$ [-]	MPE$_{Rayleigh}$ [m/s^2]
10.5	195	1863	1819	1.869	1388	1.876

It can be concluded that the calculated MPE$_{Ochi}$ value and MPE$_{Rayleigh}$ value are very similar for all signals of different bandwidth parameters. Only for the pitch acceleration signal with bandwidth parameter $\epsilon = 0.970$ a small difference in MPE values is observed but this difference is primarily caused by the fact that the extreme value corresponding to the peak of $g(\zeta_n)$ is taken instead of calculating the MPE value with Equation 4.13. This difference also confirms the following observation that although very similar MPE values for narrow-banded and non-narrow-banded signals are calculated with Equation 4.4 and Equation 4.13, the calculated values seem to be slightly lower than the extreme value for which $g(\zeta_n)$ has its peak. This can be seen back in the figures in which the extreme value density functions and MPE values have been plotted. However, the influence of this observed difference on the to be calculated reaction loads is considered to be negligibly small.

4.5. Findings

The main finding of this chapter is that equal extreme value density functions were observed for narrow-banded and non-narrow-banded stationary Gaussian process with zero mean and of fixed time period in which a large number of positive maxima is observed. Other findings are summarized below:

- The number of expected positive maxima calculated with Equation 4.12 is found to give accurate estimations of the number of observed positive maxima in the signals, independent of the spectral bandwidth of the signals.
- By visual inspection, the mathematical density function of the positive maxima given in Equation 4.8 is considered to be an accurate approximation of the obtained histograms of the positive maxima for all signals independent of the spectral bandwidth of the signals.
- The MPE values calculated with Equation 4.4 for narrow-banded signals and with Equation 4.13 for non-narrow-banded signals give very similar results.
- By comparison of the calculated MPE values with the extreme value density functions, the calculated MPE values are found to be slightly lower than expected from the extreme value density function. However, the influence of this small difference on the to be calculated reaction loads is considered to be negligibly small.
- Even though the obtained acceleration signals of the jacket CoG are found to be non-narrow-banded, it is considered to be valid to use Equation 4.4 for narrow-banded signals to calculate the MPE values for the response acceleration signals.

5

Probabilistic investigation of load combination methods

As mentioned at the beginning of the previous chapter, EVT is often applied to describe response motions and loads of vessels and structures exposed to wind and wave loads. In the current calculation method EVT is used to describe the response accelerations in terms of 3-hour MPE values. Subsequently, these probabilistic 3-hour MPE values of the accelerations, which have been obtained in different sea states, are used in a deterministic method of calculating the reaction loads. First, the inertia loads acting on the jacket are calculated with 3-hour MPE values of the accelerations after which these inertia loads are combined, according to specified load cases, with the static weight of the jacket and the static wind loading.

This chapter focuses on the method of combining these loads. First a probabilistic method based on the previously introduced EVT will be presented in section 5.1. A method to obtain time series of the reaction loads is derived such that the EVT can be applied to these reaction load time series to obtain 3-hour extreme value density functions of the reaction loads in each sea state. In section 5.2 load combination methods are introduced which are similar to the current load combination method but for which the uncertainties are reduced. In section 5.3 it is investigated whether the current partial-deterministic method and the newly introduced methods of combining loads, from which the inertia loads are calculated with probabilistic values of accelerations, can be used to obtain probabilistic results of the reaction loads in each sea state. If this is not the case, the current deterministic method of combining loads should be replaced by the probabilistic method which is presented in section 5.1 to obtain a probabilistic calculation method of the reaction loads for each sea state.

5.1. Probabilistic load combination method

In the previous chapter, EVT was applied to the response acceleration time series to describe the accelerations in a probabilistic way. In this section the aim is to obtain response reaction load time series such that EVT can be applied to these response reaction load time series.

5.1.1. Simplified rigid jacket calculation method

In section 2.5 it was explained how a static second-order FEM analysis of the jacket is performed to calculate the reaction loads on the sea fastening. It was explained that maximum 3-hour MPE values of accelerations are used to calculate the inertia loads acting on the jacket while in reality these loads are dynamic harmonic loads. Most basic FEM software packages do not offer the possibility to insert time series of loads acting on the jacket and more advanced software packages which have this option included are often expensive. Besides, performing the structural analysis of a jacket for time series of loads acting on the jacket would be time consuming especially when many different sea states are considered.

Instead of performing a FEM analysis of the jacket, a simplified calculation method is introduced here to calculate the reaction loads on the sea fastening for each time step of the obtained response acceleration time series. Instead of calculating the inertia loads with 3-hour MPE values of accelerations, now the actual accelerations at each time step are used to calculate the inertia loads acting on the jacket. At each time step these inertia loads are now combined, according to the simplified rigid jacket method, with the static weight and static wind load on the jacket.

Assumptions in the calculation method
The introduced calculation method is a simplified method to calculate the reaction loads on the sea fastening which is based on the following assumptions:

- The jacket is assumed to be a rigid body and therefore deformations are not considered. Instead of the second-order FEM analysis this is a linear calculation method.
- The inertia loads are dynamic fluctuating loads while the static weight and wind loads are assumed to be constant loads. Although the inertia loads are dynamic fluctuating loads, a static calculation of the reaction loads is performed for each time step.
- Only the vertical reaction forces are calculated with this method as only these forces are of interest when investigating the combination of loads. In general, the vertical reaction forces are caused by a combination of the horizontal inertia forces, the inertia moments, the heave inertia force and the constant self weight and wind force on the jacket. On the other hand, the horizontal reaction forces are caused only by the horizontal inertia forces and the constant wind force in the considered direction.
- The jacket legs are assumed to be supported by hinged supports and therefore the supports do not constrain rotations and there will be no reaction moments in the supports.
- The hinged supports are assumed rigid such that there will be no deflections and deformations in the supports. Besides, the deck of the vessel is assumed to be rigid as well.
- The wind loading is assumed to have the same direction as the waves which have a wave heading angle θ.

Derivation of rigid jacket calculation method
The loads acting on the jacket are composed of the inertia loads, static wind loading F_w and the static weight F_{static} of the jacket. The inertia loads are calculated with the mass of the jacket m, the moments of inertia of the jacket I_{xx} and I_{yy} and the surge acceleration a_x, sway acceleration a_y, heave acceleration a_z, roll acceleration r_x and pitch acceleration r_y. As the wind loading is assumed to have the same direction as the wave heading angle θ this load has components contributing to both F_x and F_y.

$$
\begin{aligned}
F_x &= m \cdot a_x + F_w \cdot \cos\theta \\
F_y &= m \cdot a_y + F_w \cdot \sin\theta \\
F_z &= m \cdot a_z - F_{static} \\
M_x &= I_{xx} \cdot r_x \\
M_y &= I_{yy} \cdot r_y
\end{aligned}
\tag{5.1}
$$

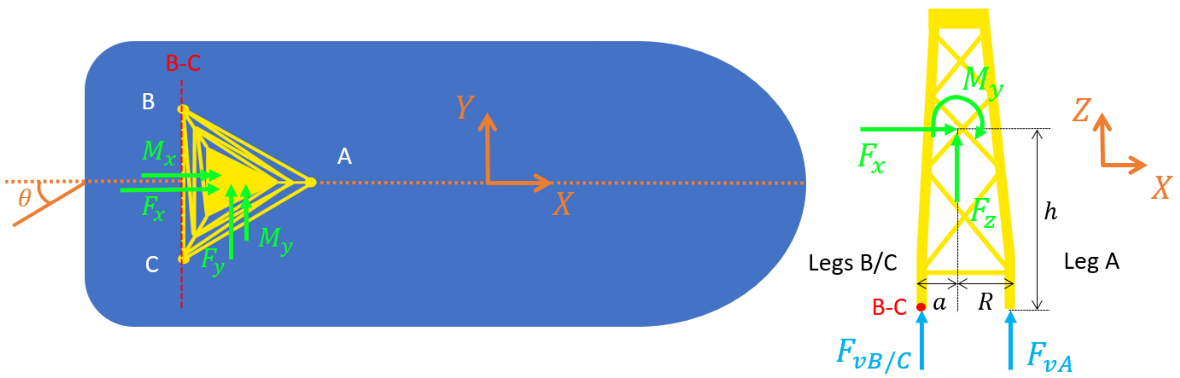

Figure 5.1: Load scheme used to calculate the vertical reaction forces on the sea fastening of leg A

The vertical reaction load F_vA on leg A is calculated from the equilibrium of moments around the B-C axis connecting legs B and C:

$$\begin{aligned} \sum M_{B-C} = 0: \quad M_y + F_x \cdot h - F_z \cdot a - F_{vA} \cdot (R+a) = 0 \\ F_{vA} = \frac{M_y + F_x \cdot h - F_z \cdot a}{R+a} \end{aligned} \tag{5.2}$$

To calculate the vertical reaction load on leg B, the equilibrium of moments around the A-C axis connecting legs A and C is considered. This axis has a different orientation than the B-C axis and therefore the $X'Y'$-coordinate system is introduced which has an angle α relative to the XY-coordinate system. F_y and M_x are now expressed in the $X'Y'$-coordinate system as F_y' and M_x':

$$\begin{aligned} \alpha &= 30^\circ \\ F_{y'} &= -F_x \cdot \sin\alpha + F_y \cdot \cos\alpha \\ M_{x'} &= M_x \cdot \cos\alpha + M_y \cdot \sin\alpha \end{aligned} \tag{5.3}$$

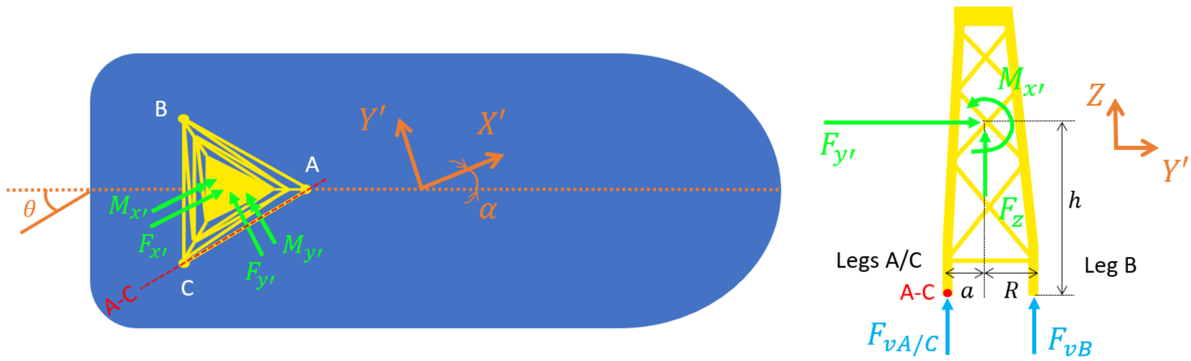

Figure 5.2: Load scheme used to calculate the vertical reaction forces on the sea fastening of leg B

The vertical reaction load F_vB on leg B is calculated from the equilibrium of moments around the A-C axis connecting legs A and C:

$$\begin{aligned} \sum M_{A-C} = 0: \quad M_{x'} + F_z \cdot a - F_{y'} \cdot h + F_{vB} \cdot (R+a) = 0 \\ F_{vB} = \frac{-M_{x'} - F_z \cdot a + F_{y'} \cdot h}{R+a} \end{aligned} \tag{5.4}$$

To calculate the vertical reaction load F_{vC} on leg C the $X''Y''$-coordinate system is introduced with an angle β relative to the XY-coordinate system. F_y and M_x are now expressed in the $X''Y''$-coordinate system as F_y'' and M_x'':

$$\begin{aligned} \beta &= 30^\circ \\ F_{y''} &= F_x \cdot \sin\beta + F_y \cdot \cos\beta \\ M_{x''} &= M_x \cdot \cos\beta - M_y \cdot \sin\beta \end{aligned} \tag{5.5}$$

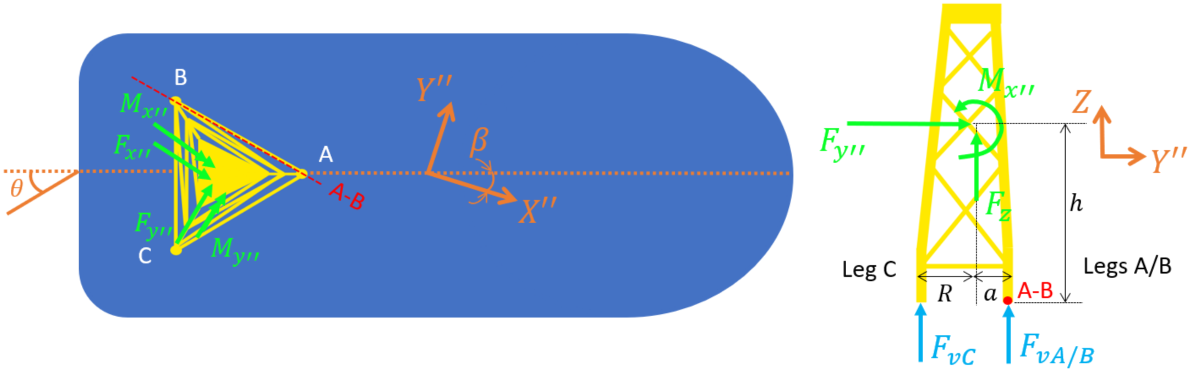

Figure 5.3: Load scheme used to calculate the vertical reaction forces on the sea fastening of leg C

The vertical reaction load F_vC on leg C is calculated from the equilibrium of moments around the A-B axis connecting legs A and B:

$$\begin{aligned} \sum M_{A-B} = 0: \quad M_{x''} - F_{y''} \cdot h - Fz \cdot a - F_{vC} \cdot (R + a) = 0 \\ F_{vC} = \frac{M_{x''} - F_{y''} \cdot h - Fz \cdot a}{R + a} \end{aligned} \tag{5.6}$$

Validation of results

The main goal of using this method is to illustrate a probabilistic load combination method. In addition, this method is used to perform a probabilistic investigation of the current calculation method. It should therefore be kept in mind that the simplified rigid jacket calculation is not introduced with the purpose of obtaining the exact reaction loads on the sea fastening. In Appendix C, the rigid jacket calculation method is validated by comparing the results of the method with the results of the static FEM analysis which was explained in section 2.5. The difference in results is considered small enough in order for the rigid jacket calculation to be valid for the purpose of illustrating a probabilistic calculation method and performing a probabilistic investigation of the current calculation method. However, when it is desired to calculate the exact reaction loads, it is still recommended to use a structural FEM analysis.

5.1.2. 3-hour extreme value density functions of reaction loads

With the introduced rigid jacket calculation method, vertical reaction loads time series are obtained for the three legs of the jacket. It should be noted that the reaction loads time series consist of a linear superposition of a static part and a harmonic part with zero mean. The static part is caused by the static wind load on the jacket and the static self weight. The harmonic part is caused by the harmonic inertia loads acting on the jacket. It is shown in Appendix D that the static part of the reaction loads is equal to the mean of the reaction loads time series and that the contribution of the inertia loads is harmonic with zero mean. Besides, the harmonic part is expected to be Gaussian distributed as this part is obtained by linear superposition of the Gaussian distributed response acceleration signals.

When the time series of the reaction loads of the three legs are obtained for all sea states, the theory described in section 4.3 is applied to the harmonic part of the reaction load time series. For the vertical reaction loads the focus is not only on the extreme values of the maximum reaction loads but also on the extreme values of the minimum reaction loads. The reason for this is that when negative vertical reaction loads are expected, the sea fastening should also be designed to constrain uplift. Therefore, the extreme values of the minimum reaction loads are also considered in the remainder of this section.

When applying the extreme value theory introduced in section 4.3, the spectral moments of the vertical reaction load energy spectra are computed from the reaction load time series. The average zero up-crossing period and average peak to peak period of the 3-hour reaction load time series are determined. Subsequently, the spectral moments are approximated with Equation 4.17. Once the spectral moments have been found, the initial density functions of positive maximum peaks and the negative minimum peaks of the reaction load time series are obtained. Finally, with these initial density functions the extreme value density function of the maximum and minimum reaction loads are determined. It should be noted that these are obtained by adding the static part of the reaction loads.

5.2. Introduced load combination methods of reduced uncertainty

In this section it will be investigated if the current deterministic method of combining loads could be used to obtain probabilistic reaction loads. Although the current load combination method is deterministic, the inertia loads which are being used have been calculated with probabilistic values of the accelerations (3-hour MPE values of accelerations). For this reason, the current load combination method could also be considered to be semi-probabilistic or partial-probabilistic.

In this section the resulting reaction loads of this partial-probabilistic method are investigated in terms of probability. For different sea states it is investigated if using inertia loads calculated with probabilistic acceleration values result in reaction loads which have a consistent probability of being exceeded by the 3-hour extreme value of the reaction loads. If consistent probabilities for the various sea states will be observed, the current partial-probabilistic method could be used to determine reaction loads which have a desired probability of being exceeded by the 3-hour extreme value of the reaction loads. Instead of using 3-hour MPE values of the accelerations, probabilistic values of accelerations which have a higher or lower probability of being exceeded by the 3-hour extreme value of the accelerations could be used to calculate the inertia loads. Moreover, the probabilistic acceleration values could be chosen such that reaction loads are obtained which have probability of being exceeded by the 3-hour reaction loads extreme value which is expected for the chosen probabilistic values of the accelerations. However, if the obtained probabilities for the different sea states are not consistent, it should be concluded that the current load combination method is not suited to obtain probabilistic reaction loads for a given sea state.

In section 3.4 it was described that the current load combination method and more specifically the use of inertia loads calculated from 3-hour extreme values of acceleration signals contains several uncertainties. Because of these uncertainties it is not expected that the current load combination method results in consistent probabilities of the calculated reaction loads being exceeded by the 3-hour extreme value of the reaction loads. Therefore, load combination methods are introduced which are similar to the current load combination method but for which the uncertainties are reduced.

The first method is the current load combination method containing several uncertainties. Each newly introduced method is introduced with the aim of reducing the uncertainties. Method 1 is therefore expected to contain the most uncertainties whereas the fourth method is is expeced to contain the least uncertainties. The different methods are described below:

> **Method 1:** ***Current method*** **-** This is the current calculation method as described in chapter 2. In this method the inertia loads for the different motions are calculated with 3-hour MPE values of the acceleration signals obtained in different sea states. The inertia loads are combined according to the load cases which are defined in the LCD in section 2.4. Depending on the load case not all motions are considered. In the load cases for beam waves only heave, sway and roll motion are considered. In the load cases for head and following waves only heave, surge and pitch motion are considered. In the load cases defined for quartering waves all motions are considered but factors are applied to surge, sway, roll and pitch motion. Besides, for the calculation of the minimum reaction loads and uplift factor of 0.85 is applied to the static weight of the jacket. In the load cases the signs of the inertia load directions are chosen such that the highest reaction loads are calculated for the load cases when focusing on maximum reaction loads and the lowest reaction loads are calculated for the load cases when focusing on the minimum reaction loads. Finally, the governing maximum and minimum reaction loads out of all load cases are taken as the final result of the current calculation method. From this it can already be concluded that the current method cannot be used to calculate the reaction loads for the various sea states but it is likely that the current method calculates reaction loads which are only expected in the governing sea states.

The second calculation method is introduced to reduced the uncertainty of combining inertia loads which have been calculated with 3-hour MPE values of accelerations obtained in different sea states.

The current load combination method will be used, but now the 3-hour MPE values of accelerations obtained in the same sea state will be used:

> **Method 2:** ***Current method same sea state -*** This method is similar to the current calculation method. The same load cases are considered. However, instead of using 3-hour MPE values of acceleration signals coming from different sea state, 3-hour MPE values calculated from acceleration signals obtained in the same sea state will be used. The current method is thus applied for every sea state individually and the resulting reaction loads will be different for every sea state. It should be noted that besides the current method, this method is also widely applied in the industry.

The third calculation method is introduced to reduce the uncertainty of the used load cases in the current load combination method:

> **Method 3:** ***Same sea state governing directions -*** In this method again the 3-hour MPE values of the acceleration motions obtained in the same sea state are used to calculate the inertia loads. But in this method the defined load cases of the current method are neglected. Instead of the load cases, the inertia loads caused by all motions are combined without factors and independent of the considered wave heading angle. The signs of the inertia loads directions are still chosen such that they result in the highest reaction loads when the maximum reaction loads are considered and the lowest reaction loads when the minimum reaction loads are considered. This can be explained with the help of Figure 5.4 in which the load scheme and formulas are given to calculate the vertical reaction load F_{vA} for leg A. It is given in Table 5.1 how the signs of the directions of the accelerations a_x, a_z and r_y are chosen such that they result in the maximum and minimum vertical reaction load for leg A.

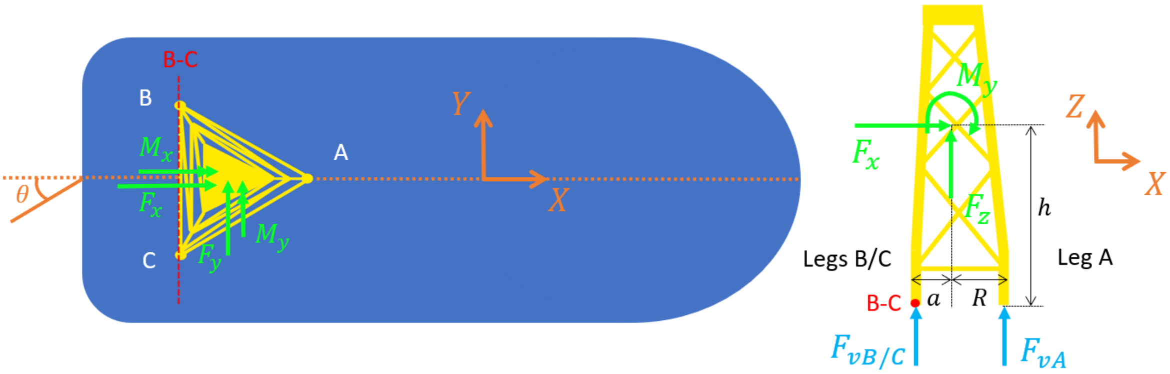

$$F_x = m \cdot a_x + F_w \cdot \cos\theta$$
$$F_z = m \cdot a_z - F_{static}$$
$$M_y = I_{yy} \cdot r_y$$

Figure 5.4: Load scheme to calculate the vertical reaction loads for leg A

Table 5.1: Signs of acceleration directions are chosen such that the inertia loads contribute to maximum and minimum reaction loads

	Maximum F_{vA}	Minimum F_{vA}
a_x	$+$ MPE-a_x	$-$MPE-a_x
a_z	$-$ MPE-a_z	$+$ MPE-a_z
r_y	$+$ MPE-r_y	$-$ MPE-r_y

The fourth calculation method is introduced to reduce the uncertainty of choosing the directions of the loads such they results in governing reaction loads. Instead, in this combination method the directions of the loads are combined according to information on the signs of the acceleration directions observed in the motion analysis for each sea state:

> **Method 4: *Same sea state empirical directions* -** This method is similar to the previous method except for the fact that the directions of the loads are not chosen such that the maximum and minimum reaction loads are calculated. Instead, the signs of the acceleration directions are chosen based on empirical information from the performed simulations. From the obtained reaction loads time series for each sea state the maximum and minimum reaction loads for each of the legs are identified. Once the maximum and minimum reaction loads for each leg have been found, the directions of accelerations at the time step of the maximum and minimum reaction loads are taken. These directions are used in this method such that the loads are combined according to empirical observed directions.

An overview of the introduced methods of combining loads is given in Table 5.2.

Table 5.2: Overview of the introduced calculation methods

1. Current method:	**2. Current method same sea state:**
• MPE values calculated for different sea states are assumed to happen at the same moment in time • Loads are combined according to load cases • Depending on the load case, not all motions are considered • The directions of the loads are chosen such that they all contribute to governing reaction loads • For the minimum reaction loads an uplift factor of 0.85 is applied to the static jacket weight • The final reaction loads are the governing maximum and minimum reaction loads out of all load cases	• MPE values from the same sea state are assumed to happen at the same moment in time • Loads are combined according to load cases • Depending on the load case, not all motions are considered • The directions of the loads are chosen such that they all contribute to governing reaction loads • For the minimum reaction loads an uplift factor of 0.85 is applied to the static jacket weight • The final reaction loads are the governing maximum and minimum reaction loads out of all load cases
3. Same sea state governing directions:	**4. Same sea state empirical directions:**
• MPE values from the same sea state are assumed to happen at the same moment in time • The load cases of the current method are neglected • The inertia loads of all motions are considered • The directions of the loads are chosen such that they all contribute to governing reaction loads	• MPE values from the same sea state are assumed to happen at the same moment in time • The load cases of the current method are neglected • The inertia loads of all motions are considered • The directions of the inertia loads are chosen based on acceleration directions observed at the time step at which the highest reaction load occurs in time series

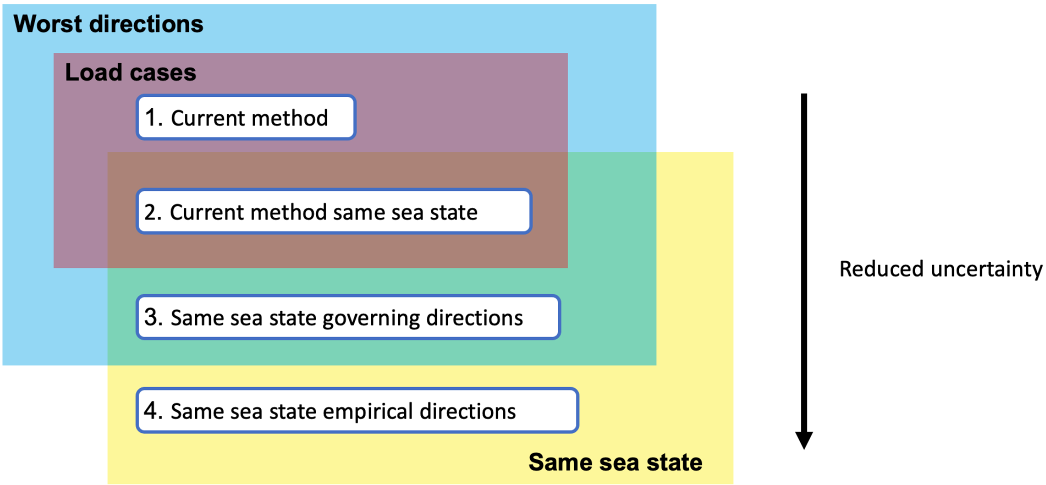

Table 5.3: Illustration of the introduced load combination methods for reduced uncertainty

5.3. Probabilistic investigation of load combination methods

To investigate the different load combination methods which have been introduced in the previous section, first the maximum and minimum reaction loads for the individual jacket legs for each sea state are calculated with these methods. The simplified rigid jacket calculation method is used to calculate the reaction loads for the different load combination methods. Once the resulting reaction loads have been obtained with the different load combination methods, the 3-hour extreme value density functions of the reaction loads are used to investigate the reaction loads in terms of probability.

In Figure 5.5 an example is given for the maximum reaction load for leg C for a simulation corresponding to a sea state with a wave heading angle θ = 90° and a peak period of T_p = 12.0s. It should be noted that this is the sea state for which the highest maximum and lowest minimum 3-hour MPE value of the vertical reaction load F_{vC} was observed. The calculated vertical reaction loads F_{vC} obtained with the different load combination methods are given in this figure by vertical lines, each having its own color. In addition, the 3-hour MPE value of F_{vC} is given by a vertical green line.

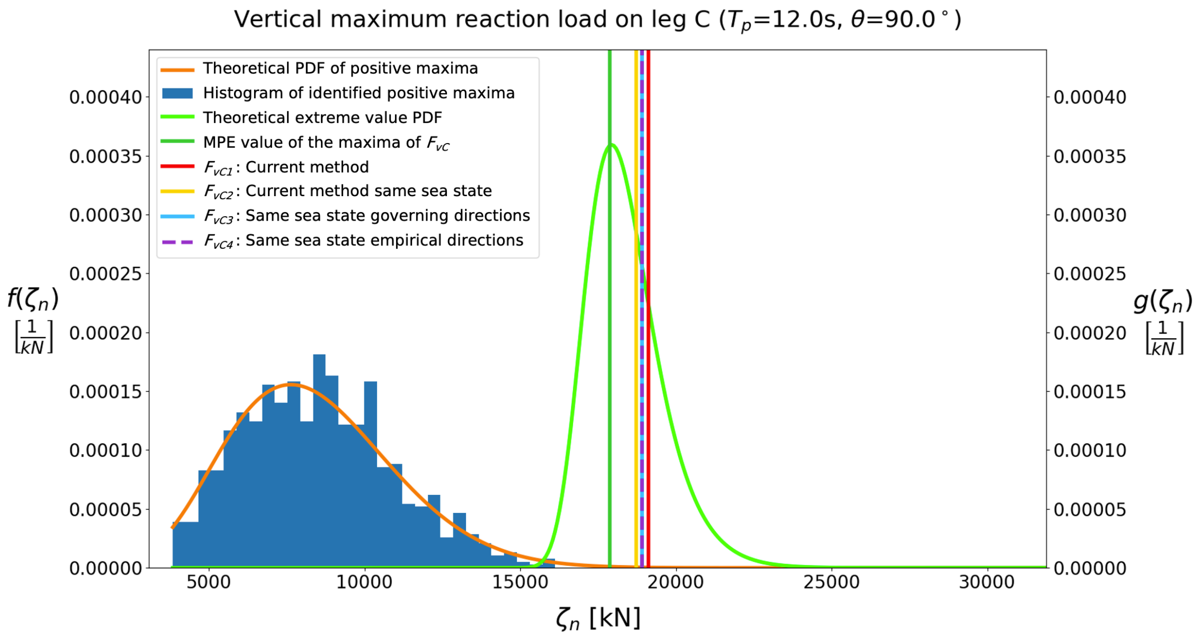

Figure 5.5: Maximum vertical reaction loads F_{vC} calculated with the different methods of combining inertia loads plotted together with the extreme value distribution for the same simulation

In Figure 5.6 the same results are presented for the minimum reaction loads F_{vC} for the same sea state.

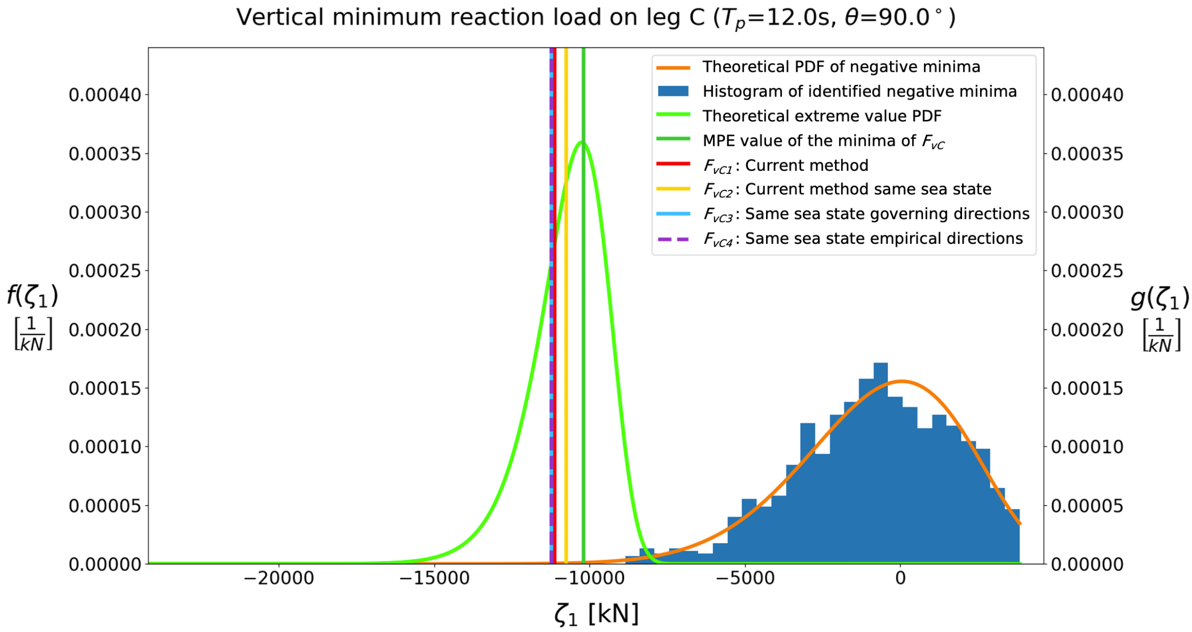

Figure 5.6: Minimum vertical reaction loads F_{vC} calculated with the different methods of combining inertia loads plotted together with the extreme value distribution for the same simulation

As a next step, the probabilities that the calculated reaction loads are exceeded by the 3-hour extreme value of the reaction loads are derived for the different load combination methods. These probabilities can be determined from the 3-hour extreme value density function of the reaction loads. For the maximum reaction loads, the probability that the 3-hour extreme value ζ_n of the reaction loads is higher than the reaction load F_v calculated with the different load combination methods is obtained by integration of the extreme value PDF of the maxima $g(\zeta_n)$:

$$P(\zeta_n \geq F_v) = \int_{F_v}^{\infty} g(\zeta_n) d\zeta_n \tag{5.7}$$

The results for the chosen sea state are given in the following table where x in the subscript of F_{vCx} corresponds to the different combination methods which have been numbered in the previous section:

Table 5.4: Calculated maximum vertical reaction loads and probabilities of being exceeded by 3-hour extreme value ζ_n

T_p [s]	Heading [deg]	MPE [kN]	$P(\zeta_n \geq$ MPE) [-]	F_{vC1} [kN]	$P(\zeta_n \geq F_{vC1})$ [-]	F_{vC2} [kN]	$P(\zeta_n \geq F_{vC2})$ [-]
12.0	90	17867	0.606	19108	0.232	18732	0.321

T_p [s]	Heading [deg]	F_{vC3} [kN]	$P(\zeta_n \geq F_{vC3})$ [-]	F_{vC4} [kN]	$P(\zeta_n \geq F_{vC4})$ [-]
12.0	90	18921	0.283	18921	0.283

For the minimum reaction loads, the probability that the 3-hour extreme value ζ_1 of the minima is lower than the calculated vertical reaction loads F_v is obtained by integration of the extreme value PDF of the minima $g(\zeta_1)$:

$$P(\zeta_1 \leq F_v) = \int_{-\infty}^{F_v} g(\zeta_1) d\zeta_1 \tag{5.8}$$

The results for the minimum reaction loads for the chosen sea state are given in the following table:

Table 5.5: Calculated minimum vertical reaction loads and probabilities of a lower 3-hour extreme value ζ_1

T_p [s]	Heading [deg]	MPE [kN]	$P(\zeta_1 \leq \text{MPE})$ [-]	F_{vC1} [kN]	$P(\zeta_1 \leq F_{vC1})$ [-]	F_{vC2} [kN]	$P(\zeta_1 \leq F_{vC2})$ [-]
12.0	90	-10181	0.606	-11123	0.302	-10747	0.430

T_p [s]	Heading [deg]	F_{vC3} [kN]	$P(\zeta_1 \leq F_{vC3})$ [-]	F_{vC4} [kN]	$P(\zeta_1 \leq F_{vC4})$ [-]
12.0	90	-11229	0.283	-11229	0.283

In Appendix E the figures and tables which have just been presented for leg C, are also presented for legs A and B. The figures and tables are again presented for the sea states for which the highest 3-hour MPE values of the reaction loads were observed for these legs.

The probabilities which have been presented in Table 5.4 for one sea state, can also be presented in figures for a range of sea states. In this section two types of figures are presented. From these figures it can be seen whether for various sea states consistent probabilities are obtained with the different load combination methods. Besides, the probability that the 3-hour MPE values of the reaction loads are exceeded by the 3-hour extreme values is also included in the figures. In Figure 5.7 the probabilities are presented for a fixed peak period $T_p = 12.0$s and for the full range of wave heading angles θ. The probabilities are given for the maximum reaction loads F_{vC} for leg C. From this type of figure it could be concluded whether consistent probabilities are obtained for sea states of different wave heading angles but a fixed peak period.

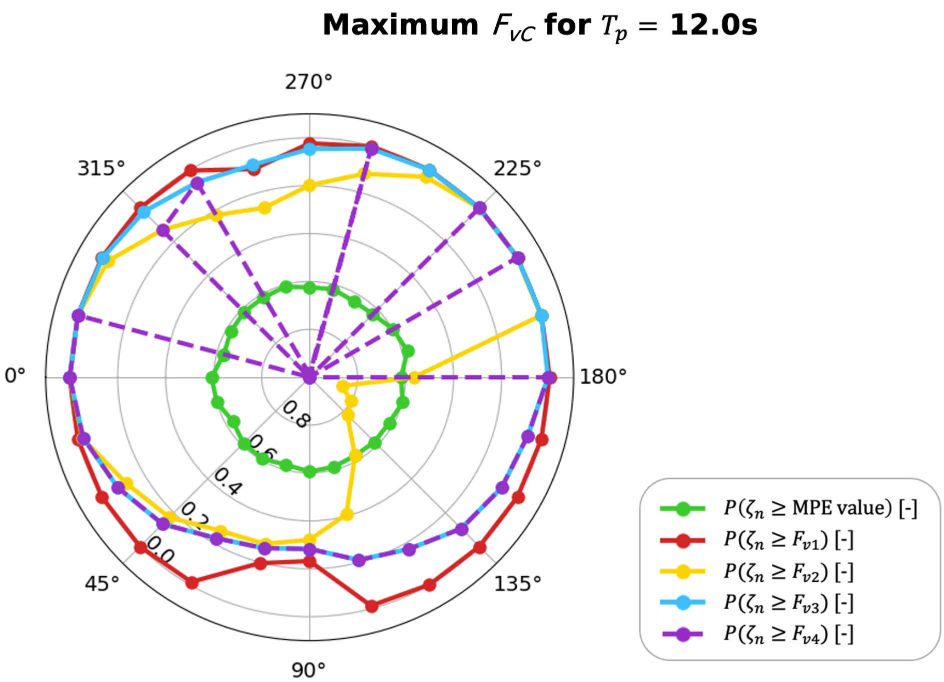

Figure 5.7: For the different load combination methods the probabilities are presented for a fixed peak period and a range of wave heading angles

The second type of figure is given in Figure 5.8. In this figure the probabilities are presented for a fixed wave heading angle $\theta = 90°$ and for the full range of peak periods T_p. The probabilities are again given for the maximum reaction loads FvC for leg C. From this type of figure it could be concluded whether consistent probabilities are obtained for sea states of different peak periods but for a fixed wave heading angle.

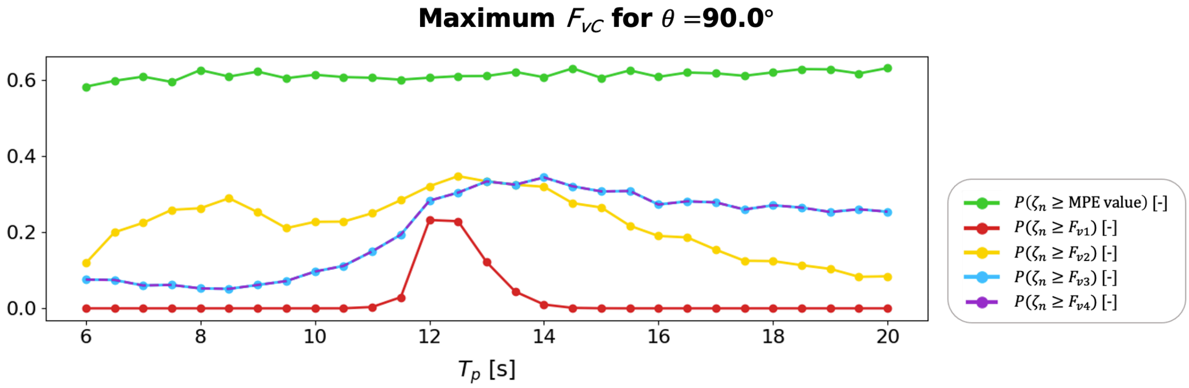

Figure 5.8: For the different load combination methods the probabilities are presented for a fixed wave heading angle and a range of peak periods

In Appendix E the plots for the maximum and minimum reaction loads of all jacket legs are presented. From these figures it can be observed:

- As concluded before, the current calculation method only calculates reaction loads which have a realistic probability of being experienced in sea states for which the highest reaction loads are expected. This is caused by the fact that in the current load combination method the inertia loads are calculated with the maximum 3-hour MPE values of the accelerations out of all 3-hour MPE values obtained for each sea state.
- However, for the sea states for which the highest reaction loads for leg A are expected, the probabilities are still considered quite small when the current method is applied: $P(\zeta_n \geq F_{vA1}) =$ 6.50$\cdot$ 10^{-5} and $P(\zeta_1 \leq F_{vA1}) =$ 1.79$\cdot$ 10^{-4}. For leg A the highest reaction loads are expected in the sea state for which the the most pitch motion is observed ($T_p =$ 9.5s and $\theta =$ 150°).
- For legs B and C the probabilities in the governing sea states are higher: $P(\zeta_n \geq F_{vB1}) =$ 0.237, $P(\zeta_1 \leq F_{vB1}) =$ 0.301, $P(\zeta_n \geq F_{vC1}) =$ 0.232 and $P(\zeta_1 \leq F_{vC1}) =$ 0.302. For these legs the highest reaction loads are expected for sea states in which the most roll motion is expected (beam waves with peak period in the range of the natural roll period $T =$ 12.6s)
- Unsurprisingly, the 3-hour MPE values of the reaction loads show consistent probabilities of approximately $P \approx$ 0.61. Although this same probability is used for the 3-hour MPE values of the accelerations which have been used as input to the partial-probabilistic load combination methods, for none of the combination methods this same probability is observed for the calculated reaction loads. It can therefore be concluded that using 3-hour MPE values of the accelerations as input to the partial probabilistic load combination method does not result in 3-hour MPE values of the reaction loads.
- In addition, none of the introduced load combination methods shows consistent results in the probability that the calculated reaction loads are exceeded by the 3-hour extreme value of the reaction loads for different sea states. This holds even for the introduced load combination methods with reduced uncertainty.
- The partial-probabilistic method is therefore considered not suited to be used to determine reaction loads in a specific sea state for which a desired probability of being exceeded by the 3-hour extreme value of the reaction loads is expected.

5.4. Findings

The main finding of this chapter is that the current load combination method which might be considered partial-probabilistic should be replaced by the probabilistic method based on EVT in order to describe the reaction loads in a true probabilistic way for each sea state. Other findings are summarized below:

- With the simplified rigid jacket calculation method a relatively quick and efficient method is introduced to obtain vertical reaction load time series from acceleration time series which have been obtained with the motion analysis. The method was found to be accurate enough for the purpose of illustrating a probabilistic calculation method of the reaction loads in this thesis. However, when it is desired to accurately calculate reaction loads it is still recommended to perform a structural FEM analysis.

- The obtained reaction load time series allowed to apply the EVT introduced in the previous chapter. With this theory, 3-hour extreme value density functions of the reaction loads have been derived. These density functions could be used to interpret reaction loads in terms of probability when it is known or assumed that that a certain sea state will be encountered.

6
Long-term probabilistic calculation method

In the previous chapter a probabilistic method of describing the reaction loads for each given 3-hour stationary sea state was introduced. However, in the design phase of a sea fastening structure it is not known which sea states will be encountered during a transport. Besides, when multiple transport are to performed the sea states which are encountered might be different for every transport. In order to obtain a true probabilistic method which can be used to estimate the probability of occurrence of reaction loads during transports, the probability of encountering various sea states should be accounted for.

In this chapter the long-term probability of encountering various sea states at an offshore location is presented in section 6.1 by introducing wave scatter diagrams. In section 6.2 a long-term probabilistic calculation method of the reaction loads is derived by combining the 3-hour extreme value density functions of the reaction loads for each sea state with the long-term probability of encountering these sea states. Thereafter, in section 6.3 this derived long-term probabilistic calculation method is used to evaluate the results of the current calculation method in terms of probability of occurrence.

6.1. Long-term sea state probability

In the planning phase of marine operations, such as a sea voyage, the environmental conditions and criteria should be determined. It is stated in DNV-ST-N001 [6] that each marine operation shall be designed to withstand the expected loads caused by the most adverse environmental conditions. For sea voyages, it is prescribed that the different areas and seasons in which the voyage will take place should be accounted for. For each phase of the voyage the design sea state, wind and if relevant current should be defined. If applicable, any mitigation measures should also be specified.

Long-term wave climatology can be used to describe the statistical probability od encountering certain sea states during a sea voyage [9]. This probability can be determined by collecting 3-hour sea state characteristic wave data given by the significant wave height H_s and peak period T_p and possibly also wave heading angle θ. This wave data can be presented in wave scatter diagrams. For the transport considered in the case study for this thesis, the $H_s - T_p$ scatter diagram for the location on the route for which the most extreme wave conditions are expected based on long-term wave data the is presented in Figure 6.2. In Figure 6.1 this location on the route is given together with the conventions for the wave heading angle θ.

Confidential information

Figure 6.1: Location on the route for which the most extreme wave conditions are expected based on long-term wave data

Confidential information

Figure 6.2: Wave scatter diagram for the location on the route for which the most extreme wave conditions are expected based on long-term wave data

This wave scatter diagram can be used to determine the long-term probability of occurrence of a 3-hour stationary sea state at the given location. The value in each cell in the diagram divided by 100 represents the long-term probability of occurrence $P(h_{s,i} \cap t_{p,j})$ of a sea state with a significant wave height and peak period within the intervals of this cell. The rows of the diagram specify the significant wave height intervals $h_{s,i}$ whereas the columns represent the peak period intervals $t_{p,j}$ for the sea states. It should be noted that cells with a given value of 0 have an actual value which is less than 0.5 and therefore rounded to 0. On the other hand, cells without a specified value have a value which is very low and approaching zero.

For the project considered in this thesis, motion analyses were performed for sea states described by a significant wave height $H_s =$?m and a range of peak periods $T_p =$?s. The sea fastening design should therefore be expected to be able to withstand loads calculated for sea states with significant waves height $H_s \leq$?m and the sea voyage should not be performed or mitigation measures should be taken when sea states with higher significant wave heights are expected. From the scatter diagram the probability that a sea state for which $H_s \geq$?m is encountered at the given offshore location can be calculated as follows:

$$P(H_s \geq \text{?m}) = \frac{5+4+9}{100} = 0.18 \tag{6.1}$$

As can be seen from the scatter diagram, sea states with a significant wave height of $H_s =$?m are exactly on the edge of two intervals. It is chosen to consider the cells in the significant wave height range $H_s =$?m as indicated with red borders. This range is conservatively chosen for as the number of observations for the simulations are higher than for the range of $H_s =$?m. The same problem holds for the peak period intervals. For every sea state described by a peak period which has a value on the edge of two intervals, the neighbouring cell containing the highest probability is conservatively chosen for. However, when constructing the wave scatter diagrams from the long term data it is recommended to choose the intervals such that the used significant wave height and peak periods for the motion analyses fall into the intervals.

In DNV-ST-N001 [6] it is prescribed that directional variations of the environmental design data may be used. Besides $H_s - T_p$ scatter diagrams, it might therefore also be interesting to consider wave scatter diagrams which contain 3-hour sea state characteristic wave data given by significant wave height H_s and wave heading angle θ. Where the wave heading angle follows the conventions presented in Figure 6.1. In such a scatter diagram the value of each cell divided by 100 represents the long term probability of occurrence $P(h_{s,i} \cap \theta_k)$ of a sea state within a H_s-interval and θ-interval. The rows of the diagram specify the significant wave height intervals $h_{s,i}$ whereas the columns represent the wave heading angle intervals θ_k of the sea states. For the specific project considered in this thesis, the $H_s - \theta$ scatter diagram for the location on the route with the most extreme wave conditions is presented in Figure 6.3. For this scatter diagram the sea states of the considered project are also conservatively assumed to be within the $H_s =$?m interval as indicated with red borders in the figure. By looking at the route in Figure 6.1 it is assumed that the orientation of the vessel at the considered offshore location is such that the wave heading angle θ of the wave scatter diagram aligns with the wave heading angle relative to the vessel as described in Figure 2.6.

Confidential information

Figure 6.3: Directional wave scatter diagram for the location on the route for which the most extreme wave conditions are expected based on long-term wave data

Seasonal scatter diagrams
It should be noted that the presented scatter diagrams are annual scatter plots which have been obtained by collecting long-term data throughout the entire year. In DNV-ST-N001 [6] it is also prescribed that seasonal variations may be used. When long term seasonal wave data is available it is possible to obtain wave scatter diagrams for each month of the year. This can be done for both the $H_s - T_p$ and the directional $H_s - \theta$ wave scatter diagrams. For most offshore locations the probability of encountering severe sea states is different for winter months than summer months. Depending on whether the sea fastening should be designed for a single sea voyage at a known time of the year or for multiple transports during multiple months or seasons, it might be beneficial to consider monthly or seasonal scatter diagrams instead of yearly diagrams.

For the considered offshore location the monthly $H_s - T_p$ wave scatter diagrams for the months January and July are presented in Figure 6.4 and Figure 6.5. From the diagrams it can be clearly seen that in the winter month January there is a much higher probability on sea states with high significant wave heights H_s than in July. As calculated from the yearly wave scatter diagram, the probability $P(H_s \geq ?\text{m})$ is equal to 0.18. While for the months January and July this probability is:

$$
\begin{aligned}
P_{Jan}(H_s \geq ?\text{m}) &= \frac{9+8+25}{100} = 0.42 \\
P_{Jul}(H_s \geq ?\text{m}) &= \frac{1+0+0}{100} = 0.01
\end{aligned}
\tag{6.2}
$$

Depending on the sea voyage it might therefore be interesting to consider long term seasonal wave data in the design process of the sea fastening.

Confidential information

Figure 6.4: Wave scatter diagram for the month January for the considered offshore location

Confidential information

Figure 6.5: Wave scatter diagram for the month July for the considered offshore location

In the monthly directional $H_s - \theta$ wave scatter diagrams it is also observed that there is a higher probabilities on sea states with high significant wave height H_s in January. For the months January and July no significant difference is observed between wave headings in the directional $H_s - \theta$ wave scatter diagrams.

6.2. Long-term probabilistic calculation method

In the previous chapter, for each sea state the 3-hour extreme value density functions of the reaction loads have been obtained for the different legs. The 3-hour extreme value density functions have been computed for a significant wave height H_s = ?m and for peak periods in the range T_p = ?s and wave headings in the range θ = 0-345deg.

Instead of using 3-hour time periods, the most accurate approach of determining the design reaction loads would be to use long-term statistics of the reaction loads. However, computing long-term response calculations for changing sea states is very challenging and time consuming. Therefore, an approach of estimating a long-term density function of the 3-hour extreme values of reaction loads for a non-stationary long-term period with changing sea states is presented in [14]. Where the formulation long-term is used to express the fact that the method accounts for the various sea states which might be encountered during this long-term period.

As mentioned, a long-term time period T is introduced which is considered non-stationary due to changing environmental conditions. This long-term duration can be interpreted as a sequence of 3-hour stationary periods in which the environmental conditions do not change. The introduced method is based on combining the conditional extreme value density functions $g(\zeta_n|h_s, t_p, \theta)$ of the reaction loads with the probability of encountering the corresponding sea state characterized by H_s, T_p and θ. To be accurate, conditional extreme value distributions of the reaction loads should be determined for all sea states even though some sea states are expected to have little influence on the design reaction loads. After the conditional extreme value distributions are obtained, a long-term PDF of the 3-hour extreme value ζ_n of the reaction loads is approximated as follows:

$$g_{LT}(\zeta_n) = \int_{h_s}\int_{t_p}\int_{\theta} g(\zeta_n|h_s, t_p, \theta) \cdot f_{H_s T_p \theta}(h_s, t_p, \theta) dh_s dt_p d\theta \tag{6.3}$$

Where $f_{H_s T_p \theta}(h_s, t_p, \theta)$ reflects the relative frequency of encountering the various sea states during the long-term period T. When it is known which sea state will be encountered when passing the considered location on the route, the 3-hour conditional extreme value distribution provides information on the extreme value of the reaction load during this 3-hour sea state. However, during the design phase of the sea fastening it is unknown which sea state will be encountered when passing the considered location on the route. In case it is unknown which sea state will be encountered, the long-term extreme value distribution $g_{LT}(\zeta_n)$ provides information on the 3-hour extreme value of the reaction loads in an unknown 3-hour sea state.

When adequate $H_s - T_p$ and $H_s - \theta$ scatter diagrams are available, $f_{H_s T_p \theta}(h_s, t_p, \theta)$ can be approximated with the information contained in these scatter diagrams. The long-term PDF $g_{LT}(\zeta_n)$ of the 3-hour extreme values can be written as:

$$g_{LT}(\zeta_n) \approx \sum_{i=1}^{N_{H_s}} \sum_{j=1}^{N_{T_p}} \sum_{k=1}^{N_\theta} g(\zeta_n|h_i, t_j, \theta_k) \cdot P(h_{s,i} \cap t_{p,j} \cap \theta_k) \tag{6.4}$$

By using scatter diagrams the PDF $f_{H_s T_p \theta}(h_s, t_p, \theta)$ is discretized into N_{H_s} significant wave height intervals, N_{T_p} peak period intervals and N_θ wave heading intervals. The probability of encountering a sea state with characteristic parameters within the intervals given by $h_{s,i}$, $t_{p,j}$ and θ_k is denoted by $P(h_{s,i} \cap t_{p,j} \cap \theta_k)$. By assuming the probabilities $P(h_{s,i})$, $P(t_{p,j})$ and $P(\theta_k)$ to be independent, $P(h_{s,i} \cap t_{p,j} \cap \theta_k)$ can be computed with the probabilities $P(h_{s,i} \cap t_{p,j})$ and $P(h_{s,i} \cap \theta_k)$ coming from the scatter diagrams:

$$P(h_{s,i} \cap t_{p,j} \cap \theta_k) = \frac{P(h_{s,i} \cap t_{p,j}) \cdot P(h_{s,i} \cap \theta_k)}{P(h_{s,i})} \tag{6.5}$$

It is shown here that this holds when the probabilities are assumed to be independent:

$$
\begin{aligned}
P(h_{s,i} \cap t_{p,j} \cap \theta_k) &= \frac{P(h_{s,i} \cap t_{p,j}) \cdot P(h_{s,i} \cap \theta_k)}{P(h_{s,i})} \\
&= \frac{P(t_{p,j}|h_{s,i}) \cdot P(h_{s,i}) \cdot P(\theta_k|h_{s,i}) \cdot P(h_{s,i})}{P(h_{s,i})} \\
&= P(t_{p,j}|h_{s,i}) \cdot P(\theta_k|h_{s,i}) \cdot P(h_{s,i}) \\
&= P(t_{p,j}) \cdot P(\theta_k) \cdot P(h_{s,i})
\end{aligned} \tag{6.6}
$$

As mentioned in [14], one should be careful when using scatter diagrams in this long-term probabilistic method. Especially, when scatter diagrams are not very refined as is the case with the scatter diagrams presented in the previous section. When scatter diagrams are not very refined, the resolution in tail-regions might be poor and as a result the long-term extreme value estimates of the reaction loads may be inaccurate. In case of scatter diagrams with poor resolution it is recommended to use smooth joint PDFs for the parameters characterizing the short-term sea states.

When the long-term PDF $g_{LT}(\zeta_n)$ of the 3-hour extreme value has been obtained, it can be used to calculate the probability that a design reaction load F_v is exceeded by the 3-hour extreme value ζ_n of the reaction load in an unknown 3-hour sea state:

$$
\begin{aligned}
P_{LT}(\zeta_n \geq F_v) &= \int_{F_v}^{\infty} g_{LT}(\zeta_n) d\zeta_n \\
&\approx \sum_{i=1}^{N_{H_s}} \sum_{j=1}^{N_{T_p}} \sum_{k=1}^{N_\theta} \int_{F_v}^{\infty} g(\zeta_n|h_{s,i}, t_{p,j}, \theta_k) d\zeta_n \cdot P(h_{s,i} \cap t_{p,j} \cap \theta_k)
\end{aligned} \tag{6.7}
$$

It should be noted here that per sea state interval only one 3-hour conditional extreme value distribution $g(\zeta_n|h_i, t_j, \theta_k)$ should be used. Otherwise the summation of the sea state probabilities would not add up to one:

$$
\sum_{i=1}^{N_{H_s}} \sum_{j=1}^{N_{T_p}} \sum_{k=1}^{N_\theta} P(h_{s,i} \cap t_{p,j} \cap \theta_k) \neq 1 \tag{6.8}
$$

Since the calculated long-term probability $P_{LT}(\zeta_n \geq F_v)$ accounts for the various sea states which might be encountered during the long-term non-stationary time period, this probability can be expressed by a return period. The return period is determined as follows:

$$
\begin{aligned}
T_{r,years} &= \frac{1}{365 \cdot 8 \cdot P_{LT}(\zeta_n \geq F_v)} \\
T_{r,days} &= \frac{1}{8 \cdot P_{LT}(\zeta_n \geq F_v)}
\end{aligned} \tag{6.9}
$$

The return period denotes the expected average long-term non-stationary period T_r between successive events of the design reaction load F_v being exceeded by 3-hour extreme values of the reaction loads in the various sea states. For the design of sea fastening structures, this introduced method can also be used in reverse to determine the design reaction loads. By using the method in reverse, the design reaction loads F_v can be determined for acceptable return periods. Acceptable return periods to ensure a required target reliability could be defined by performing structural reliability analyses of the sea fastening structures.

In this section the method was introduced for the maximum reaction loads, but the same method can be applied for the minimum reaction loads as well.

6.3. Probabilistic investigation of current calculation method

Although the current calculation method is often referred to as being conservative, it remains unknown what is the probability of occurrence of the reaction loads during transports. Therefore, in this section the introduced long-term probabilistic method is applied to determine the return periods T_R for the reaction loads calculated with the current method. The return periods are calculated for both the maximum and minimum reaction loads of the different jacket legs.

As a first step Equation 6.7 is used to calculate the probabilities that the design reaction loads F_v calculated with the current method are exceeded by the 3-hour extreme value in an unknown sea state:

$$\begin{aligned} P_{LT}(\zeta_n \geq F_v) &\approx \sum_{i=1}^{N_{H_s}} \sum_{j=1}^{N_{T_p}} \sum_{k=1}^{N_\theta} \int_{F_v}^{\infty} g(\zeta_n | h_{s,i}, t_{p,j}, \theta_k) d\zeta_n \cdot P(h_{s,i} \cap t_{p,j} \cap \theta_k) \\ &\approx \sum_{i=1}^{N_{H_s}} \sum_{j=1}^{N_{T_p}} \sum_{k=1}^{N_\theta} P(\zeta_n | h_{s,i}, t_{p,j}, \theta_k \geq F_v) \cdot P(h_{s,i} \cap t_{p,j} \cap \theta_k) \end{aligned}$$

Once the probabilities are obtained, these are used in Equation 6.9 to calculate the return periods for the different reaction loads calculated with the current method:

$$\begin{aligned} T_{r,years} &= \frac{1}{365 \cdot 8 \cdot P_{LT}(\zeta_n \geq F_v)} \\ T_{r,days} &= \frac{1}{8 \cdot P_{LT}(\zeta_n \geq F_v)} \end{aligned}$$

In the previous chapter the probabilities ($P(\zeta_n \geq F_{vA1})$, $P(\zeta_n \geq F_{vB1})$, $P(\zeta_n \geq F_{vC1})$, $P(\zeta_1 \leq F_{vA1})$, $P(\zeta_1 \leq F_{vB1})$, $P(\zeta_1 \leq F_{vC1})$) that the reaction loads calculated with the current method are exceeded by the 3-hour extreme value during have been computed for all sea states with significant wave height $H_s =$?m.

The motion analyses have only been performed for sea states with significant wave height $H_s =$?m. In the previous section it was assumed that the sea states for which the motion analyses have been performed fall into the interval $H_s =$?m. The significant wave height $H_s =$?m is considered to be the upper limit which means that it should be avoided to sail in sea states described by higher significant wave heights. The contributions of sea state intervals of $H_s >$?m to the return periods are therefore neglected.

As mentioned in the previous section, it is most accurate to consider all possible sea states when calculating the return period. However, for the purpose of illustrating the introduced method for the reaction loads calculated with the current calculation method, the sea state intervals for $H_s \leq$?m are neglected. In the previous chapter it was shown for legs B an C that the current calculation method only has significant probabilities $P(\zeta_n \geq F_{v1})$ and $P(\zeta_1 \leq F_{v1})$ for sea states in which the highest reaction loads are expected (beam waves with peak periods close to the natural roll period $T_p =$?s). For leg A small probabilities were observed even for the sea state in which the highest reaction loads are expected (quartering waves with peak period $T_p =$?s). Although this is not entirely correct, it is assumed that the probabilities $P(\zeta_n \geq F_{v1})$ and $P(\zeta_1 \leq F_{v1})$ are low enough for sea state intervals with $H_s \leq$?m such that these sea states have little influence on $P_{LT}(\zeta_n \geq F_{v1})$ and $P_{LT}(\zeta_1 \leq F_{v1})$. In reality probabilities might approach zero but they are never exactly zero and therefore they will always have an influence on $P_{LT}(\zeta_n \geq F_{v1})$ and $P_{LT}(\zeta_1 \leq F_{v1})$. As a result of neglecting the sea state intervals of $H_s \leq$?m slightly higher return periods will be obtained.

As mentioned as well, for each sea state interval only one probability $P(\zeta_n \geq F_{v1})$ or $P(\zeta_1 \leq F_{v1})$ should be considered when calculating the return periods. It is chosen to take the highest probability obtained for the sea states within each sea state interval. The sea state probabilities $P(h_{s,i} \cap t_{p,j} \cap \theta_k)$ are computed from the scatter diagrams with Equation 6.5. It is explained in more detail in Appendix F how the sea state probabilities are determined from the wave scatter diagrams.

In the table below the calculated return periods for the maximum and minimum reaction loads calculated with the current method are given for the different legs.

Table 6.1: Calculated return periods for the reaction loads calculated with the current method

Load	T_r
Max. F_{vA}	850 years
Min. F_{vA}	248 years
Max. F_{vB}	18 days
Min. F_{vB}	16 days
Max. F_{vC}	23 days
Min. F_{vC}	45 days

For the maximum and minimum reaction loads F_{vA} for leg A, very long return periods have been obtained. This is not surprising as the probabilities $P(\zeta_n \geq F_{vA1})$ and $P(\zeta_1 \leq F_{vA1})$ for the sea state ($T_p =$ 9.5s, $\theta = 150$deg) in which the highest maximum and lowest minimum reaction loads F_{vA} are observed are already very low as can be seen from Appendix E. Besides, this sea state has a low probability of being encountered. The difference in the return periods for the maximum and minimum reaction loads is caused by the fact that for the sea states in the range of (T_p = 9.5s, $\theta = 150$deg) higher values for $P(\zeta_1 \leq F_{vA1})$ are calculated than for $P(\zeta_n \geq F_{vA1})$. The probability $P(\zeta_1 \leq F_{vA1})$ for the minimum reaction load is higher because in the current method an uplift factor is applied to the static weight of the jacket. Moreover, the wind loading is assumed to be in the same direction as the waves and for $\theta = 150$deg this causes the maximum loads to be lower such that $P(\zeta_n \geq F_{vA1})$ decreases and the negative minimum loads to be lower such that $P(\zeta_1 \leq F_{vA1})$ increases.

As shown in the previous chapter the highest maximum and lowest minimum reaction loads for legs B and C are observed for beam waves ($\theta = 90$deg and $\theta = 270$deg). The probabilities $P(\zeta_n \geq F_{vB1})$, $P(\zeta_1 \leq F_{vB1})$, $P(\zeta_n \geq F_{vC1})$ and $P(\zeta_1 \leq F_{vC1})$ are therefore relatively high for beam waves. As beam waves with $\theta = 270$deg have a high probability of being encountered the return periods for legs B and C are much shorter than for leg A.

The highest maximum and lowest minimum reaction loads for leg C are observed for $\theta = 90$deg while the highest maximum and lowest minimum reaction loads for leg B are observed for $\theta = 270$deg. This is likely to be caused by asymmetry in the motion analysis. In the case study used for this thesis the vessel is assumed to be symmetrically loaded and the jacket CoG is assumed to be perfectly aligned above the center line of the vessel. However, the input which has been used for the motion analysis is coming from a problem which is not perfectly symmetric. Because beam waves with $\theta = 270$deg have a high probability of being encountered the return periods for leg B are shorter than for leg C. For beam waves with $\theta = 270$deg, $P(\zeta_1 \leq F_{vC1})$ is significantly lower than $P(\zeta_n \geq F_{vC1})$ and therefore the return period for the minimum reaction load F_{vC} is longer than for the maximum reaction load F_{vC}.

The causes of the significant differences in return periods for the different reaction loads have just been explained. It is therefore expected that these significant differences are not caused by the uncertainties involved in the introduced calculation method of the return periods. However, one should be cautious when utilizing or interpreting the return periods as they might not be very accurate due to uncertainties incorporated in this calculation. Despite these uncertainties involved in the calculation of the return periods, the results can be used to asses the current calculation method:

- Depending on the position and orientation of the jacket on the vessel, the highest maximum and lowest minimum reaction loads for the individual legs are observed for different sea states. The current method does not account for the probability of encountering the various sea states which might be encountered. For this reason, significant differences in the return periods for the reaction loads corresponding to the different legs of the jacket may be observed when the reaction loads are calculated with the current method.
- As the calculated return periods may be very different for the individual legs, the structural reliability of the sea fastening structures for the individual legs may be far from consistent as well. While for some legs the structural reliability might just be ensured such that over conservative design is avoided, for other legs the structural reliability might easily be ensured resulting in over

conservative sea fastening structures. However, without knowing the acceptable return periods, it cannot be concluded whether structural reliability is ensured for sea fastening designs based on reaction loads calculated with the current method.

- As the calculated return periods for leg A are very long, it can be expected that the structural reliability of the sea fastening design based on the current calculation method will be ensured for this leg, even for very low structural target reliabilities. It is therefore also expected that the sea fastening design for leg A based on the reaction loads calculated with the current method is over-conservative.
- Without knowing the acceptable return periods to ensure a required target reliability, it can not be concluded whether the structural reliability is ensured for legs B and C. However, if the structural reliability of these sea fastening designs would be ensured it is not expected that the designs are over-conservative given the obtained short return periods.
- The fact that the introduced long-term probabilistic method accounts for the probability of encountering various sea states might be used as advantage during the design phase of sea fastening structures. The method could for example be used to find the optimal position and orientation of the jacket on the vessel based on the probabilities of various sea states. Depending on the route of the transport this might result in different orientations of the jacket.

Uncertainties in calculated return periods
As mentioned, one should be cautious when utilizing or interpreting the calculated return periods as they might not be very accurate due to uncertainties incorporated in this calculation. Some of these uncertainties are described below.

It was mentioned already that the continuous PDF $f_{H_sT_p\theta}(h_s, t_p, \theta)$ has been discretized and approximated by scatter diagrams. The used scatter diagrams are not very refined and poor resolution in the tail-regions might cause the calculated return periods to be not very accurate. If sufficient environmental data is available it is recommended to construct more refined scatter diagrams to reduce the uncertainty in the return periods.

It should also be taken into account that the return periods are calculated with wave scatter diagrams which are based on yearly long-term wave conditions. This might be a fair approach when during the design phase of the sea fastening it is not known yet in which month of the year the sea voyage will take place. However, when it is known in which period of the year the sea voyage will take place, more reliable return periods could be calculated by considering monthly or seasonal wave scatter diagrams.

It should also be noted that in the motion analysis of the current method non-linear viscous effects are accounted for. It was explained in section 3.3 that viscous damping effects are determined only for the sea states in which the governing roll motions are expected. It was also mentioned that when this same roll damping is applied to the motion analysis for sea states in which less roll motion is expected, the obtained roll, sway and yaw motions are likely to be underestimated. If the correct roll damping would be applied for the motion analysis of each sea state, slightly shorter return periods are expected.

6.4. Findings

The main finding of this chapter is that the introduced long-term probabilistic method, which accounts for the probability of encountering various sea states, can be used to make tailored sea fastening designs based on the characteristics of a specific transport. In addition, once acceptable return periods are determined through structural reliability analysis, the long-term probabilistic approach can be employed to determine design reaction loads which ensure a certain structural target reliability without being over-conservative. Other findings are summarized below:

- Depending on whether the sea fastening is to be designed for a repetitive sea voyage in multiple seasons or for a single sea voyage at a known time of the year is considered, seasonal or monthly wave conditions might be considered as input for the long-term probabilistic method. This might influence the design reaction loads in a positive way.
- Depending on the position and orientation of the jacket on the vessel and on the probabilities of the various sea states which might be encountered, significant differences in return periods

might be obtained for the individual jacket legs. As a result, different structural reliabilities for the sea fastening structures of the individual jacket legs may be ensured. In addition, for different transports the structural reliabilities of the same sea fastening structures might be very different due to the heading of the vessel and differences in probability of encountering various sea states.

- Even for very low structural target reliabilities, it is very likely that the target reliability will be ensured for the sea fastening structure of leg A designed for the reaction loads which have been calculated with the current calculation method. This can be concluded based on the long return period obtained for this leg.
- Without knowing the acceptable return periods to ensure certain structural target reliabilities, it cannot be concluded whether the structural reliability of the sea fastening structures of legs B and C would be ensured. However, if a certain structural target reliability would be ensured it is not expected that the designs of the sea fastening structures are over-conservative due to the short return periods calculated for these legs.

7 Discussion

In the future, OWT components and their support structures are expected to keep increasing in size and weight. As a result, the reaction loads on sea fastening structures of these items during future transports are also expected to increase. The increasing reaction loads have various negative consequences which might become limiting factors for future transports. The current method of calculating the reaction loads which is widely used in the industry is often referred to as being conservative. In addition, when this method is used to calculate the reaction loads it remains unknown what is the probability of occurrence of these loads during transports. For these reasons the objective of this research was to enhance the current method of calculating the reaction loads by shifting from a conservative approach towards an optimized method of determining the reaction loads based on an acceptable probability of occurrence during transports.

7.1. Main findings

With the aim of this research in sight, the following main findings were uncovered:

- Statistical EVT was introduced for stationary Gaussian process with zero mean. By applying this EVT to the response acceleration signals, it was found that the extreme value density functions for narrow-banded processes and non-narrow-banded processes are similar when a fixed time period is considered.
- Consequently, this EVT was applied to reaction load time series which were obtained with an introduced simplified rigid jacket calculation method. By applying this EVT to the reaction load time series, 3-hour extreme value density functions of the reaction loads were obtained for every sea state.
- With these extreme value density functions it was shown that the current load combination method which might be considered partial-probabilistic, does not determine design reaction loads which have consistent probabilities of being exceeded by the 3-hour extreme value of the reaction loads for different sea states. For this reason it was recommended to use the 3-hour extreme value density functions of the reaction loads in a probabilistic calculation method instead of the current partial-probabilistic load combination method.
- A long-term probabilistic method was introduced, which accounts for the probability of encountering various sea states at the location on the route for which the most severe environmental conditions are expected. The method can be used to approximate the return periods of the 3-hour extreme values of the reaction loads exceeding the design reaction loads for the sea fastening structures. In addition, the method can be used in reverse to determine the design reaction loads based on acceptable return periods to ensure structural reliability of the sea fastening structures.
- The long-term probabilistic calculation method was used to approximate the return periods for the design reaction loads which have been obtained by using the current calculation method. Significant differences in return periods were obtained for the reaction loads of the individual jacket legs.

7.2. Interpretation of results

Depending on the orientation and the position of the jacket on the vessel, the governing reaction loads for the individual jacket legs are expected for different sea states. In this thesis, jacket leg A was positioned on the centerline while legs B and C were positioned close to the side shell of the vessel. It was observed that the governing reaction loads were mainly caused by roll and pitch motion of the vessel. From the orientation of the jacket it follows that the governing reaction loads for leg A were observed for sea states for which the largest pitch motion was observed (bow-quartering waves in the range of the natural pitch period T_{pitch}= ?s) while for legs B and C the governing reaction loads were observed for sea states in which the largest roll motion was observed (beam waves in the range of the natural roll period T_{roll} = ?s).

The return-periods which can be calculated with the introduced long-term probabilistic method are highest when the sea states for which the governing reaction loads are expected have a relatively high probability of being encountered. From the scatter diagrams in Figure 6.2 and Figure 6.3 it can be seen that the governing sea states for legs B and C have a relatively high probability of being encountered unlike the governing sea states for leg A. For these reasons very short return-periods were approximated for legs B and C and very long return periods for leg A. The combination of orientation of the jacket, the heading of the vessel and the probabilities of encountering various sea states at the chosen location on the route causes the considered case study being the perfect example to illustrate the introduced long-term probabilistic calculation method of the reaction loads.

For other transports, it is unlikely that worse combinations of jacket orientation and probability of encountering governing sea states for this orientation will be experienced. For this reason it can be expected that for other transports the return periods will be longer than those calculated for legs B and C and shorter than the return period of leg A. If it is assumed that the return periods for legs B and C are sufficiently long to ensure a desired structural reliability of the sea fastening structures, it is therefore expected that for all other transports a higher structural reliability is ensured for the sea fastening structures of legs B and C when the current calculation method is applied. This would confirm the presumption that the current calculation method can be considered conservative.

7.3. Implications of the research

The performed research provides a new insight into the method of designing sea fastening structures. In this research, the long-term probabilistic calculation method was introduced which could be applied in practice to design sea fastening structures for design reaction loads which have an acceptable probability of being experienced at the location for which the most severe wave conditions are expected. When acceptable return periods to ensure a desired target reliability are known, the introduced method can be applied to determine design reaction loads which ensure this desired structural target reliability while avoiding over-conservative design of the sea fastening structures. Instead of determining the design reaction loads in a conservative way without knowing what is the probability of experiencing these loads during transport, the design reaction loads can now be determined based on a desired structural target reliability.

In DNV-ST-N001 [6] it is prescribed that weather-unrestricted marine operations, such as a sea voyage, should be designed for environmental criteria which are determined from statistical environmental data with the of use prescribed return periods for waves and wind. It is stated that the intention of these prescribed return periods is to ensure a structural failure probability of less than $1 \cdot 10^{-4}$ per operation when being used with load, safety and material factors from the Load and Resistance Factor Design (LRFD) design method. However, instead of designing sea fastening structures for environmental conditions which have a prescribed return period, the design reaction loads could be optimized by designing for acceptable return periods of the reaction loads to ensure a desired structural target reliability.

The methodology of the long-term probabilistic calculation method could be applied in practice to design sea fastening structures which are tailored for the characteristics of a specific transport. This can be illustrated with two different transports which are shown in Figure 7.1. Transport 1 is the transport considered in this thesis whereas transport 2 is a hypothetical one. In the figure the dominant wave heading, described as the wave heading which has the highest probability of being encountered at the given location, is shown. For transport 1, this dominant wave heading corresponds to beam waves which would result is short return periods of the design reaction loads for legs B and C compared to leg A. For transport 2, this dominant wave heading corresponds to bow-quartering waves which might result in short return periods of the design reaction loads for leg A compared to legs B and C. With this simplified example it is shown that the long-term probabilistic calculation method could be applied to optimize the sea fastening designs for specific transports.

Confidential information

Figure 7.1: Illustration of two different transports which have different vessel headings at a given offshore location for which a dominant wave heading is expected

The introduced method of constructing the 3-hour extreme value density functions of the reaction loads, contributes to better understanding of the reaction loads in specific sea states. This might contribute to advancements regarding the planning and safety of sea voyages. By continuous monitoring of weather conditions just before and during transports, it can be estimated which sea states will be encountered. Since a better understanding of the reaction loads in specific sea states is gained, this information can be used to make decisions regarding which sea states should be avoided and which actions should be taken to minimize risks when these sea states will be encountered.

7.4. Limitations of the research

While this study has provided valuable insights, it is essential to acknowledge the limitations that may affect the applicability of the findings. The limitations are summarized below:

- The introduced EVT which is used in the long-term probabilistic method of determining the design reaction loads is only valid for stationary Gaussian process with zero mean. However, for response processes of motions or loads to be Gaussian distributed, these wave-induced responses should have a linear relation with the wave process. As stated in [14], the Gaussian assumption of the wave process gives a reasonably good approximation to reality. For these reasons, the introduced EVT should only be applied to linear wave-induced response signals. When a non-linear motion analysis is performed, other EVT should be applied for the long-term probabilistic method. In addition, when a linear-motion analysis is performed but the reaction load calculation in non-linear also other EVT should be applied.
- In this research, current is neglected and the wind loading is assumed to be a constant and static loading which is aligned with the wave heading angle. However, to obtain true probabilistic designs of sea fastening structures, a simultaneous probabilistic model of wind, wave and current loads should be obtained [14].
- To be able to conclude whether return periods of loads approximated with the long-term probabilistic method ensure a desired structural target reliability, first a structural reliability should be performed to determine the acceptable return periods corresponding to a desired structural target reliability. This structural reliability analysis should account for all the uncertainties regarding the reaction loads (for example those described in chapter 3) and the uncertainties regarding the resistance of the sea fastening structures. Once acceptable return periods of the loads to ensure a desired structural target reliability have been determined, these return periods can be used to determine the optimized reaction loads with the long-term probabilistic method.
- In the introduced long-term probabilistic method only one location on the route is considered. For the purpose of illustration the long-term probabilistic method it is chosen to only consider the location on the route for which the most severe environmental conditions are expected. However, it would be more accurate to perform the long-term probabilistic analysis for multiple locations on the route, especially when a long transport is considered. If nevertheless it is chosen for to consider only one location on the route, it is recommended to chose this location not only based

on most severe conditions but also on the orientation of the jacket, the heading of the vessel and the sea state probability for the different locations on the route.

- The long-term probabilistic method is considered an optimized method of calculating the design reaction loads in terms of probability of experiencing these loads during transport. However, since the simplified rigid jacket calculation method was used to obtain the 3-hour extreme value density functions of the reaction loads, the reaction loads obtained with the long-term probabilistic method might be considered optimized but not necessarily accurate. Even if a static FEM analysis of the jacket is performed, this is still a simplification and it would be most accurate to perform a dynamic structural analysis to obtain the exact reaction loads.
- In addition, when performing the structural analysis of the jacket in this research, the supports were considered to be rigid hinged supports. In reality the jacket is supported by the sea fastening structures which have a certain stiffness. Besides, the vessel structure and deck are also not rigid and have a certain stiffness as well. As the sea fastening structures of the individual legs are expected to be designed for different reaction loads, for each leg the combined stiffness of the structure and the vessel are expected to be different. To accurately perform a structural analysis to determine the reaction loads, the relative stiffness of the sea fastening structures and vessel should be accounted for.

8 Conclusion and future work

8.1. Conclusion

This research aimed to enhance the current calculation method of the reaction loads by shifting from a conservative approach towards an optimized method of calculating reaction loads based on an acceptable probability of occurrence during transports.

To achieve this research objective, a case study was performed for an existing sea fastening project from industry. The current calculation method was elaborated and applied to the chosen sea fastening project. Subsequently, EVT for stationary Gaussian processes with zero mean was introduced and investigated by applying this theory to the 3-hour linear wave-induced response accelerations of the jacket CoG. Thereafter, a simplified linear calculation method was introduced to obtain time series of the reaction loads from the response acceleration time series of the jacket CoG. Since a linear calculation method was used, the EVT could also be applied to the reaction load time series to obtain 3-hour extreme value density functions of the reaction loads for each sea state. These 3-hour extreme value density functions of the reaction loads were used to investigate whether the current load combination method could be applied in a probabilistic way. Finally, sea state probability was introduced and combined with the 3-hour extreme value density functions of the reaction loads for each sea state.

The findings of this research show that optimized reaction loads can be obtained by replacing the current calculation method by a long-term probabilistic method. It was found that this long-term probabilistic method could be derived by combining 3-hour extreme value density functions of reaction loads with the probabilities of encountering the various sea states at the location on the route for which the most severe environmental conditions are expected. The long-term probabilistic method was used to perform a probabilistic investigation of the reaction loads calculated with the current calculation method. It was found that the return periods of the reaction loads calculated with the current method were significantly different for the individual jacket legs. Moreover, it was found that the sea fastening design for at least one of the jacket legs was expected to be over-conservative. By presenting the long-term probabilistic calculation method, a methodology was introduced which determines reaction loads based on acceptable return periods while avoiding over-conservative sea fastening designs.

In conclusion, this research has provided a new inside into the method of designing sea fastening structures. The long-term probabilistic calculation method can be applied in practice to determine optimized reaction loads incorporated in sea fastening designs. This research therefore makes a valuable contribution to preparing the reaction load calculation method for future transports which are expected to become more critical due to OWT components and their support structures growing in size and weight.

8.2. Future work

While this research has provided valuable insights in the optimization of the reaction loads incorporated in sea fastening designs, the limitations discussed in the previous chapter suggest that there are still challenges and opportunities for future investigations. These challenges and opportunities are summarized below:

- In this research a long-term probabilistic method was derived in which only the wave-induced reaction loads were modelled in a probabilistic way. Current was neglected and wind loading was assumed to be constant, static and aligned with the wave heading angle. Further research on how the long-term probabilistic method can be expanded to include probabilistic descriptions of wind and current loads is recommended.
- With the introduced long-term probabilistic calculation method, the design reaction loads could be determined for acceptable return periods. Future research should be performed which focuses on the structural reliability analysis to determine acceptable return periods of the reaction loads to ensure desired structural target reliabilities .
- In the current calculation method a static FEM analysis of the jacket is performed to calculate the reaction loads on the sea fastening. In this research this static structural analysis is simplified by introducing the linear rigid jacket calculation method. Future research focusing on the influence of performing a static structural analysis of the jacket instead of a dynamic structural analysis may lead to more accurate reaction load calculations.
- Future investigations should address how the relative stiffness of the sea fastening structures of each leg can be implemented in the long-term probabilistic method.

References

[1] Classification Note no. 30.6. *Structural Reliability Analysis of Marine Structures*. Det Norske Veritas, 1991.

[2] Subrata Chakrabarti. "Empirical calculation of roll damping for ships and barges". In: *Ocean Engineering* 28.7 (2001), pp. 915–932.

[3] *Clean Energy Is Approaching a Tipping Point - Bloomberg*. URL: `https://www.bloomberg.com/news/articles/2017-09-19/tipping-point-seen-for-clean-energy-as-monster-turbines-arrive#xj4y7vzkg`.

[4] G. Costanzo, G. Brindley, and P. Cole. *Wind energy in Europe - 2022 Statistics and the outlook for 2023-2027*. Feb. 2023.

[5] DNV-RP-205. *Environmental Conditions and Environmental Loads*. DNVGL, 2010.

[6] DNV-ST-N001. *Marine operations and Marine warranty*. DNVGL, 2018.

[7] O.M. Faltinsen. *Sea Loads on Ships and Offshore Structures*. Cambridge University Press, 1993.

[8] Victor Igwemezie, Ali Mehmanparast, and Athanasios Kolios. "Current trend in offshore wind energy sector and material requirements for fatigue resistance improvement in large wind turbine support structures – A review". In: *Renewable and Sustainable Energy Reviews* 101 (Mar. 2019), pp. 181–196. ISSN: 18790690. DOI: `10.1016/J.RSER.2018.11.002`.

[9] J. M. J. Journée and W. W. Massie. *Offshore Hydromechanics*. First Edition. 2001.

[10] A. D. Kiureghian and O. Ditlevsen. "Aleatory or epistemic? Does it matter?" In: *Structural Safety* 31 (2 Mar. 2009), pp. 105–112. ISSN: 01674730. DOI: `10.1016/j.strusafe.2008.06.020`.

[11] M. Manohar, I.E. Mobarek, and N.A. El Sharaky. "CHARACTERISTIC WAVE PERIOD". In: *Coastal Engineering* Volume 1 (1976), pp. 273–288.

[12] Alexandre Mathern, Christoph von der Haar, and Steffen Marx. "Concrete support structures for offshore wind turbines: Current status, challenges, and future trends". In: *Energies* 14 (7 Apr. 2021). ISSN: 19961073. DOI: `10.3390/EN14071995`.

[13] R. E. Melchers and A.T. Beck. *Structural reliability analysis and prediction*. Third edition. John Wiley & Sons, Incorporated, 2018.

[14] A. Naess and T. Moan. *STOCHASTIC DYNAMICS OF MARINE STRUCTURES*. 2013.

[15] Asle Natskår. "Reliability-based assessment of marine operations with emphasis on sea transport on barges". Norwegian University of Science and Technology, Dec. 2020. ISBN: 9788232651122.

[16] Michel K Ochi. *Applied probability and stochastic processes*. Wiley New York, 1990.

[17] Michel K Ochi. "On Prediction of Extreme Values". In: *Journal of Ship Research* (1973), pp. 29–37. DOI: `https://doi.org/10.5957/jsr.1973.17.1.29`.

[18] *Offshore wind power Saint Brieuc | News Mecanizados Acebrón*. URL: `https://acebrongroup.com/en/offshore-wind-power-saint-brieuc/`.

[19] Ki Yong Oh et al. "A review of foundations of offshore wind energy convertors: Current status and future perspectives". In: *Renewable and Sustainable Energy Reviews* 88 (May 2018), pp. 16–36. ISSN: 18790690. DOI: `10.1016/J.RSER.2018.02.005`.

[20] Lizet Ramírez, Daniel Fraile, and Guy Brindley. *Offshore Wind in Europe*. 2021.

[21] Silvio Rodrigues et al. "A Multi-Objective Optimization Framework for Offshore Wind Farm Layouts and Electric Infrastructures". In: *Energies* 9 (2016). DOI: `10.3390/en9030216`. URL: `www.mdpi.com/journal/energies`.

[22] *The jackets to the Saint-Brieuc offshore wind farm have arrived off the coast of Brittany - YouTube*. URL: `https://www.youtube.com/watch?v=DDjpe2yf008`.

B
Extreme value analysis of acceleration time series

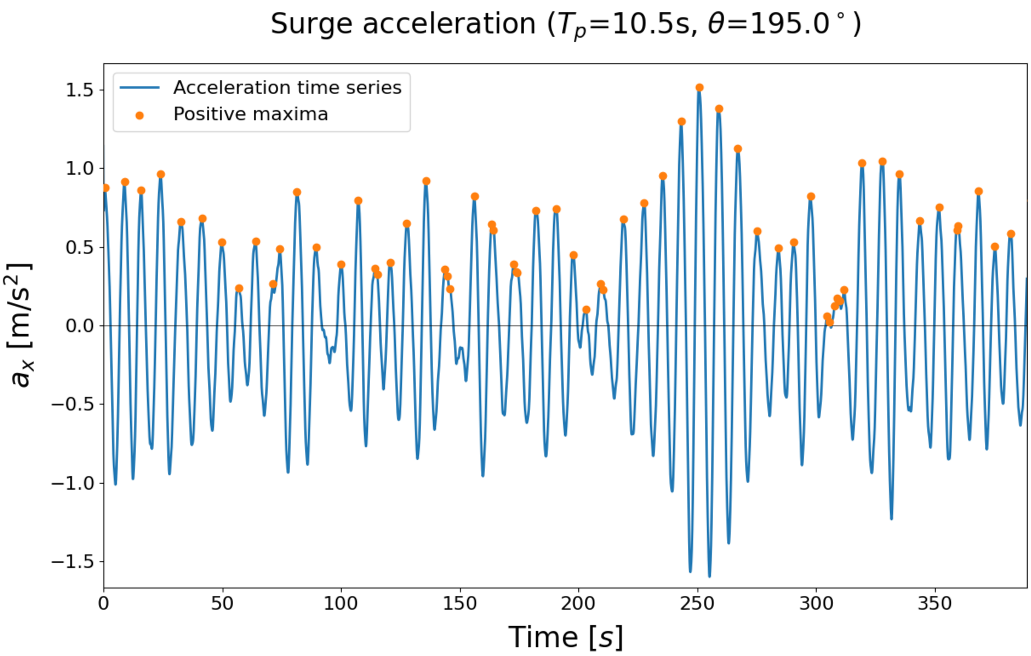

Figure B.1

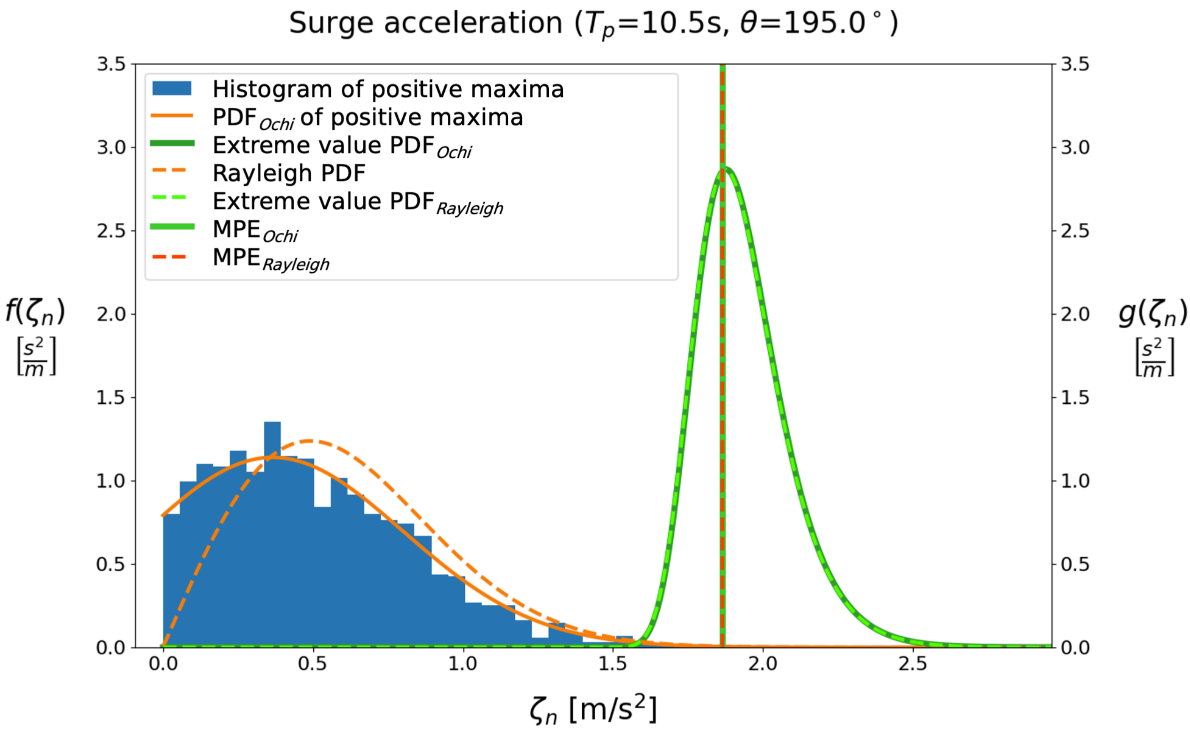

Figure B.2

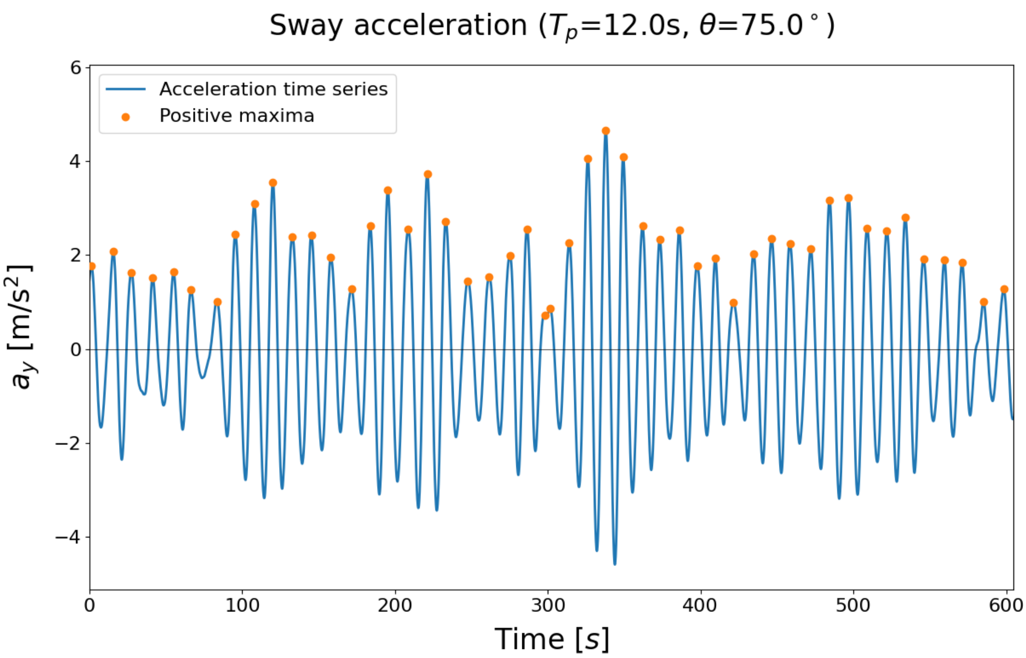

Figure B.3

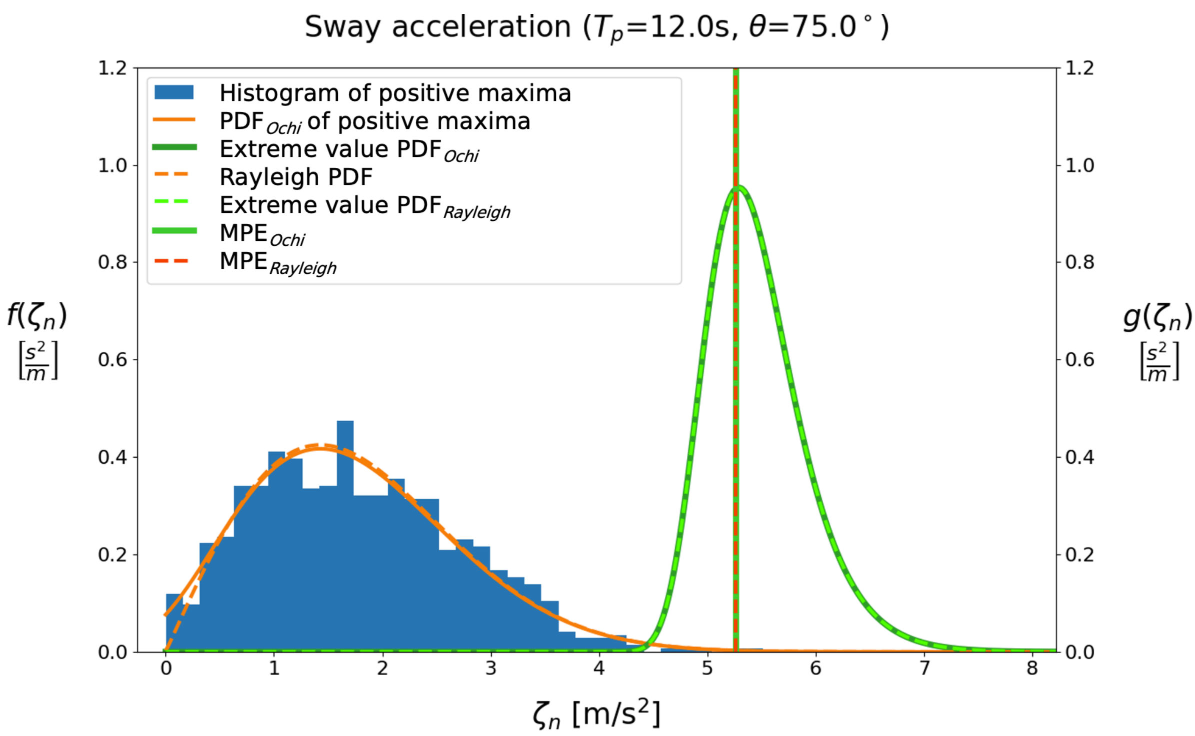

Figure B.4

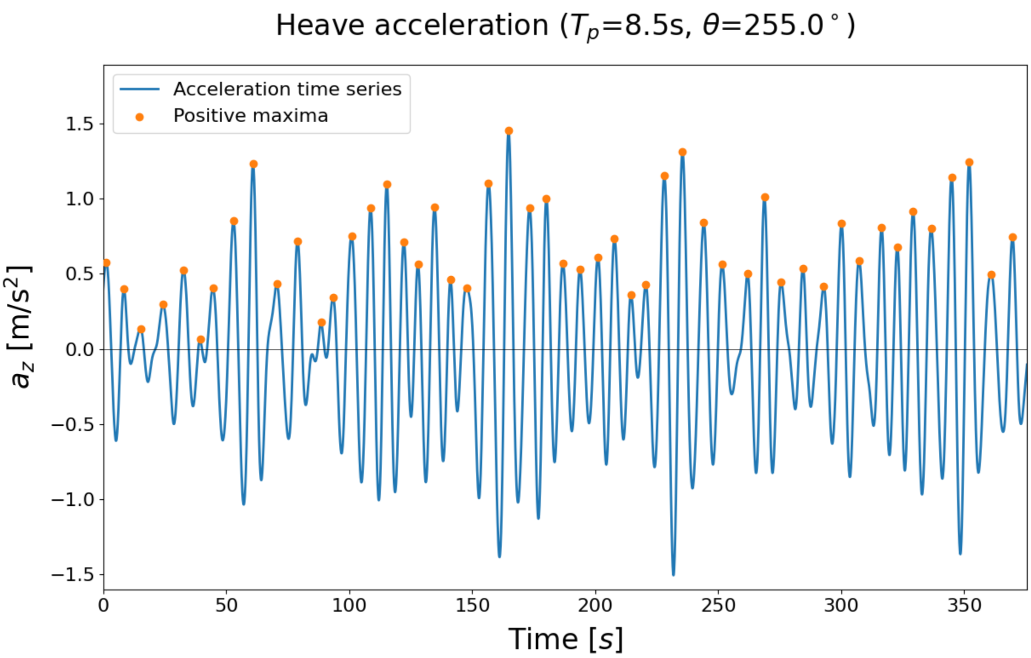

Figure B.5

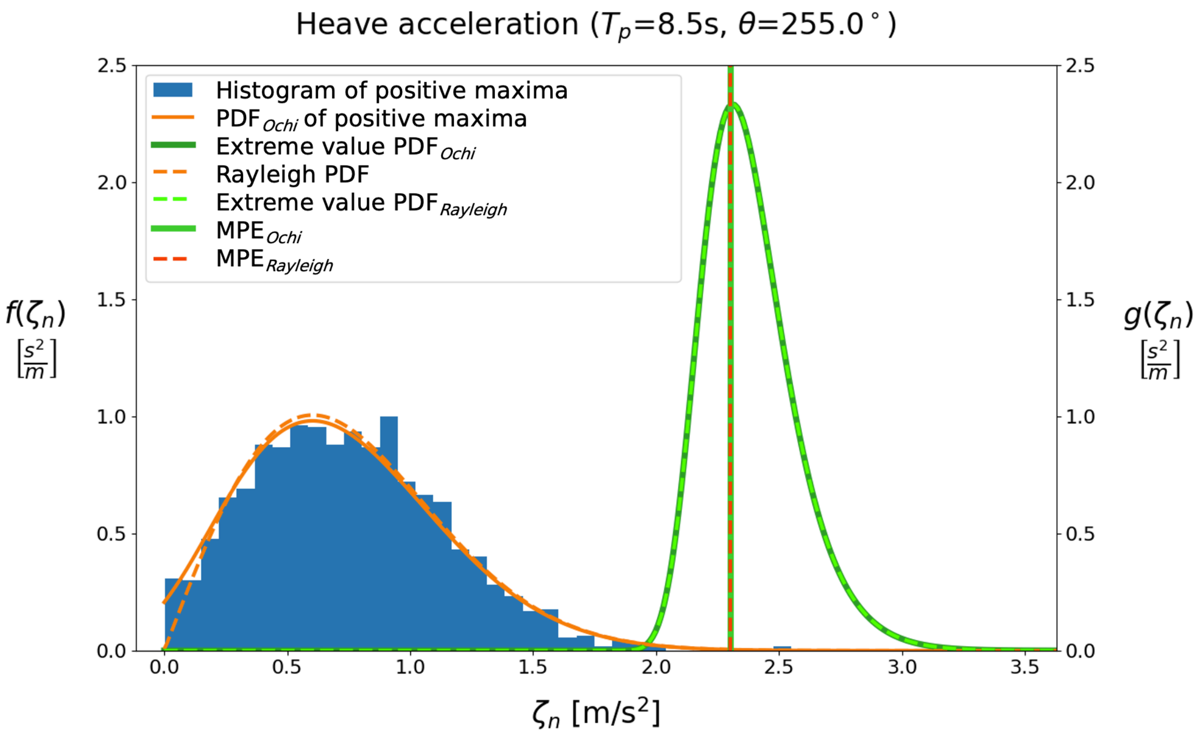

Figure B.6

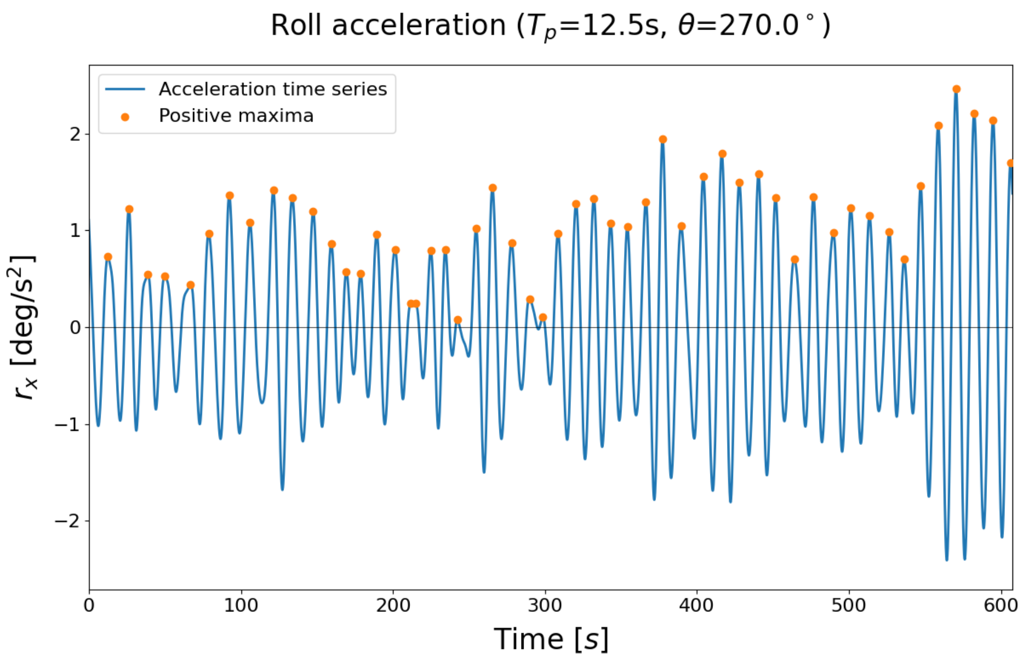

Figure B.7

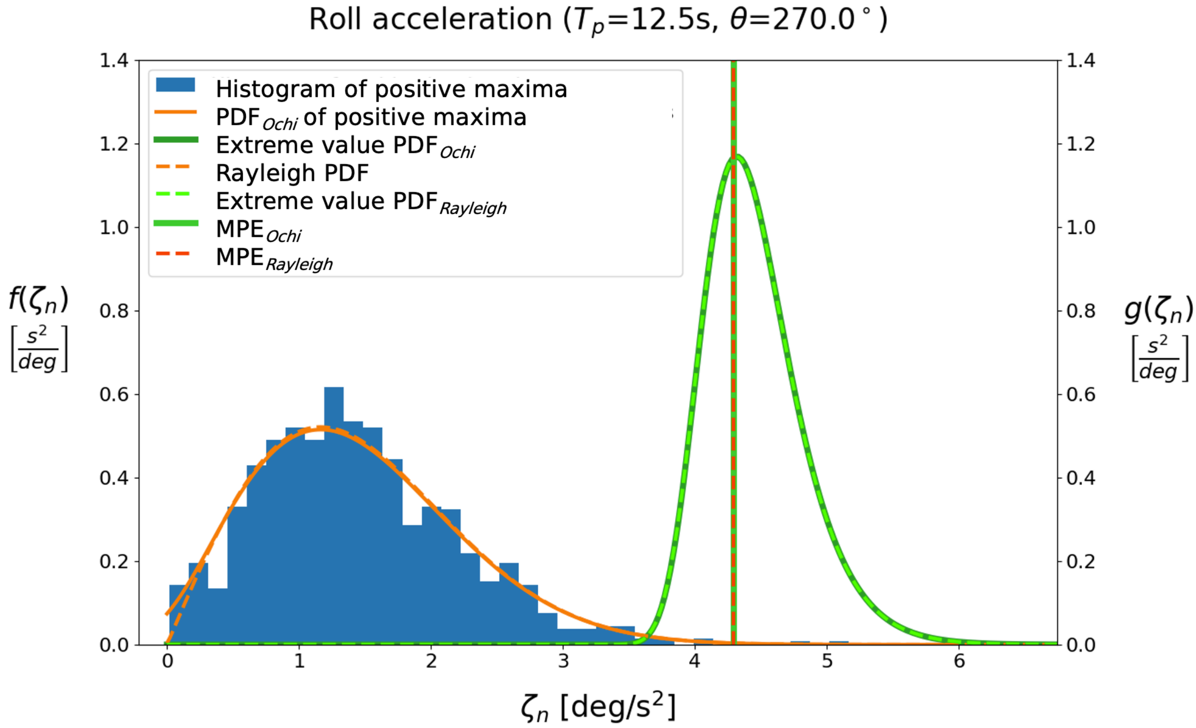

Figure B.8

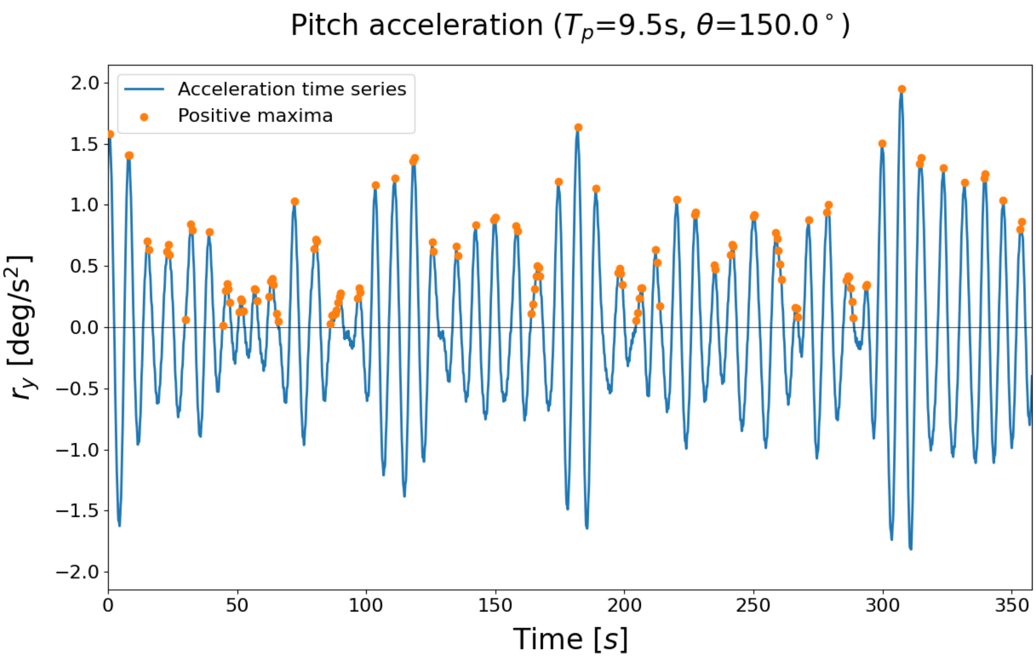

Figure B.9

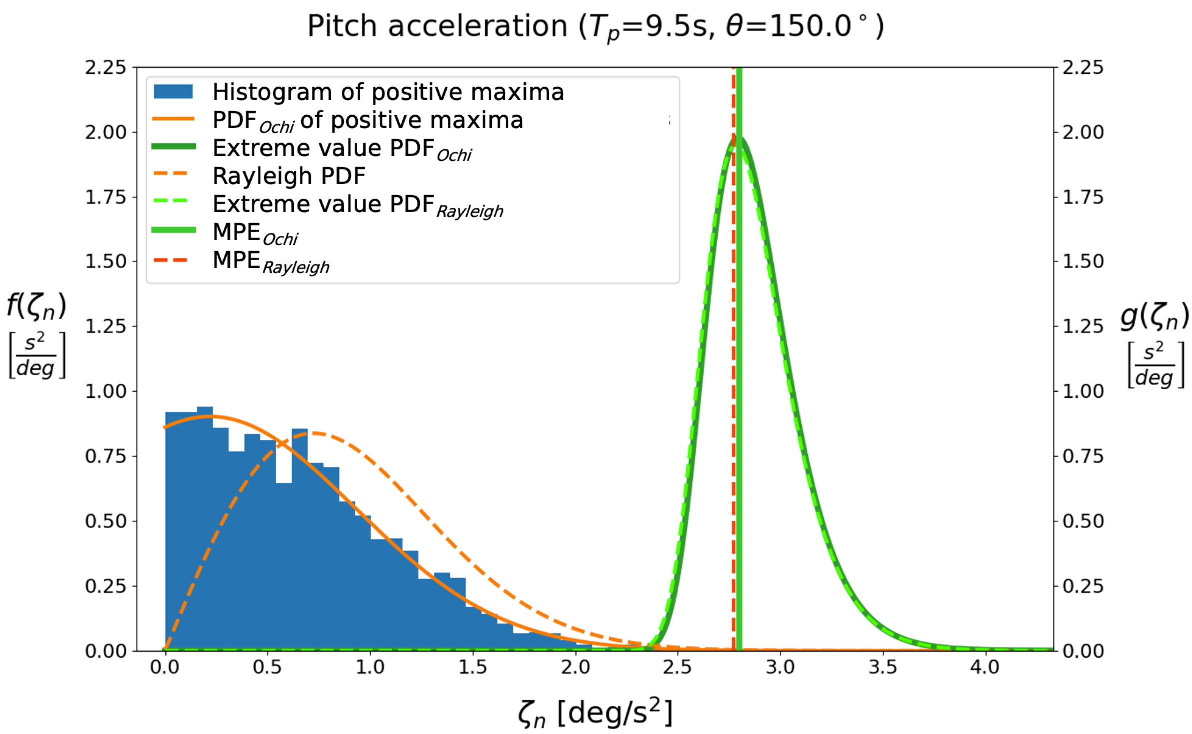

Figure B.10

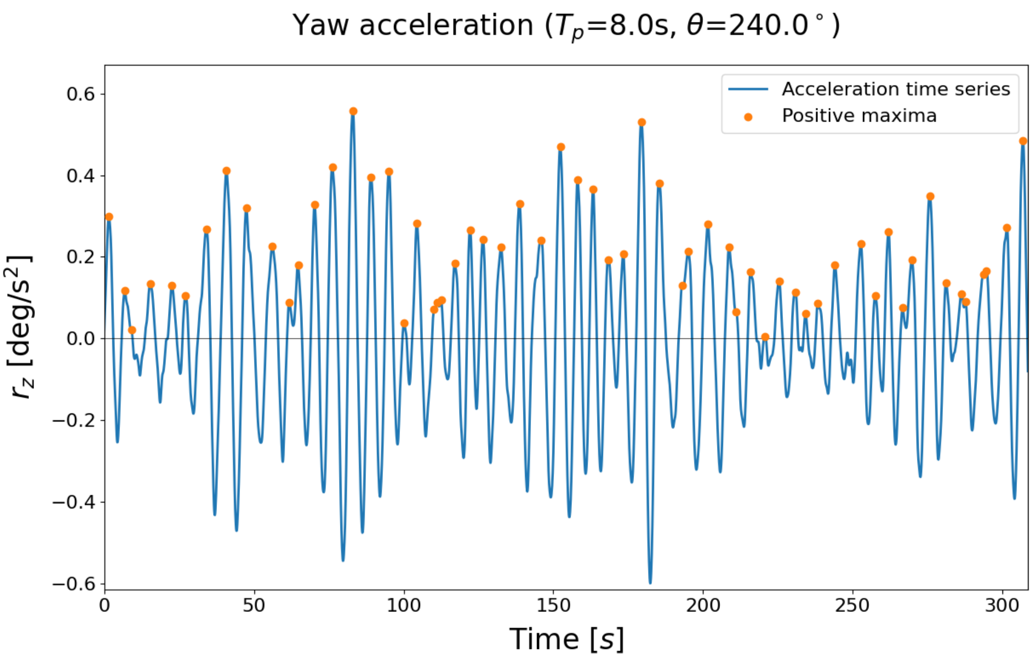

Figure B.11

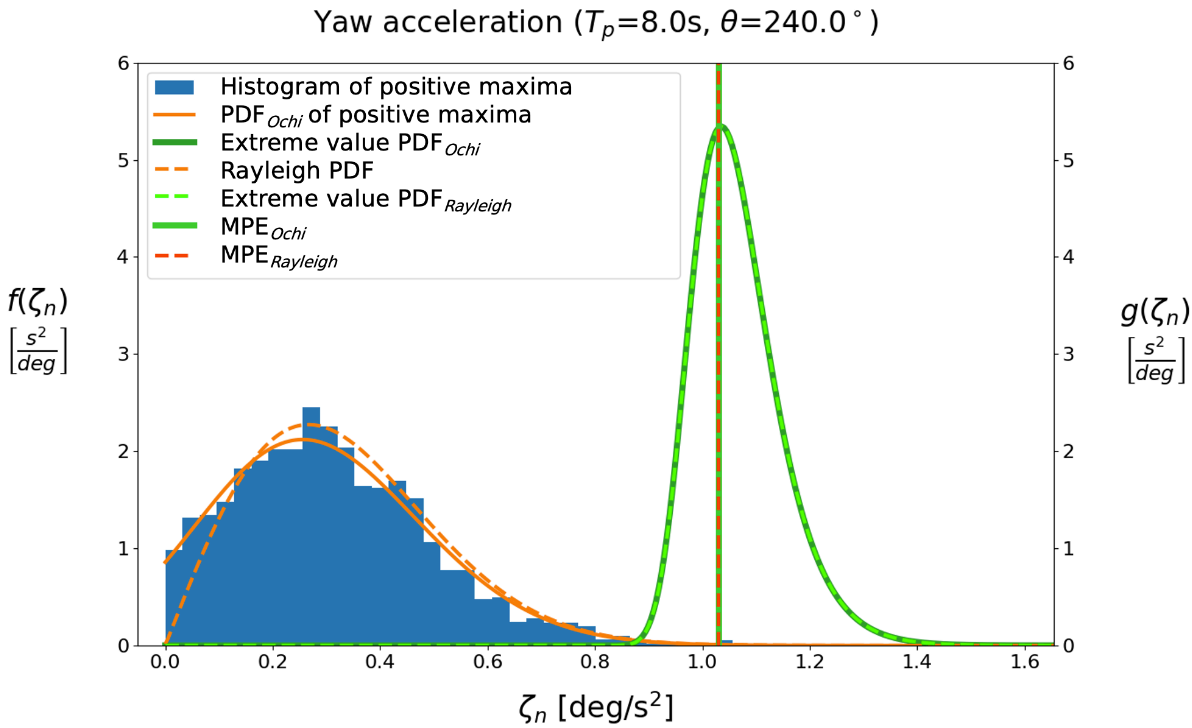

Figure B.12

Table B.1

	T_p [s]	Heading [deg]	σ [m/s^2]	m_0 [m^2/s^4]	m_2 [m^2/s^6]	m_4 [m^2/s^8]	T_z [s]	T_c [s]	ϵ [-]
Surge	10.5	195	0.490	0.241	$3.98\cdot 10^{-3}$	$1.73\cdot 10^{-4}$	7.78	4.80	0.787
Sway	12.0	75	1.428	2.038	$1.40\cdot 10^{-2}$	$1.03\cdot 10^{-4}$	12.09	11.66	0.264
Heave	8.5	255	0.603	0.364	$6.45\cdot 10^{-3}$	$1.26\cdot 10^{-4}$	7.51	7.16	0.304

Table B.2

	T_p [s]	Heading [deg]	σ [deg/s^2]	m_0 [deg^2/s^4]	m_2 [deg^2/s^6]	m_4 [deg^2/s^8]	T_z [s]	T_c [s]	ϵ [-]
Roll	12.5	270	1.165	1.356	$9.19\cdot 10^{-3}$	$6.53\cdot 10^{-5}$	12.15	11.85	0.220
Pitch	9.5	150	0.724	0.524	$1.02\cdot 10^{-2}$	$3.41\cdot 10^{-3}$	7.16	1.73	0.970
Yaw	8.0	240	0.267	$7.12\cdot 10^{-2}$	$1.87\cdot 10^{-3}$	$6.83\cdot 10^{-5}$	6.17	5.24	0.530

Table B.3

	T_p [s]	Heading [deg]	$n_{identified}$ [-]	$E[n]$ [-]	MPE$_{Ochi}$ [m/s^2]	$n_{Rayleigh}$ [-]	MPE$_{Rayleigh}$ [m/s^2]
Surge	10.5	195	1863	1819	1.869	1388	1.876
Sway	12.0	75	911	909	5.264	893	5.263
Heave	8.5	255	1465	1473	2.300	1438	2.288

Table B.4

	T_p [s]	Heading [deg]	$n_{identified}$ [-]	$E[n]$ [-]	MPE$_{Ochi}$ [deg/s^2]	$n_{Rayleigh}$ [-]	MPE$_{Rayleigh}$ [deg/s^2]
Roll	12.5	270	903	900	4.292	888	4.291
Pitch	9.5	150	3801	3873	2.799	1508	2.770
Yaw	8.0	240	1900	1905	1.031	1750	1.031

D

Static and harmonic contributions of reaction load time series

In section 5.1 the simplified rigid jacket calculation method is introduced. This linear calculation method can be used to calculate the vertical reaction loads for the three legs of the jacket. In this method it is described that the following loads are acting on the jacket:

$$
\begin{aligned}
F_x &= m \cdot a_x + F_w \cdot \cos\theta \\
F_y &= m \cdot a_y + F_w \cdot \sin\theta \\
F_z &= m \cdot a_z - F_{static} \\
M_x &= I_{xx} \cdot r_x \\
M_y &= I_{yy} \cdot r_y
\end{aligned}
$$

The loads acting on the jacket can be separated into static loads and loads which are harmonic with zero mean. The wind load acting on the jacket is assumed to be static just as the static weight of the jacket. The linear wave-induced loads on the jacket are harmonic loads since the wave elevation signal is harmonic as well.

The vertical reaction load for leg A is given by Equation 5.2:

$$F_{vA} = \frac{M_y + F_x \cdot h - F_z \cdot a}{R + a}$$

Which can be rewritten into a static and a harmonic part:

$$F_{vA} = \underbrace{\frac{F_w \cdot \cos\theta \cdot h + F_{\text{static}} \cdot a}{R + a}}_{\text{Static}} + \underbrace{\frac{I_{yy} \cdot r_y + m \cdot a_x \cdot h - m \cdot a_z \cdot a}{R + a}}_{\text{Harmonic}} \tag{D.1}$$

The vertical reaction load for leg B is given by Equation 5.4:

$$F_{vB} = \frac{-M_{x'} - F_z \cdot a + F_{y'} \cdot h}{R + a}$$

With:

$$
\begin{aligned}
\alpha &= 30^\circ \\
F_{y'} &= -F_x \cdot \sin\alpha + F_y \cdot \cos\alpha \\
M_{x'} &= M_x \cdot \cos\alpha + M_y \cdot \sin\alpha
\end{aligned}
$$

The vertical reaction load for leg B can also be rewritten into a static and a harmonic part:

$$F_{vB} = \underbrace{\frac{F_{\text{static}} \cdot a - F_w \cdot \cos\theta \cdot \sin\alpha \cdot h + F_w \cdot \sin\theta \cdot \cos\cdot\alpha \cdot h}{R+a}}_{\text{Static}} + \underbrace{\frac{-I_x x \cdot r_x \cdot \cos\alpha - I_y y \cdot r_y \cdot \sin\alpha - m \cdot a_z \cdot a - m \cdot a_x \cdot \sin\alpha \cdot h + m \cdot a_y \cdot \cos\cdot\alpha \cdot h}{R+a}}_{\text{Harmonic}} \tag{D.2}$$

The vertical reaction load for leg C is given by Equation 5.6:

$$F_{vC} = \frac{M_{x''} - F_{y''} \cdot h - Fz \cdot a}{R+a}$$

With:

$$\beta = 30^\circ$$
$$F_{y''} = F_x \cdot \sin\beta + F_y \cdot \cos\beta$$
$$M_{x''} = M_x \cdot \cos\beta - M_y \cdot \sin\beta$$

The vertical reaction load for leg C can also be rewritten into a static and a harmonic part:

$$F_{vC} = \underbrace{\frac{-F_w \cdot \cos\theta \cdot \sin\beta \cdot h - F_w \cdot \sin\theta \cdot \cos\beta \cdot h + F_{\text{static}} \cdot a}{R+a}}_{\text{Static}} + \underbrace{\frac{I_x x \cdot r_x \cdot \cos\beta - I_y y \cdot r_y \cdot \sin\beta - m \cdot a_x \cdot \sin\beta \cdot h - m \cdot a_y \cdot \cos\beta \cdot h - m \cdot a_z \cdot a}{R+a}}_{\text{Harmonic}} \tag{D.3}$$

In Figure D.1 it is graphically shown how a total reaction load times series F_{vB} for leg B is obtained by superposition of the static and harmonic part of the reaction load.

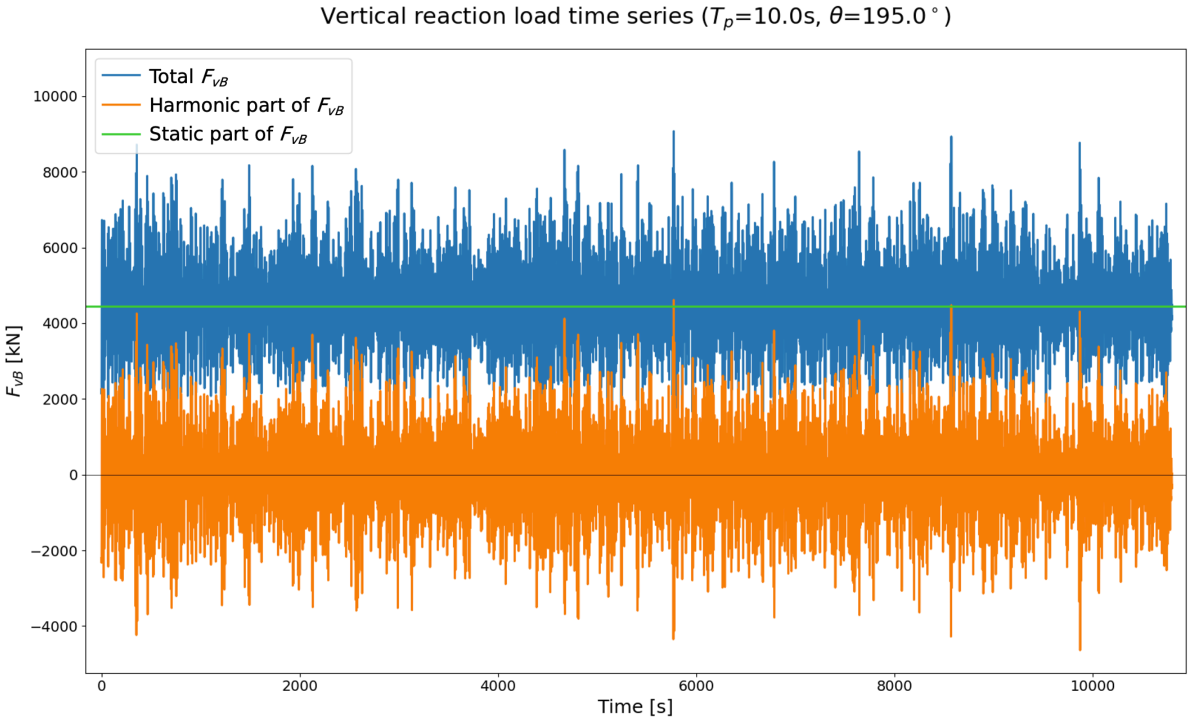

Figure D.1

E
Load combination methods results

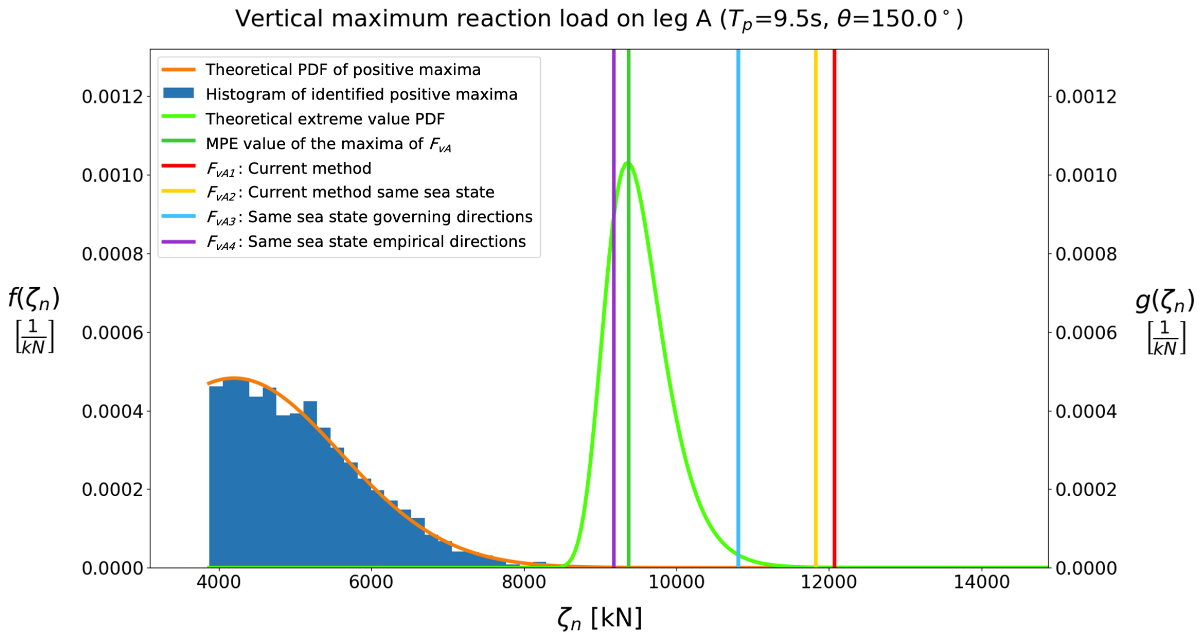

Figure E.1

Table E.1

T_p [s]	Heading [deg]	MPE [kN]	$P(\zeta_n \geq \text{MPE})$ [-]	F_{vA1} [kN]	$P(\zeta_n \geq F_{vA1})$ [-]	F_{vA2} [kN]	$P(\zeta_n \geq F_{vA2})$ [-]
9.5	150	9373	0.594	12075	$6.50\cdot 10^{-5}$	11826	$1.79\cdot 10^{-4}$

T_p [s]	Heading [deg]	F_{vA3} [kN]	$P(\zeta_n \geq F_{vA3})$ [-]	F_{vA4} [kN]	$P(\zeta_n \geq F_{vA4})$ [-]
9.5	150	10812	$9.00\cdot 10^{-3}$	9179	0.759

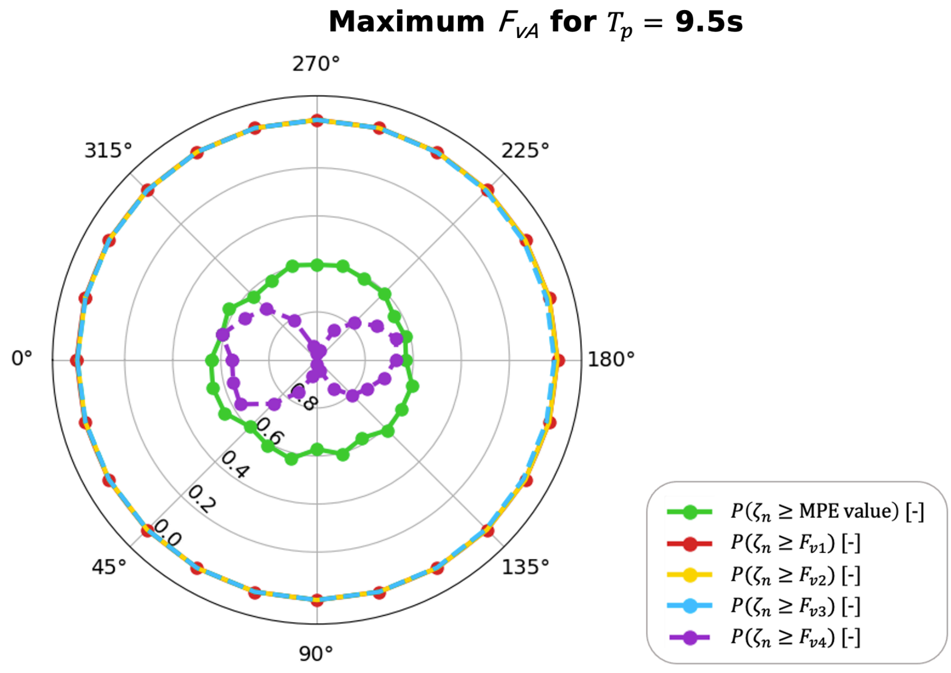

Figure E.2

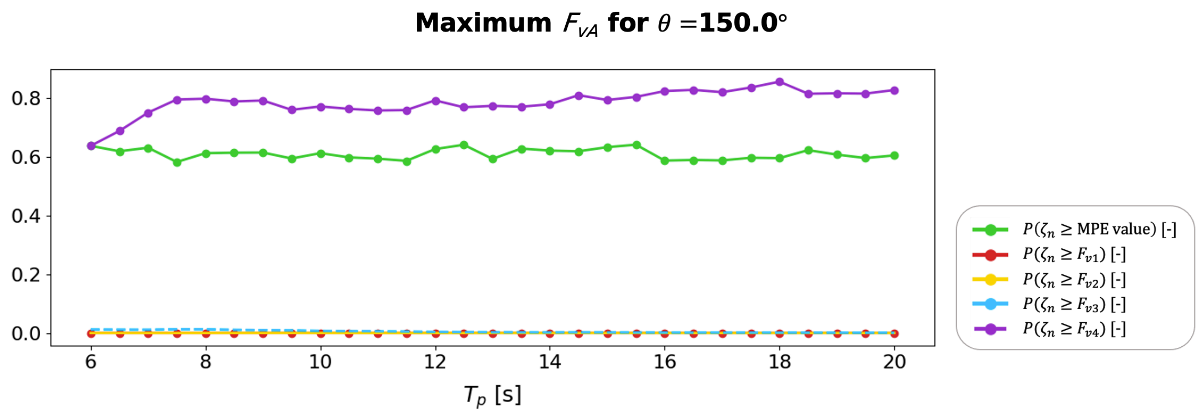

Figure E.3

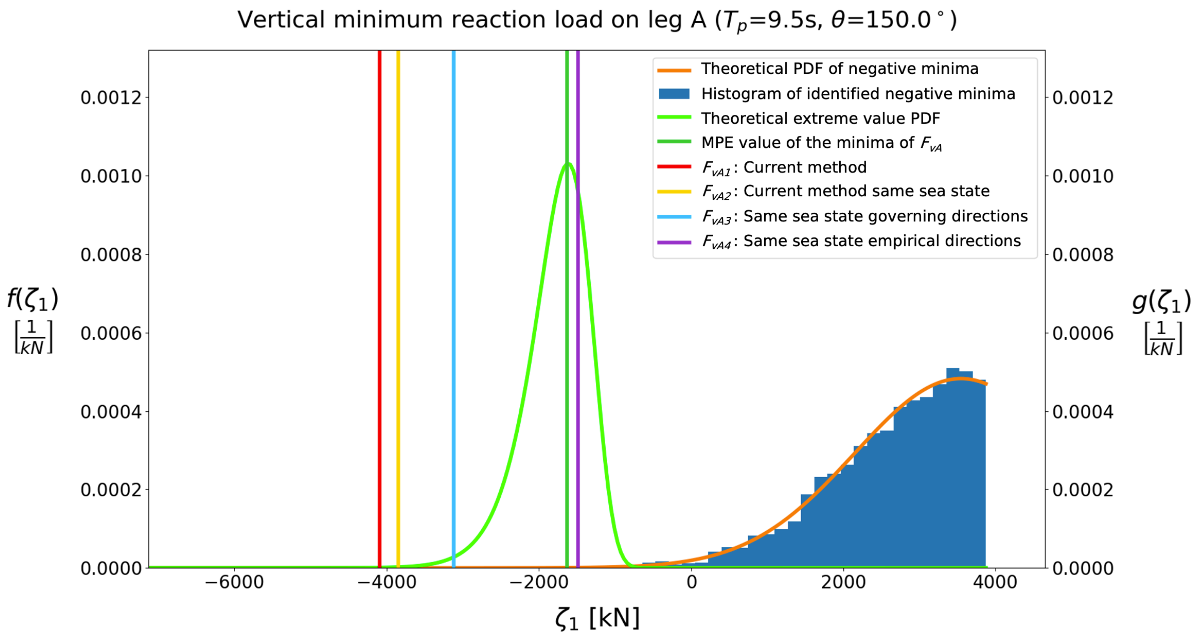

Figure E.4

Table E.2

T_p [s]	Heading [deg]	MPE [kN]	$P(\zeta_1 \leq \text{MPE})$ [-]	F_{vA1} [kN]	$P(\zeta_1 \leq F_{vA1})$ [-]	F_{vA2} [kN]	$P(\zeta_1 \leq F_{vA2})$ [-]
9.5	150	-1627	0.594	-4090	$1.79 \cdot 10^{-4}$	-3841	$4.82 \cdot 10^{-4}$

T_p [s]	Heading [deg]	F_{vA3} [kN]	$P(\zeta_1 \leq F_{vA3})$ [-]	F_{vA4} [kN]	$P(\zeta_1 \leq F_{vA4})$ [-]
9.5	150	-3120	$6.71 \cdot 10^{-3}$	-1487	0.720

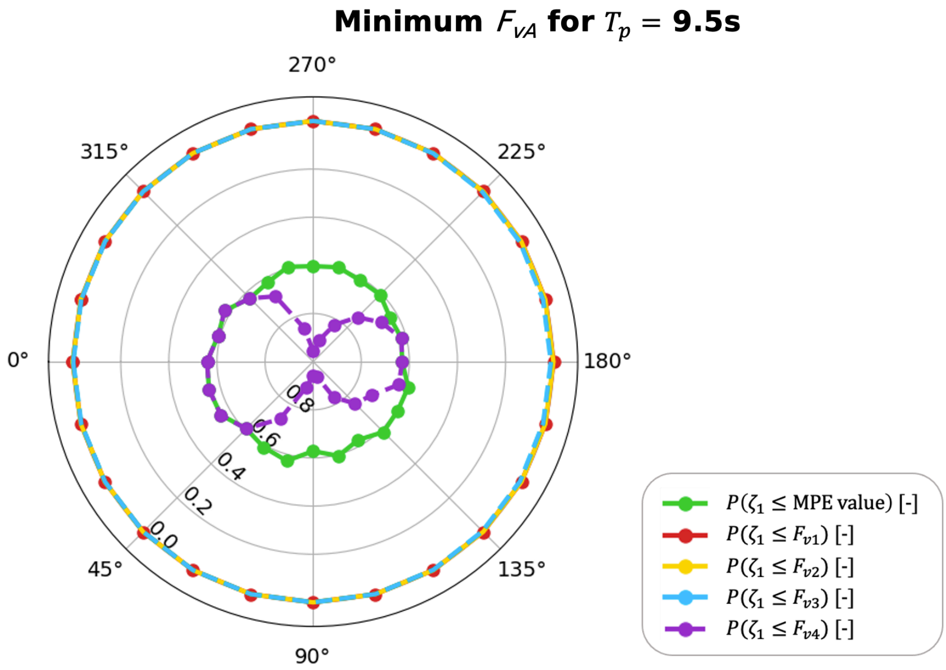

Figure E.5

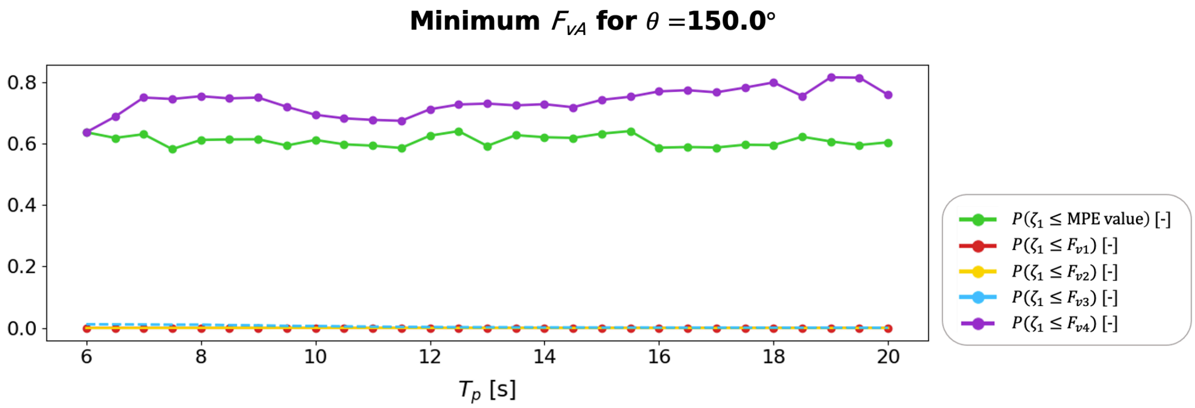

Figure E.6

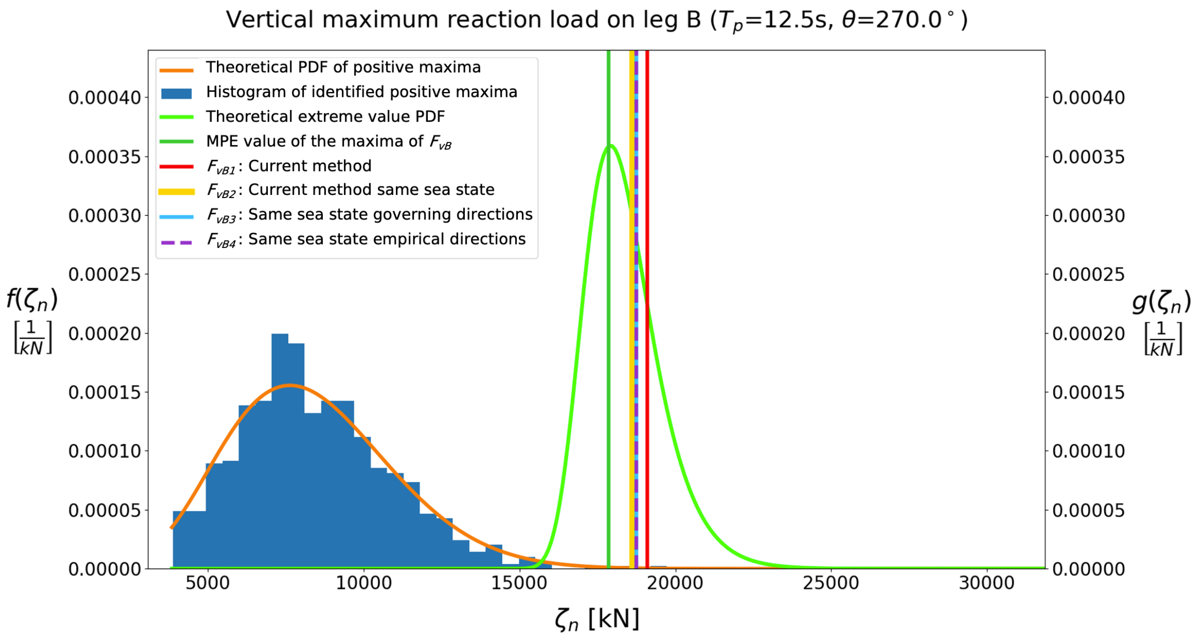

Figure E.7

Table E.3

T_p [s]	Heading [deg]	MPE [kN]	$P(\zeta_n \geq \text{MPE})$ [-]	F_{vB1} [kN]	$P(\zeta_n \geq F_{vB1})$ [-]	F_{vB2} [kN]	$P(\zeta_n \geq F_{vB2})$ [-]
12.5	270	17850	0.617	19108	0.237	18623	0.350

T_p [s]	Heading [deg]	F_{vB3} [kN]	$P(\zeta_n \geq F_{vB3})$ [-]	F_{vB4} [kN]	$P(\zeta_n \geq F_{vB4})$ [-]
12.5	270	18738	0.325	18738	0.325

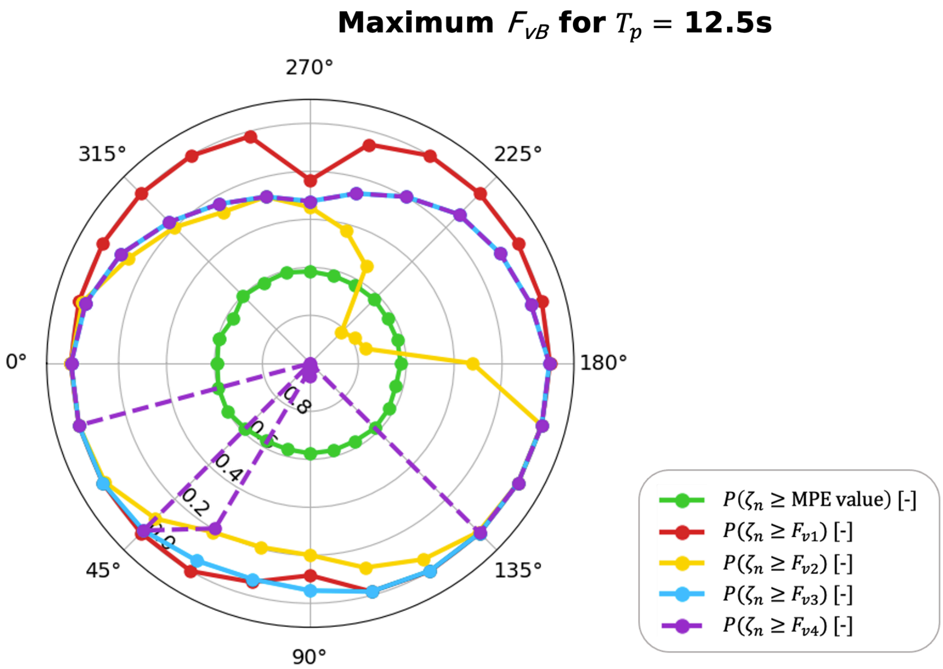

Figure E.8

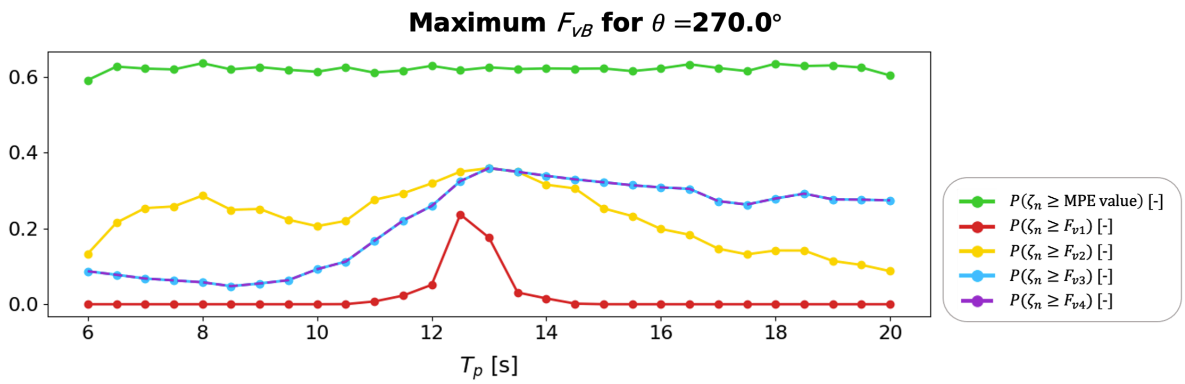

Figure E.9

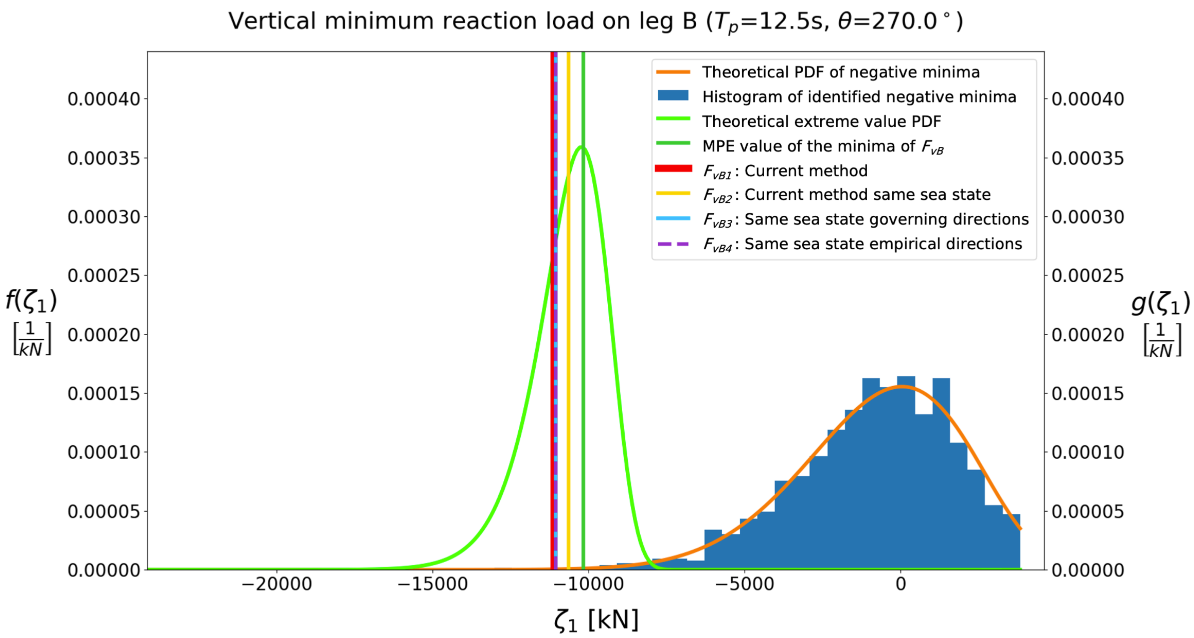

Figure E.10

Table E.4

T_p [s]	Heading [deg]	MPE [kN]	$P(\zeta_1 \leq \text{MPE})$ [-]	F_{vB1} [kN]	$P(\zeta_1 \leq F_{vB1})$ [-]	F_{vB2} [kN]	$P(\zeta_1 \leq F_{vB2})$ [-]
12.5	270	-10158	0.617	-11123	0.301	-10637	0.461

T_p [s]	Heading [deg]	F_{vB3} [kN]	$P(\zeta_1 \leq F_{vB3})$ [-]	F_{vB4} [kN]	$P(\zeta_1 \leq F_{vB4})$ [-]
12.5	270	-11046	0.325	-11046	0.325

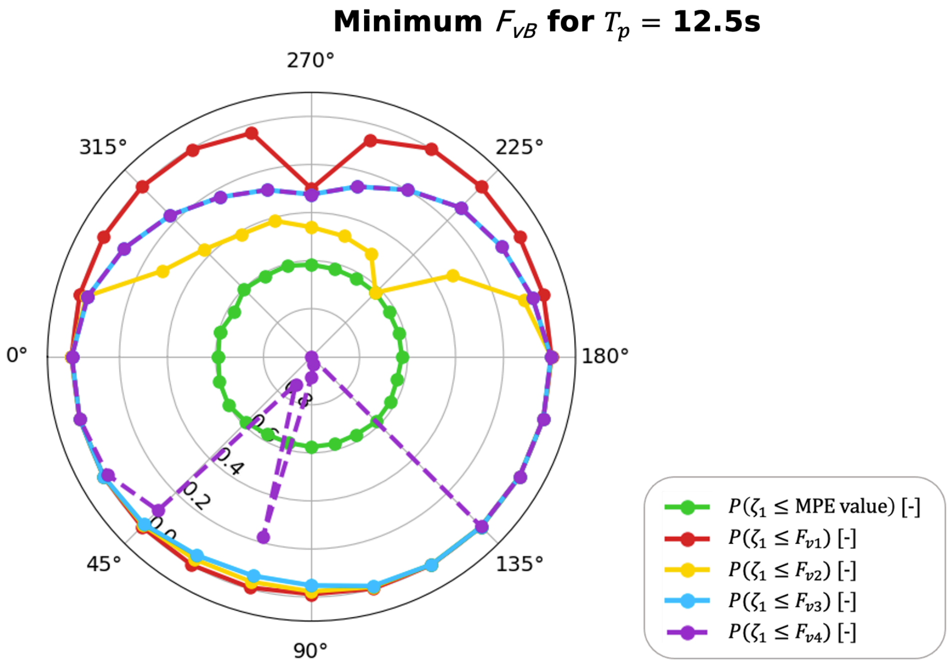

Figure E.11

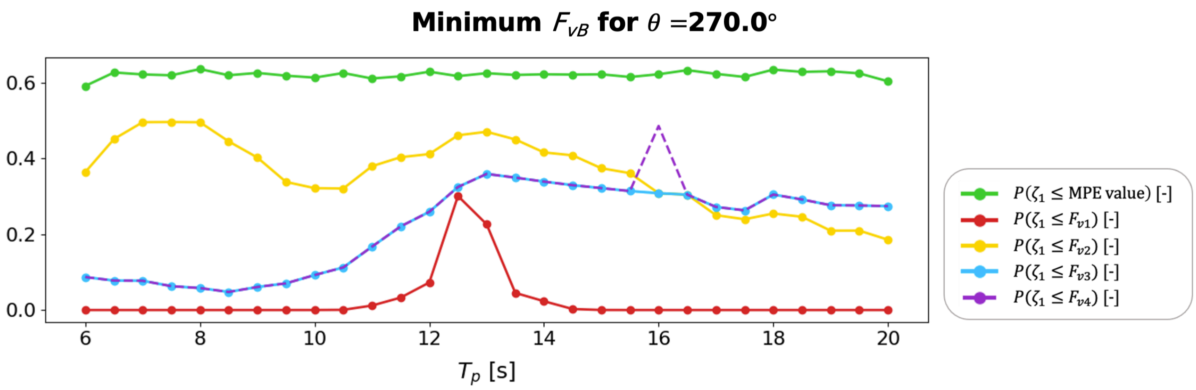

Figure E.12

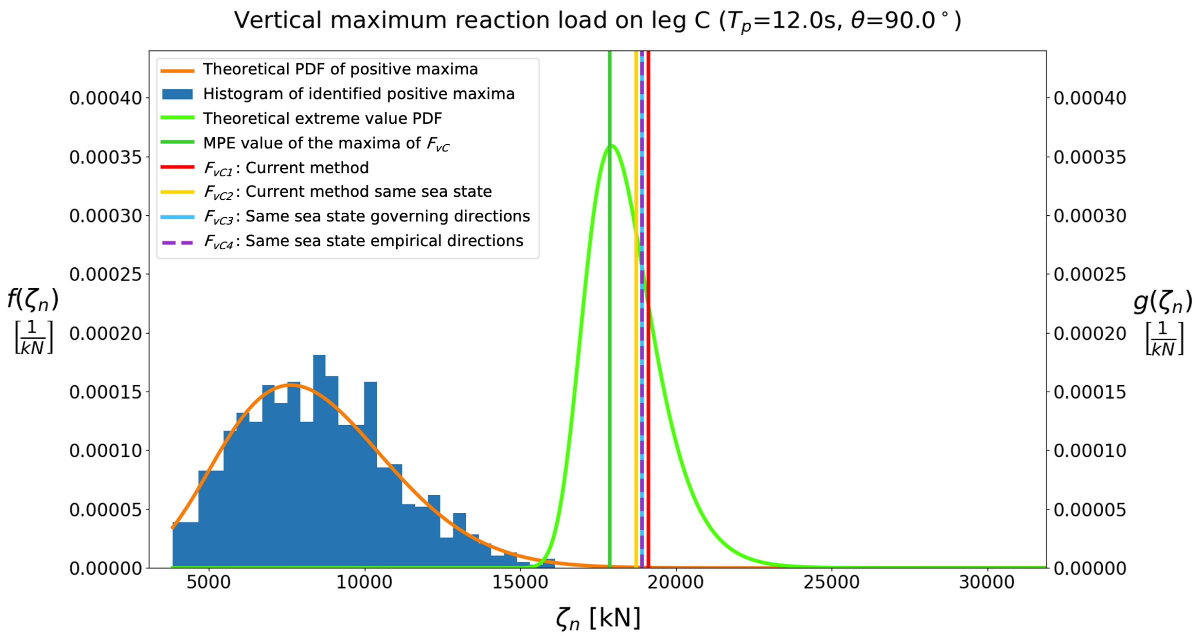

Figure E.13

Table E.5

T_p [s]	Heading [deg]	MPE [kN]	$P(\zeta_n \geq \text{MPE})$ [-]	F_{vC1} [kN]	$P(\zeta_n \geq F_{vC1})$ [-]	F_{vC2} [kN]	$P(\zeta_n \geq F_{vC2})$ [-]
12.0	90	17867	0.606	19108	0.232	18732	0.321

T_p [s]	Heading [deg]	F_{vC3} [kN]	$P(\zeta_n \geq F_{vC3})$ [-]	F_{vC4} [kN]	$P(\zeta_n \geq F_{vC4})$ [-]
12.0	90	18921	0.283	18921	0.283

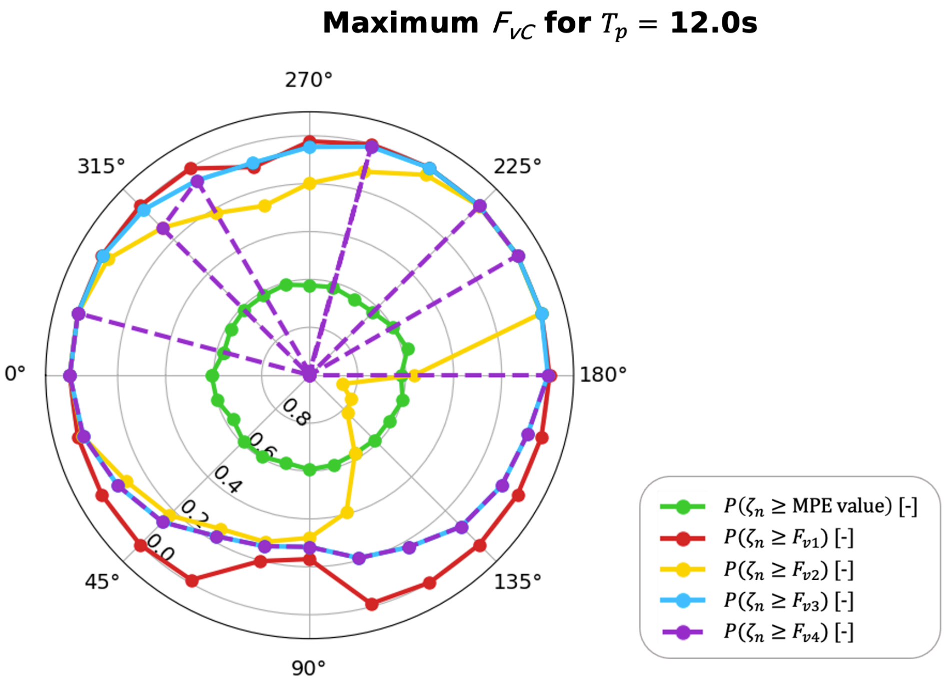

Figure E.14

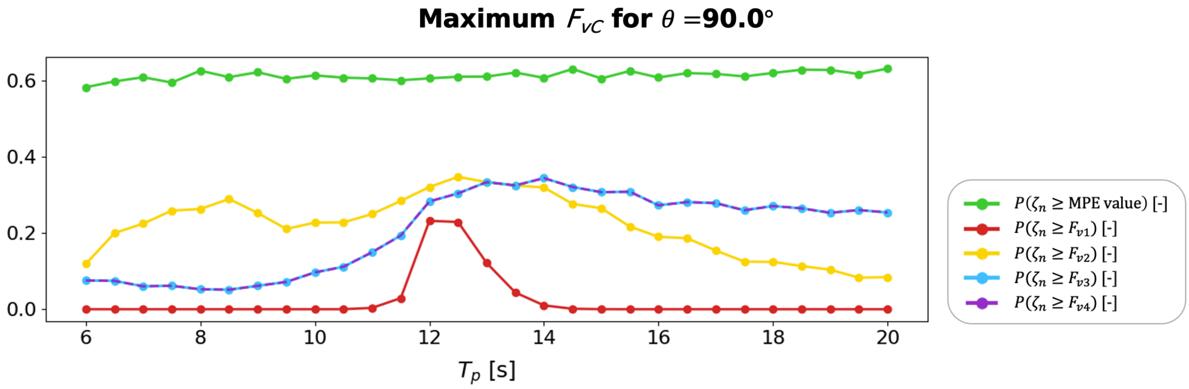

Figure E.15

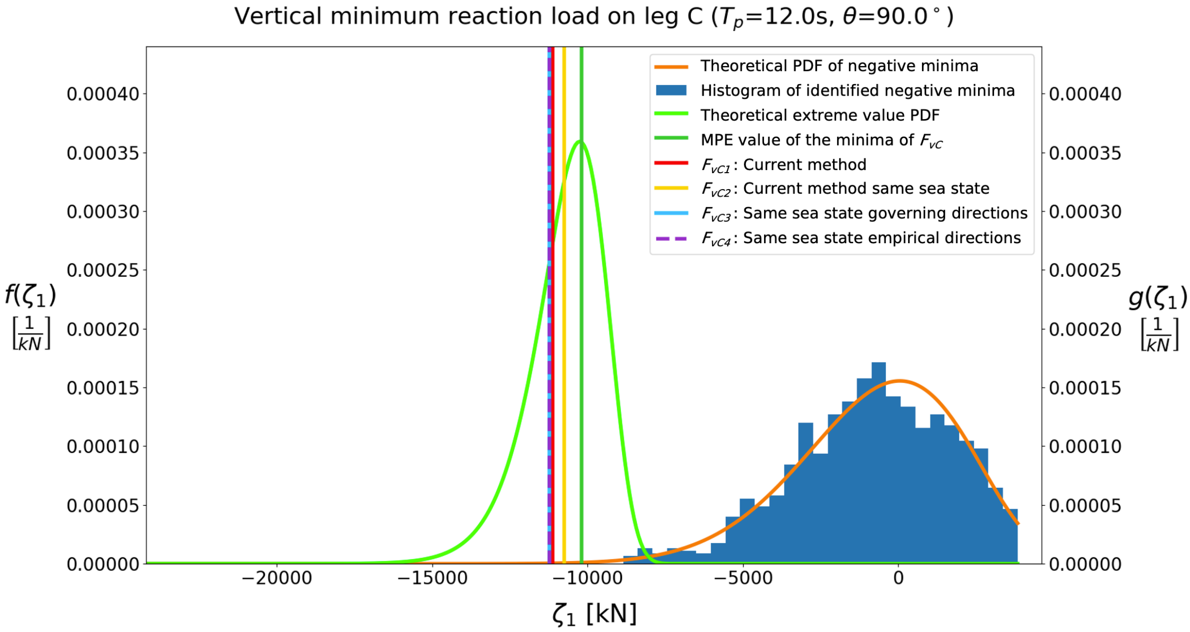

Figure E.16

Table E.6

T_p [s]	Heading [deg]	MPE [kN]	$P(\zeta_1 \leq \text{MPE})$ [-]	F_{vC1} [kN]	$P(\zeta_1 \leq F_{vC1})$ [-]	F_{vC2} [kN]	$P(\zeta_1 \leq F_{vC2})$ [-]
12.0	90	-10181	0.606	-11123	0.302	-10747	0.430

T_p [s]	Heading [deg]	F_{vC3} [kN]	$P(\zeta_1 \leq F_{vC3})$ [-]	F_{vC4} [kN]	$P(\zeta_1 \leq F_{vC4})$ [-]
12.0	90	-11229	0.283	-11229	0.283

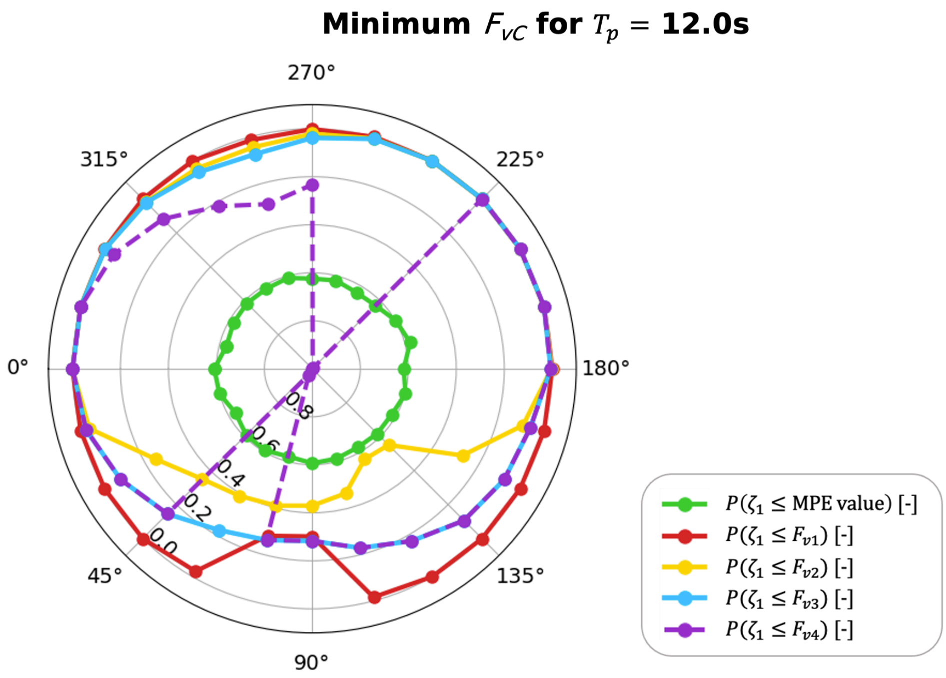

Figure E.17

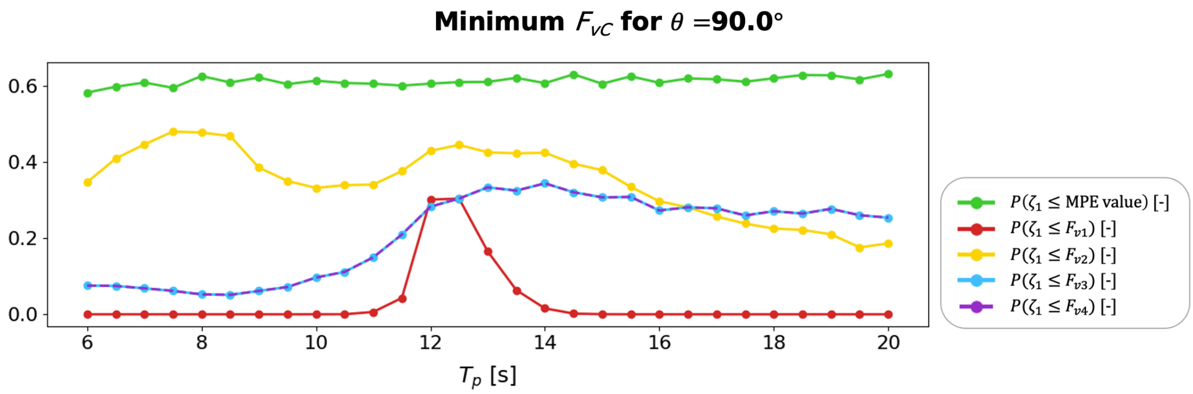

Figure E.18

F

Sea state probability

As explained in section 6.2 the probability $P(h_{s,i} \cap t_{p,j} \cap \theta_k)$ of encountering a sea state within the intervals given by $h_{s,i}$, $t_{p,j}$ and θ_k is determined with the probabilities $P(h_{s,i} \cap t_{p,j})$ and $P(h_{s,i} \cap \theta_k)$ obtained from the scatter diagrams. The probability $P(h_{s,i} \cap t_{p,j} \cap \theta_k)$ is derived with:

$$P(h_s \cap t_p \cap \theta) = \frac{P(h_s \cap t_p) \cdot P(h_s \cap \theta)}{P(h_s)} \tag{F.1}$$

Confidential information

Figure F.1: Wave scatter diagram for the location on the route which has the most extreme statistical wave conditions

Confidential information

Figure F.2: Directional wave scatter diagram for the location on the route which has the most extreme statistical wave conditions

From these wave scatter diagrams the probabilities on sea states with H_s = ?m are computed. The probability on a sea state with H_s = ?m, T_p = ?s and θ = 285-315deg is for example computed as follows:

$$P(h_s \cap t_p \cap \theta) = \frac{0.03 \cdot 0.03}{0.06} = 0.015 \tag{F.2}$$

In the table below, the probabilities for all other sea states with H_s = ?m are given. It can be seen that when all probabilities are summed, the total probability 0.06 is equal to $P(H_s =$?m).

Confidential information

Conservative approach

It was explained in section 6.1 that cells in the wave scatter diagrams with a given value of 0 have an actual value which is less than 0.5 and therefore rounded to 0. To be conservative, values of 0.5 will be used in the calculation method for cells which have a given value of 0. This is done without changing the rest of the scatter diagrams such that the total number of observations remains 100 for both scatter diagrams. In this way the probabilities for the other sea states remain the same. The wave scatter diagrams with cells which have given a conservative value of 0.5 instead of 0 are shown below.

Confidential information

Figure F.3: Wave scatter diagram for the location on the route which has the most extreme statistical wave conditions

Confidential information

Figure F.4: Directional wave scatter diagram for the location on the route which has the most extreme statistical wave conditions

The resulting probabilities for all sea states within the $H_s =$?m interval are given in the table below. It can be seen that only the cells which had values of 0 in the non-conservative approach are influenced. The cells with non-zero values remain the same. As expected the total probability of sea states within the $H_s =$?m interval is increased from 0.06 to 0.14 since some sea state intervals are conservatively given higher probabilities.

Confidential information

The probabilities $P(h_s \cap t_p \cap \theta)$ obtained with the conservative approach are used for the probabilistic investigation of the current method in section 6.3.


TU Delft
TWD
NTNU